AD-A072 724 ADAPTRONICS INC MCLEAN VA F/G 14/2
EXPLORATORY DEVELOPMENT OF ADHESIVE BOND FLAW DETECTION.(U)
DEC 78 M H LOEW, J M FITZGERALD F33615-76-C-5079
UNCLASSIFIED AFML-TR-78-206 NL

1 OF 2
ADA 072724

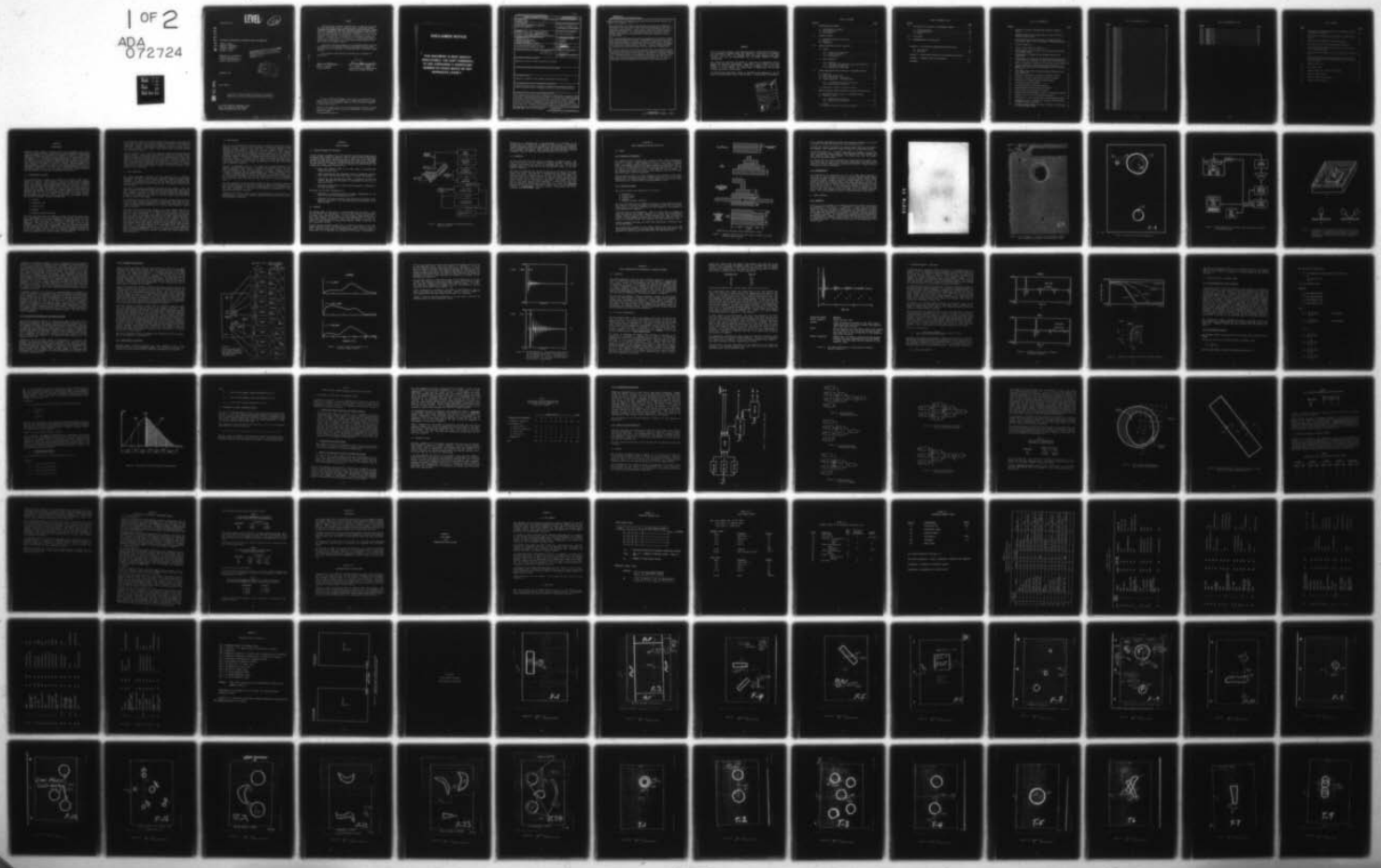

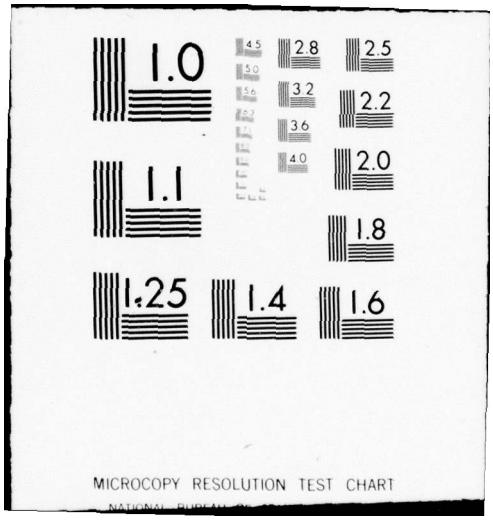
1.0
1.1
1.25
1.4
1.6
1.8
2.0
2.2
2.5
2.8
3.2
3.6
4.0
4.5
5.0
5.6
6.3
MICROCOPY RESOLUTION TEST CHART

AFML-TR-78-206

EXPLORATORY DEVELOPMENT OF ADHESIVE BOND FLAW DETECTION

Murray H. Loew
James M. Fitzgerald
Anthony N. Mucciardi
Richard K. Elsley
George A. Alers

Adaptronics, Incorporated
Westgate Research Park
7700 Old Springhouse Road
McLean, Virginia 22102

DECEMBER 1978

Final Report

AIR FORCE MATERIALS LABORATORY (AFSC)
Attn: Mr. James Holloway AFML/LLP
WRIGHT-PATTERSON AFB, OHIO 45433

NOTICE

When Government drawings, specifications, or other data are used for any purpose other than in connection with a definitely related Government procurement operation, the United States Government thereby incurs no responsibility nor any obligation whatsoever; and the fact that the Government may have formulated, furnished, or in any way supplied the said drawings, specifications, or other data, is not to be regarded by implication or otherwise as in any manner licensing the holder or any other person or corporation, or conveying any rights or permission to manufacture, use, or sell any patented invention that may in any way be related thereto.

This report has been reviewed by the Information Office (IO) and is releasable to the National Technical Information Service (NTIS). At NTIS, it will be available to the general public, including foreign nations.

This technical report has been reviewed and is approved for publication.

James A. Holloway

JAMES A. HOLLOWAY
Project Engineer

D. M. FORNEY, Jr., Chief
Nondestructive Evaluation Branch
Metals and Ceramics Division

"If your address has changed, if you wish to be removed from our mailing list, or if the addressee is no longer employed by your organization please notify AFML/LLP, WPAFB, OH 45433 to help us maintain a current mailing list."

Copies of this report should not be returned unless return is required by security considerations, contractual obligations, or notice on a specific document.

AIR FORCE/56780/7 August 1979 — 840

DISCLAIMER NOTICE

THIS DOCUMENT IS BEST QUALITY PRACTICABLE. THE COPY FURNISHED TO DDC CONTAINED A SIGNIFICANT NUMBER OF PAGES WHICH DO NOT REPRODUCE LEGIBLY.

SECURITY CLASSIFICATION OF THIS PAGE (When Data Entered)

REPORT DOCUMENTATION PAGE

READ INSTRUCTIONS BEFORE COMPLETING FORM

1. REPORT NUMBER: AFML-TR-78-206	2. GOVT ACCESSION NO.
3. RECIPIENT'S CATALOG NUMBER	
4. TITLE (and Subtitle): EXPLORATORY DEVELOPMENT OF ADHESIVE BOND FLAW DETECTION.	5. TYPE OF REPORT & PERIOD COVERED: Final rept. 1 Apr 76 - 30 Nov 78
	6. PERFORMING ORG. REPORT NUMBER
7. AUTHOR(s): Murray H. Loew, James M. Fitzgerald, and Anthony N. Mucciardi - Adaptronics, Inc. Richard K. Elsley and George A. Alers (Block 18)	8. CONTRACT OR GRANT NUMBER(s): F33615-76-C-5079
9. PERFORMING ORGANIZATION NAME AND ADDRESS: Adaptronics, Inc. Westgate Research Park 7700 Old Springhouse Road McLean, VA 22102	10. PROGRAM ELEMENT, PROJECT, TASK AREA & WORK UNIT NUMBERS: 7351/09/53
11. CONTROLLING OFFICE NAME AND ADDRESS: Air Force Materials Laboratory (LLP) Wright-Patterson AF Base, OH 45433	12. REPORT DATE: Dec 1978
	13. NUMBER OF PAGES: 125
14. MONITORING AGENCY NAME & ADDRESS (if different from Controlling Office): 135 p.	15. SECURITY CLASS. (of this report): Unclassified
	15a. DECLASSIFICATION/DOWNGRADING SCHEDULE

16. DISTRIBUTION STATEMENT (of this Report)

Approved for public release; distribution unlimited.

17. DISTRIBUTION STATEMENT (of the abstract entered in Block 20, if different from Report)

18. SUPPLEMENTARY NOTES

Prepared in cooperation with Rockwell International Science Center.

19. KEY WORDS (Continue on reverse side if necessary and identify by block number)

Nondestructive Evaluation; Ultrasonics, Adhesive Bond Inspection; Adaptive Learning Networks; Signal Processing; Quantitative Defect Characterization

62102 F

20. ABSTRACT (Continue on reverse side if necessary and identify by block number)

This project sought to establish the feasibility of automatic detection and classification of bond line defects in multiple-layer adhesively bonded structures. Bond strength was not the issue in this work; rather, the detection and classification of a bond line flaw per layer into one of three classes - unbond, void, porosity - independent of part geometry was the main objective. Each part was scanned from one flat surface using a 0.5-inch transducer in the pulse-echo mode. A decision was rendered automatically regarding the existence

DD FORM 1 JAN 73 1473 EDITION OF 1 NOV 65 IS OBSOLETE

UNCLASSIFIED

SECURITY CLASSIFICATION OF THIS PAGE (When Data Entered)

003 350

and classification of defects in each layer for each pulse-echo return in an overall scan pattern. Results

The results show that flaws in multiple-layer structures can be found with accuracies of 91% as to defect versus non-defect discrimination, and 92% as to the correct type of defect. In this work, a false-alarm rate of 19% (non-defects called defects) and a false dismissal rate of 2% (defects called non-defects) was obtained. It is believed that the false alarm rate could be greatly reduced by use of multiple-point (contextual) information from contiguous scans.

Data recording and parameter extraction are described and the design of Adaptive Learning Networks is indicated. Recommendations are made for future work that would concentrate on providing more data for certain defect conditions, with particular emphasis on lowering the false-alarm rate so that the capabilities required by a field system are achieved. A current existing instrument is proposed that would make possible real-time inspection of bonded parts.

It has been shown that it is feasible and practical to use ultrasound to detect and classify defects and flaws in multiple-layer adhesively bonded structures, regardless of the layers in which they lie. The method is, by design, insensitive to moderate variations in transducer orientation and to construction geometry. The accuracies on a blind evaluation test compare very well with the data used to train the ALN classifier system, indicating that the system can be expected to perform comparably under future, similar NDE conditions.

FOREWORD

This is the final technical report under Contract No. F33615-76-C-5079, "Exploratory Development of Adhesive Bond Flaw Detection." The period of performance was from 1 April 1976 to 30 November 1978. The prime contractor was Adaptronics, Inc., and the subcontractor was the Science Center of Rockwell International.

Drs. Anthony N. Mucciardi and Murray H. Loew were the Adaptronics Project Manager and Principal Investigator, respectively. Drs. George A. Alers and Richard K. Elsley occupied similar roles for Rockwell. The latter wrote Section 1 of this report. Mr. David Weber of Adaptronics also provided valuable assistance in this project.

The guidance and enthusiastic support of the AFML Project Engineers -- Dr. Rod Panos, Dr. Thomas Moran, and Mr. James Holloway -- are gratefully acknowledged.

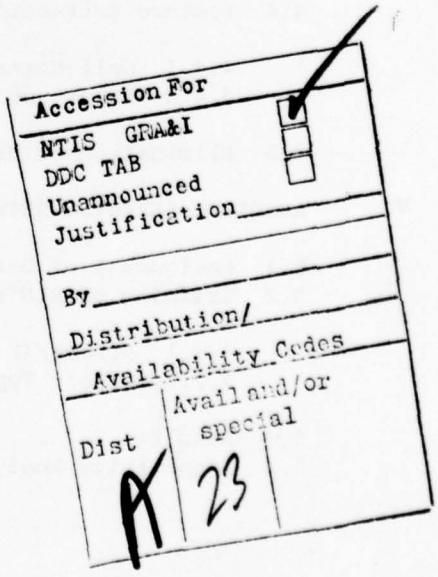

TABLE OF CONTENTS

TABLE OF CONTENTS (cont.)

LIST OF ILLUSTRATIONS

LIST OF ILLUSTRATIONS (cont.)

LIST OF ILLUSTRATIONS (cont.)

LIST OF TABLES

SECTION I

INTRODUCTION

Adhesively bonded airframe structures exhibit many improvements over conventional construction methods. Unfortunately, currently available nondestructive evaluation methods are inadequate for reliable in-service or manufacturing inspection and hence represent a serious deterrent to the exploitation of these improvements. As a step toward overcoming this problem, a joint program involving Adaptronics, Inc. and Rockwell International was initiated to incorporate new methods of signal processing and waveform analysis with quantitative ultrasonic inspection techniques to achieve a greatly improved capability for characterization of bond line defects. This characterization should lead to quantitative measurement of the size, shape, location and nature of defects in the adhesive bond line, so that full use can ultimately be made of fracture mechanics methods for predicting the remaining life in a part.

1.1 CONFIGURATION OF SAMPLES

Four different kinds of samples were provided by the sponsor (AFML) shown in Section III, Figure 2. Each consists of from one to four layers of aluminum bonded to one another, thereby providing from zero to three layers of adhesive bonds. The thickness of the aluminum plates ranged from 0.025 in. to 0.080 in. and the adhesive layers were typically 0.005 in. thick. The samples were 6 in. across and 9 in. long. Each sample had one flat surface so that inspection could be done primarily from that side. Fifteen samples of each of the four geometries were provided, 10 with documentation to explain what kind of defects had been built in, and five without documentation, for testing purposes. Several examples of each type of defect were built into each geometry or part. The five basic categories of defects provided were:

- Porosity
- Crack-like voids
- Circular voids
- Disbonds
- Bondline thickness variations

The first three types were all examples of regions of missing adhesive material. They differ in the sizes and shapes of the regions. Pores are "zero-dimensional" defects in that their dimensions are small compared to the wavelength of sound being used for inspection. Crack-like voids are one-dimensional. They are thinner than a wavelength of sound but have lengths comparable to or larger than the wavelength. Circular voids are regions both of whose dimensions are large. Disbonds are regions where adhesive is present, but for some reason, such as a layer of grease or an unremoved release film, bonding to the metal plate did not occur. Bondline thickness variations can result from insufficient or excessive pressure during bonding.

The documentation which the sponsor supplied with the samples indicated that four of the five defect types had been created successfully. Direct thickness measurements indicated that bondline thicknesses of as little as one-half of normal were present. Disbonds were successfully created by leaving release film atop the adhesive when bonding. These regions would be readily detected in a conventional C-scan.

Porosity and large (i.e., "circular") voids were prepared by removing adhesive prior to bonding. In some cases, large adhesive cutout regions entirely filled themselves during the bonding process due to the temperature and pressure used. However, in other cases, large voids were successfully obtained. These large voids were also readily detected by conventional means. The defects which most closely approached the configuration of crack-like voids are collections of small voids (or large pores) which were found strung together in a manner reminiscent of "leaves" and "branches." Figure 3 in Section III shows an x-ray picture of such a collection.

1.2 DATA ACQUISITION

The primary measurement technique used was pulse-echo (i.e., reflection) measurements made with a high frequency, broadband, unfocused, large diameter transducer. The reasons for this choice reflect the desire to include as much information as possible in the data so that the analysis could determine what types of data are useful and what types are not. The reasons for each choice are given below.

The choice of pulse-echo measurements was made for two reasons. First, the samples simulate airframe structures, which are often inspectable from only one side. Second, it is easier to unfold the data from each of the various layers when analyzing pulse-echo, as opposed to through transmission measurements, because in the pulse-echo case, not all of the received signal has passed through all layers of the sample.

The transducer used was a 15 MHz broadband unit which provided useable information from 1 MHz to 20 MHz when operated in a pulsed mode. The reason for using a high frequency broadband transducer is to inspect the sample with as wide a variety of frequencies as possible so as to find out which frequencies contain useful information.

The choice of an unfocused, large diameter (1/2 inch) transducer may seem at odds with the desire to detect and characterize small flaws. However, the purpose of these measurements is to obtain as much information as possible about the flaws. An unfocused, large diameter sound beam returns substantially more information from a layered structure such as these samples than does a focused beam. The reason this is true is that a pulse of sound can reverberate many times within the layers before returning to the transducer. The rather long duration signal which results contains precise information about the layers. However, if the sound beam is focused or is generated by a small diameter transducer, it will diverge rapidly as it reverberates within the layers and most of the reverberation information is lost. Once it has been determined which information is important, the goal of finding and characterizing small flaws can be pursued by means of focused sound beams which retain enough of the needed information.

1.3 DATA ANALYSES

The role of the subcontractor (Science Center of Rockwell International) was to generate ultrasonic data on defects contained in specimens supplied by AFML. Flexible acoustic techniques were used along with digital analysis of the experimental measurements to record data of high precision. This approach required the use of precise mechanical scanning systems to maintain accurate alignment of the specimen and transducer orientations coupled to new commercial electronic apparatus capable of providing high resolution (short time duration) ultrasonic pulses. In addition, special signal processing and display procedures were developed to ensure that the digitally recorded waveforms possess high accuracy and to provide visual representations of the data which would help in subsequent analyses.

The role of Adaptronics was to: (1) divide each recorded pulse-echo into segments related with each layer; (2) eliminate the negative effects of transducer misalignment and/or surface warpage; (3) extract features from the resultant UT waveform that are layer-specific; (4) design a classifier system -- based on Adaptive Learning Network classifiers -- that would decide if an echo from a given bondline in a multi-layered structure contained a defect and, if so, decide on the defect type; and (5) conduct a final test of the designed ALN system using parts that had not been seen before in a blind evaluation mode.

The major advantages of the approach adopted are that a pulse-echo inspection can be carried out easily in the field, standard commercial UT equipment can be used, and the designed ALN system can be implemented in a current Adaptronics NDE "smart instrument" -- ALN 4000 Process Analysis Microcomputer -- that employs microprocessor technology.

Therefore, the results of this project have demonstrated the feasibility and practicability of a field unit, based on adaptive learning networks, for multi-layered bondline inspection.

SECTION II

PROJECT OVERVIEW

2.1 PROBLEM STATEMENT AND OBJECTIVES

It has long been recognized that more efficient and effective Nondestructive Evaluation (NDE) methods are needed in order to evaluate reliably the quality of adhesive bonds between metal parts such as those used in the AFML PABST program. The objective of the work described in this report was to investigate new, quantitative nondestructive testing methods that utilize advanced waveform analysis techniques to establish a basis for inspection of adhesive bonds. The methods were to demonstrate the ability to:

- Locate and classify flaws in the bond lines of multiple-layer adhesively-bonded parts.
- Assess quantitatively the information content of parameters extracted from acoustic NDE waveforms with respect to bondline flaw geometry.
- Identify the most discriminating subset of parameters derived from acoustic NDE waveforms with respect to determining the size (area) of each of the flaws.
- Determine the sensitivity of each of the flaw models to variations of its input parameters.

Additional work included investigation of:

- Feasibility of measuring bondline thickness independently of the velocity of sound in the adhesive layer; and
- Examination of unusual ultrasonic wave interactions involving surface waves and Lamb waves in the metal adherends and guided modes in the adhesive layers.

2.2 APPROACH

The approach taken in this project is shown schematically in Figure 1. Each echo was divided into responses from each layer and a decision of "non-defect vs. defect" was rendered per layer. If the automatic system decided that a defect was present, a second decision was made regarding which of three possible defect classes was present. Thus, using this system, an operator can receive as many decisions as pulse-echoes analyzed during a scan over the part's accessible surface.

Adaptive Learning Networks (ALN's) (Ref. 1) provide the basis for the techniques developed to meet the program objectives. Because ALN's can use the data to determine which subset of candidate parameters is the most useful, a large number of such candidates may be proposed at the outset. As described in

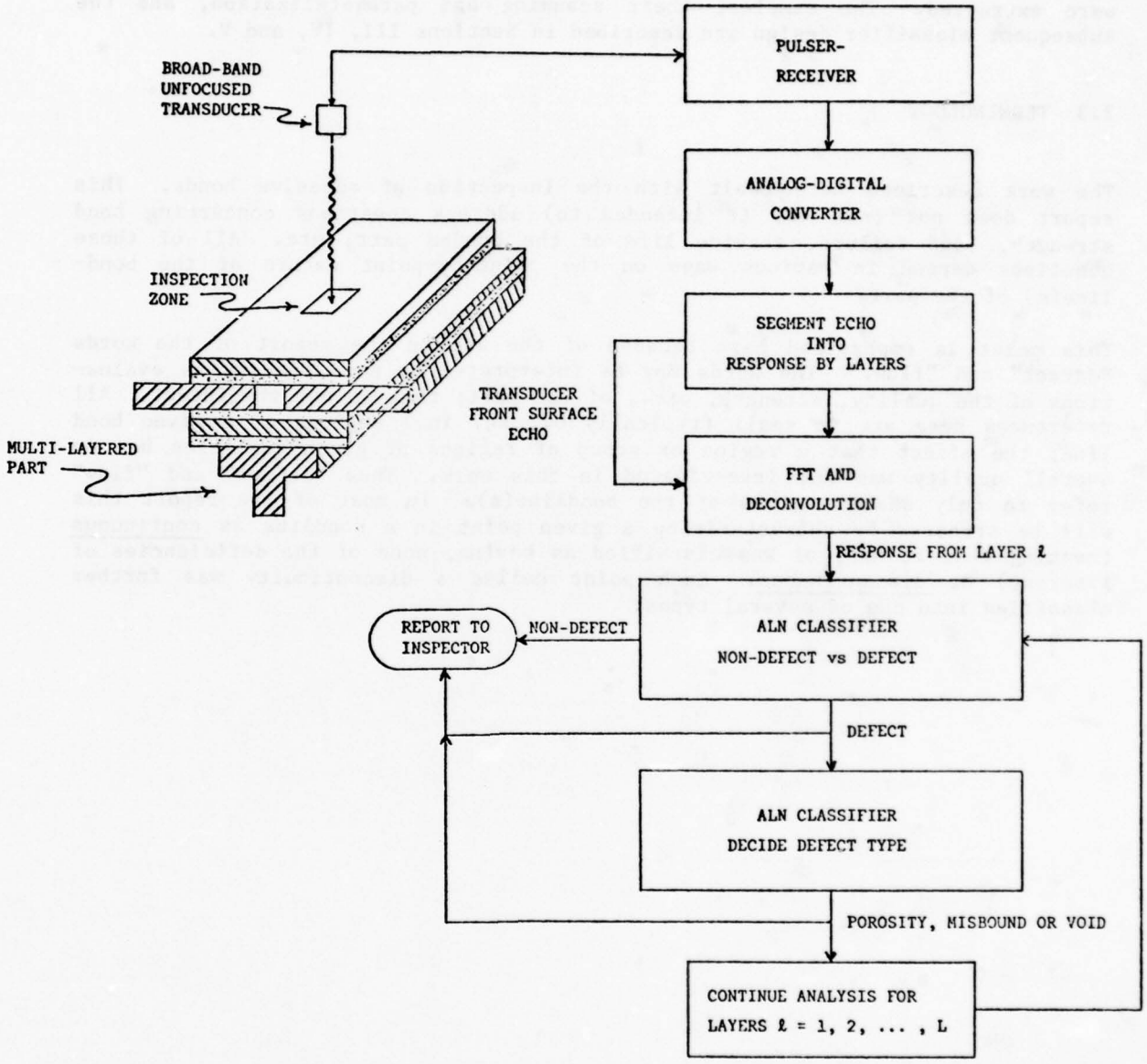

Figure 1. Overview of Automatic Multiple-Layer Bondline Inspection System

Section 5.2, an important step in the development of a classifier is the identification of a training set of samples of known classes. A training set of adhesively-bonded samples was provided by the Air Force Materials Laboratory (AFML); ultrasound scans of the samples yielded waveforms from which parameters were extracted. The samples, their scanning and parameterization, and the subsequent classifier design are described in Sections III, IV, and V.

2.3 TERMINOLOGY

The work described here dealt with the inspection of adhesive bonds. This report does not (nor was it intended to) address questions concerning bond strength, bond failure, service life of the bonded part, etc. All of those questions depend in various ways on the point-by-point nature of the bondline(s) of the part.

This point is emphasized here because of the use in the report of the words "defect" and "flaw." The words may be interpreted by some readers as evaluations of the quality, strength, etc., of the part; that is not the intent. All references here are to small (typically 0.2 sq. in.) regions of a given bond line; the effect that a region or group of regions of given qualities has on overall quality was not investigated in this work. Thus "defect" and "flaw" refer to only small regions of the bondline(s). In most of the report this will be stressed by characterizing a given point in a bondline as <u>continuous</u> (meaning that it has, or was classified as having, none of the deficiencies of interest) or <u>discontinuous</u>. Each point called a discontinuity was further classified into one of several types.

SECTION III

SAMPLE PREPARATION AND DATA COLLECTION

3.1 SAMPLES

3.1.1 Geometry and Dimensions

Four different kinds of samples were provided by AFML. Their configurations are shown in Figure 2. Each consisted of from one to four layers of aluminum glued to one another, thereby providing from zero to three layers of adhesive bonds. The aluminum plates were of various thicknesses, ranging from 0.025 in. to 0.080 in. and the adhesive layers were typically 0.005 in. thick. The samples were 6 in. across and 9 in. deep. Each sample had one flat surface. It was intended that inspection would be done primarily from the flat side, especially during in-service inspections.

Fifteen samples of each of the four geometries were provided, 10 with documentation for determining what kinds of defects were built in, and five without documentation, for testing purposes. Several examples of each type of defect (see Section 3.1.2) have been built into each geometry or part.

3.1.2 Layers and Defects

Five types of defects were identified in the contract:

- Porosities
- Cracklike voids
- Circular voids
- Disbonds
- Bondline thickness variations

The first three types are all examples of regions of missing adhesive material. They differ in the sizes and shapes of the regions. Pores are "zero" dimensional defects in that their dimensions are small compared to the wavelength of sound being used for inspection.

Crack-like voids are one-dimensional. They are thinner than a wavelength of sound but generally have lengths comparable to or larger than the wavelength. Circular voids are regions both of whose dimensions are large. Disbonds are regions in which adhesive is present but for some reason, such as a layer of grease or an unremoved release film, bonding to the metal plate did not occur.

Bondline thickness variations can result from insufficient or excessive pressure during bonding.

The documentation supplied with the samples indicated that four of the five defect types (namely, all but cracklike voids) were created successfully. That assessment was confirmed upon later destructive test (see Section 5.3).

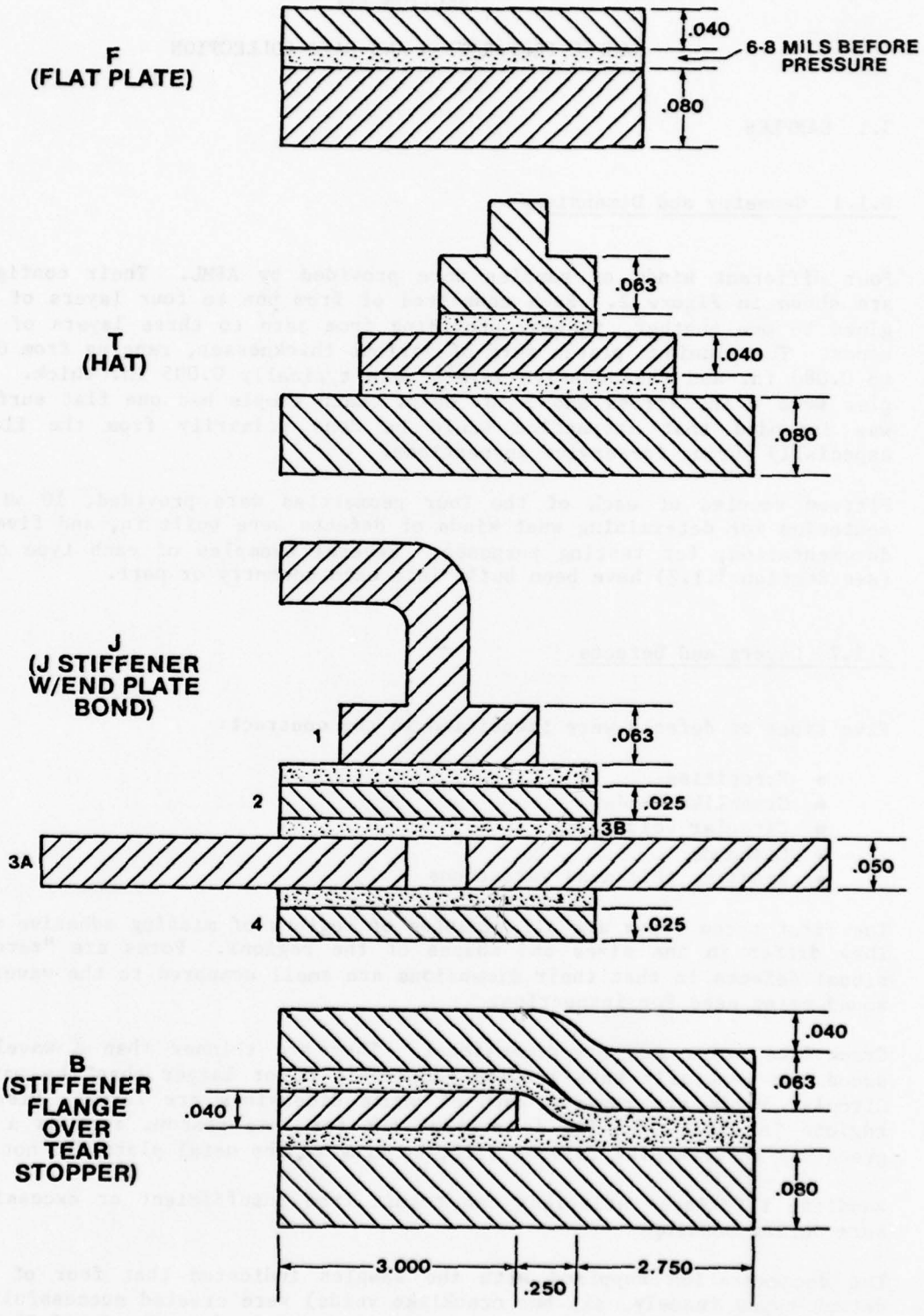

Dimensions are the metal plate thicknesses in inches.

Figure 2. Schematic Drawing of the Metal Layers in Each of the Four Specimen Types Provided.

Direct thickness measurements indicated that bondline thicknesses of as little as one-half of normal were present, but rare (see Section 5.1).

Disbonds were created successfully by leaving release film atop the adhesive when bonding. Those regions were readily detected in a conventional C-scan.

Porosity and large (i.e., "circular") voids were also supplied. In some cases regions of adhesive cutout entirely filled themselves in during bonding; however, numerous large voids remained. The large voids were also readily detected by conventional means.

The defects that most closely approached the configuration of cracklike voids were collections of small voids (or large pores) which were found strung together in a manner reminiscent of "leaves" and "branches." Figure 3 shows an X-ray picture of such a collection.

3.1.3 Documentation

The documentation that accompanied each of 40 of the AFML samples comprised an X-ray, one or more C-scans, and a set of plastic overlays (layout sheets) indicating the kinds of defects intended to be induced and the layers in which they were to appear. Examples of each are included (Figures 3, 4, and 5). The nominal locations of the defects shown on the layout sheets were plotted on the X-rays and the C-scans to estimate which of the intended defects were realized. Paths were then laid out for the ultrasound transducer to follow as it was tracked across the part. A consensus estimate of the documentation at each point of each track served as the true class label for initial classifier design. This class assignment procedure is discussed further in Section 5.1.

3.2 DATA COLLECTION

3.2.1 Apparatus

Figure 6 is a block diagram of the computer-controlled ultrasonic system which was assembled for this project. It consisted of a water tank with scanning apparatus (shown in more detail in Figure 7(a)), in which samples and transducers were located; electronics for generation and detection of ultrasound (using commercial instruments); and equipment to digitize ultrasonic waveforms for computer processing. This equipment was controlled by the subcontractor's Interpretive Signal Processor, a minicomputer-based research tool which allows the experimenter to evaluate quickly a variety of data acquisition and signal processing techniques. A more detailed description of the components of this system follows.

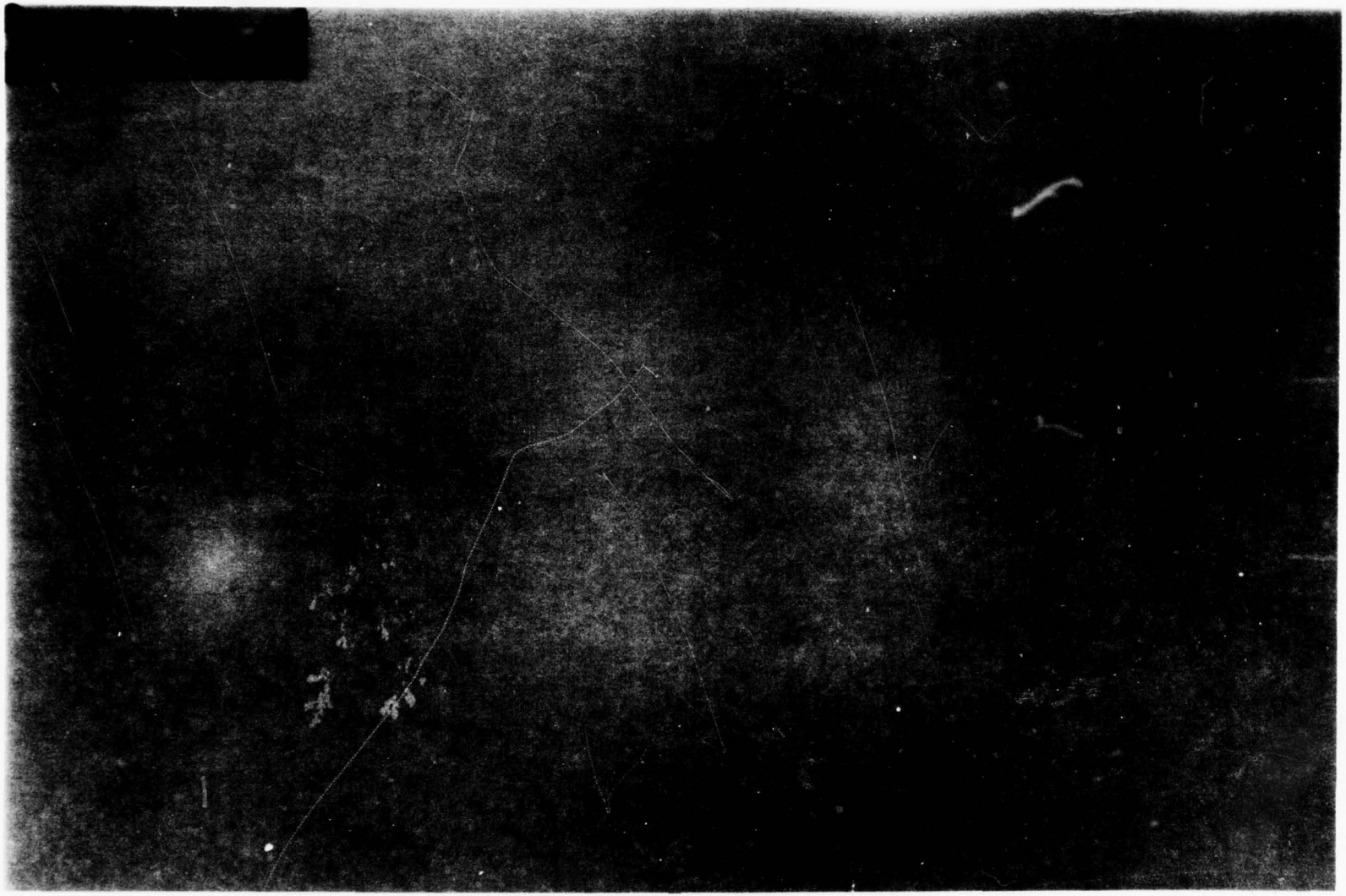

Figure 3. Print Taken from the X-ray Negative of a Sample Showing a Collection of Small Voids in the Shape of Leaves and Branches.

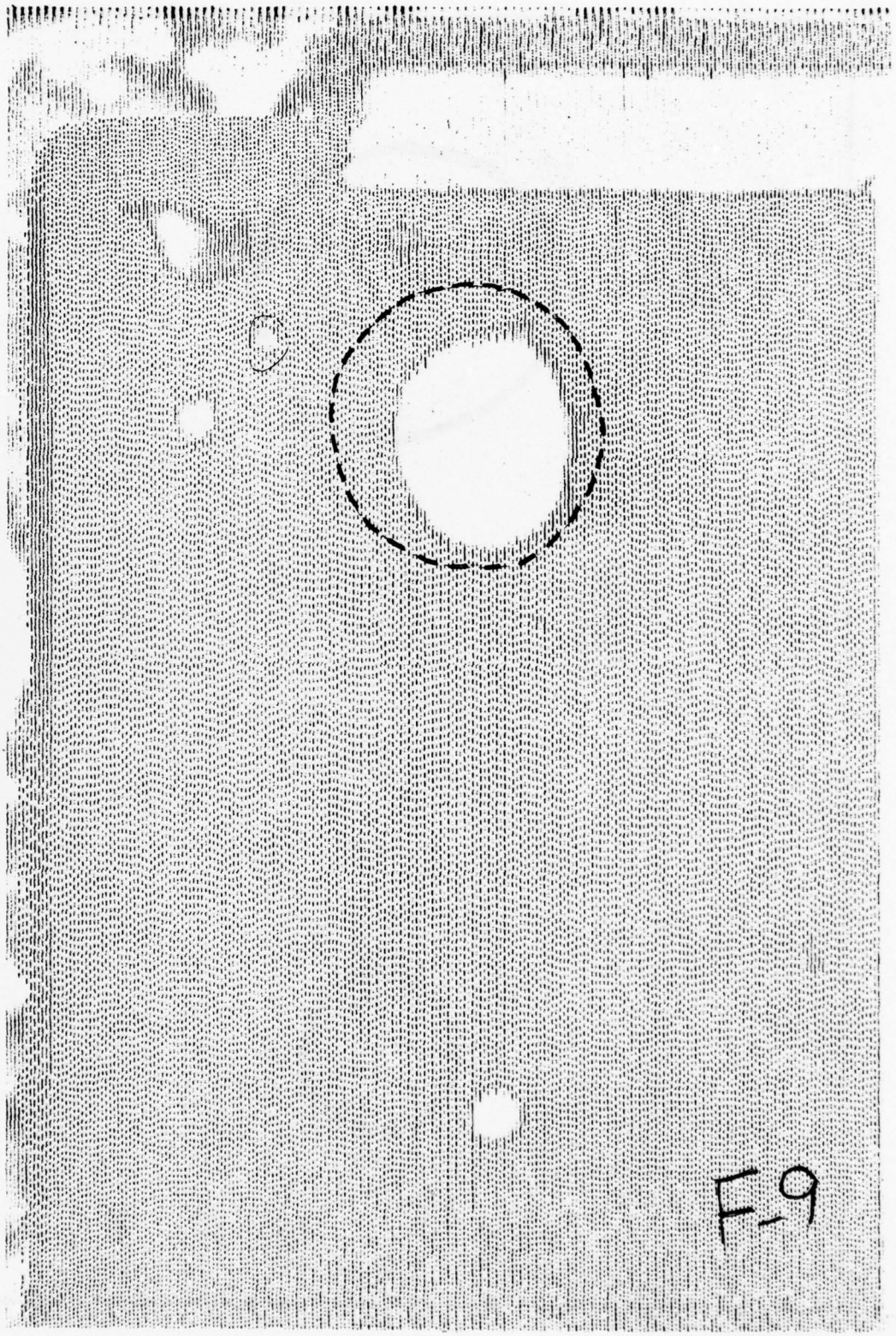

Figure 4. C-Scan of Sample F-9. Oozing in of the void region is clearly seen as compared to the original void region shown in dashes.

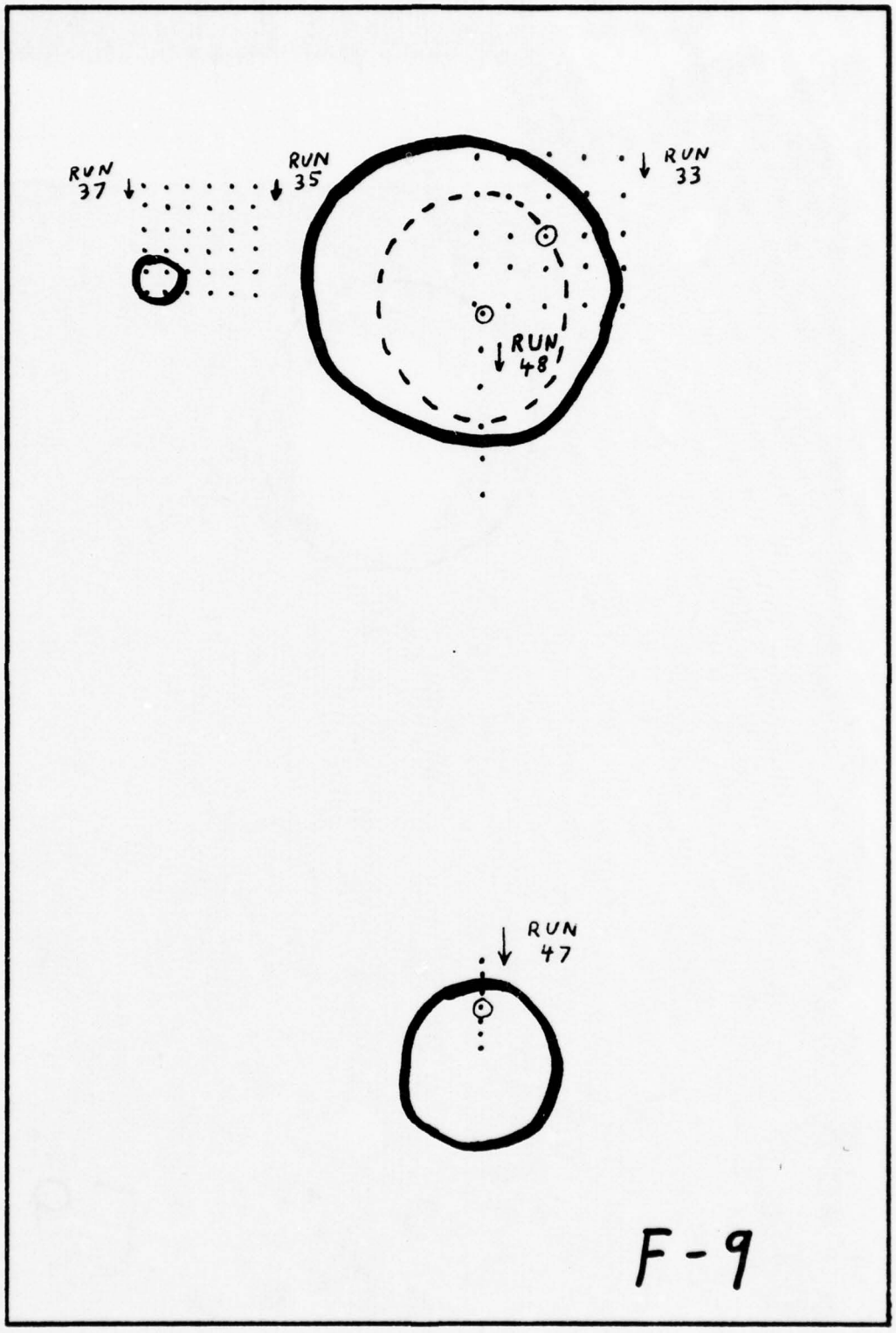

Figure 5. Layout of Scan Tracks for Sample F-9

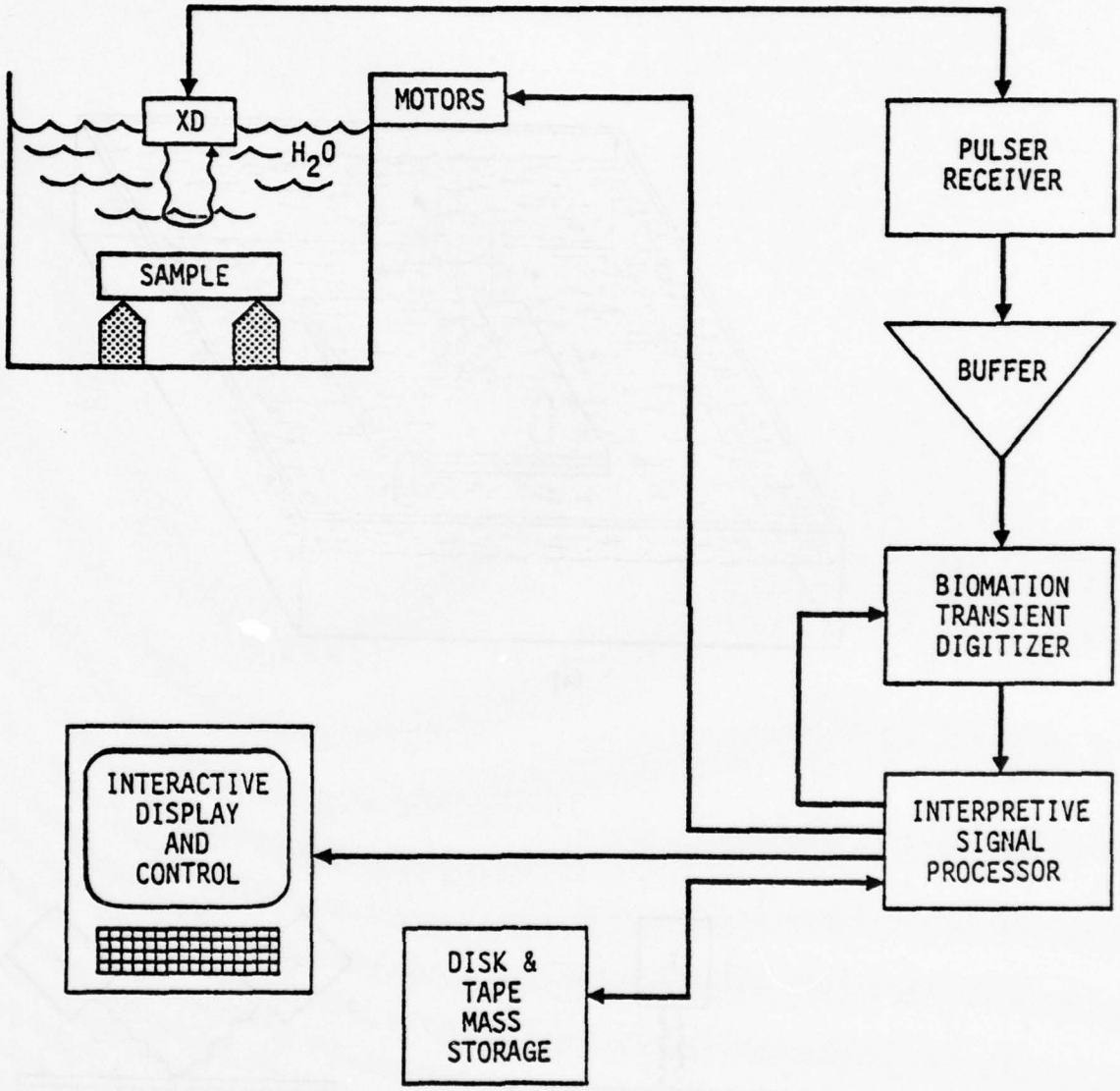

Figure 6. Block Diagram of the Ultrasonic Data Collection, Processing, and Recording System

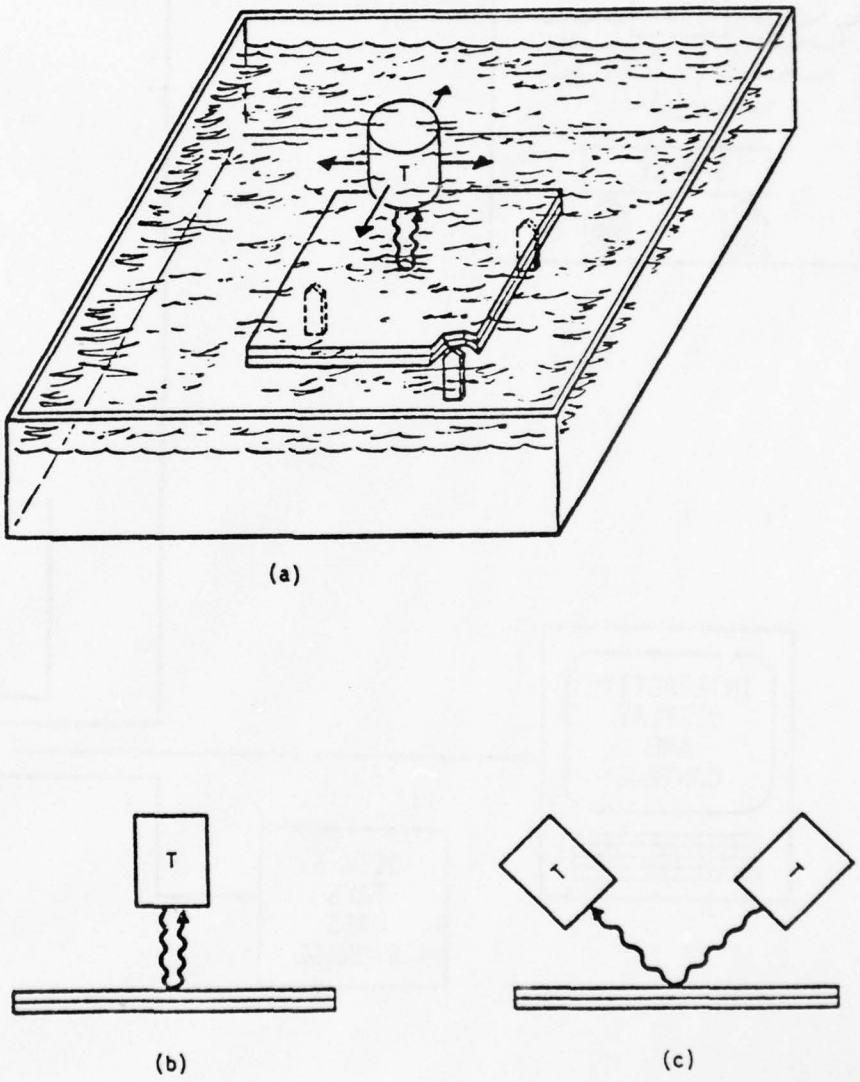

Figure 7. Configuration of Transducers and Specimens Used for the Inspections. (a) Schematic representation of water tank apparatus. (b) Normal, pulse-echo inspection technique. (c) Angle beam configuration for bond line thickness measurements.

A capacity for scanning a transducer or pair of transducers over a specimen was provided by a custom-built mechanical scanner equipped with stepping motors to drive a platform along two orthogonal axes. Electrical signals for controlling and measuring the motion of the platform could be generated manually or by the computer so that the platform could be positioned at any location over a specimen. Three mechanisms were available to control the alignment of the sound beam relative to the surface of the specimen. One adjusted the angular orientation of the transducer above the specimen support platform; the transducer was attached to a Lansing mount (Model 10.203) fixed to the scanning platform. Another adjusted the orientation of the specimen support platform; the third was the use of the pair of angle beam transducer holders described in the next paragraph. All of the scanning apparatus, including the specimen support platform, was attached to a rigid frame above a stainless steel water tank 40 cm wide x 66 cm long x 25 cm deep. This permitted an area 22 cm x 16 cm to be scanned in one pass, while the transducer-to-specimen separation could be varied from 0 to 20 cm.

A subsidiary objective of this work was to determine whether it is feasible to deduce the thickness of the adhesive bond from ultrasonic measurements alone. It was proposed that, by combining a measurement of the time for an ultrasonic wave to traverse the bond with a measurement of the physical separation of the reflections from the top and bottom boundaries of the bond when the incident ultrasonic wave was not normal to the bond plane, it would be possible to determine the thickness of the adhesive layer. A special pair of transducer holders was designed for the scanning apparatus which would support a transmitter and a receiver transducer so that their angular orientation relative to the specimen normal could be adjusted (Figure 7(c)) and so that one could be translated relative to the other by the scanning motors. This work is discussed in Appendix C.

3.2.2 Ultrasound Instrumentation and Signal Recording

The ultrasonic apparatus consists of a Reflectoscope Model UM 721 with a 50S db plug-in for applying a high voltage, short-time duration voltage pulse to a high frequency broadband transmitter-transducer and for providing at its output the amplified RF waveform of the reflected ultrasonic signal. This combination of ultrasonic test equipment was chosen because it is readily available commercially and because it generates ultrasonic signals containing a broad spectrum of frequencies with each pulse. Details of the ultrasonic signal generators, transducers, and receivers are omitted because their effects on the signal are measured and corrected in the digital analysis carried out by the computer in each case.

Digitization of the ultrasonic signals is accomplished by a Biomation 8100 transient recorder which captures the RF waveforms of the ultrasonic pulses, digitizes up to 2048 points (1001 points were used for this work) and transfers the digitized data into the computer for processing. The minicomputer upon which the Interpretive Signal Processor program system is based is a Data General Eclipse S/200 equipped with real-time displays of waveforms being processed as well as disc memory and industry-compatible 9-track magnetic tape for archival storage of data.

3.2.3 Alignment Considerations

Early in the project normal-incidence pulse-echo data for seven runs on single-adhesive-layer samples were received. Each run contained a set of time-domain waveforms, each of which was acquired at a different position on the sample under test. The sample was scanned in a 1- or 2-dimensional pattern to include the defect and a defect-free region. Analyses of the power spectra of the front-surface echoes, which should be independent of any underlying defects, revealed substantial differences within each sample. Re-examination of the scanning transducer and its mounting jig indicated that much of the variation was due to differing amounts of misalignment of the ultrasound beam and to small regions of warpage of the samples.

Figure 8 illustrates the problem. Selected points along the track taken by the scanning jig were chosen for analysis because they were expected to reveal the characteristics of the transducer and the defects. The front-surface echo starting time was approximately standardized and the power spectrum computed. Note the change in scales of the power spectrum amplitude plots (right-hand column of graphs) and the change as well in relative spectral composition. The change from the topmost to bottommost points, for example, or from the alignment point to either of the previous two, probably is due only to misalignment and, in any case, makes difficult the accurate deconvolution (see Section 4.4) of the transducer-only response from the response at a defect.

There are a number of reasons to expect that in a practical inspection system the sound beam may not always be normal to the surface of the part. These reasons include defective transducers, imprecise scanning mechanisms and part placement and unintentionally as well as intentionally curved part surfaces. This non-normal incidence results, as was evident above, in frequency-dependent destructive interference of the sound wavefronts. Another example is provided by the upper curve in Figure 9, which shows the envelope of the spectrum of a 15 MHz transducer whose sound beam has been carefully aligned to be normal to an aluminum surface by maximizing the amplitude of the top surface reflection. The second curve is the same configuration, but with the transducer translated 6 inches to one side. Because the present scanning apparatus does not maintain perfect alignment, and because the specimens are not perfectly flat, the spectrum has been changed noticeably. The lowest curve shows the spectrum which results when the transducer is realigned at the new position. It is very similar to the first spectrum.

Section 4.4 describes in detail a procedure that obviates the need for realignment of the transducer at each position.

3.2.4 Description of Data Base

Broadband normal incidence pulse-echo data were acquired for all of the discontinuities in the 40 documented samples. This provided a data base for testing the bondline characterization algorithms developed in this contract.

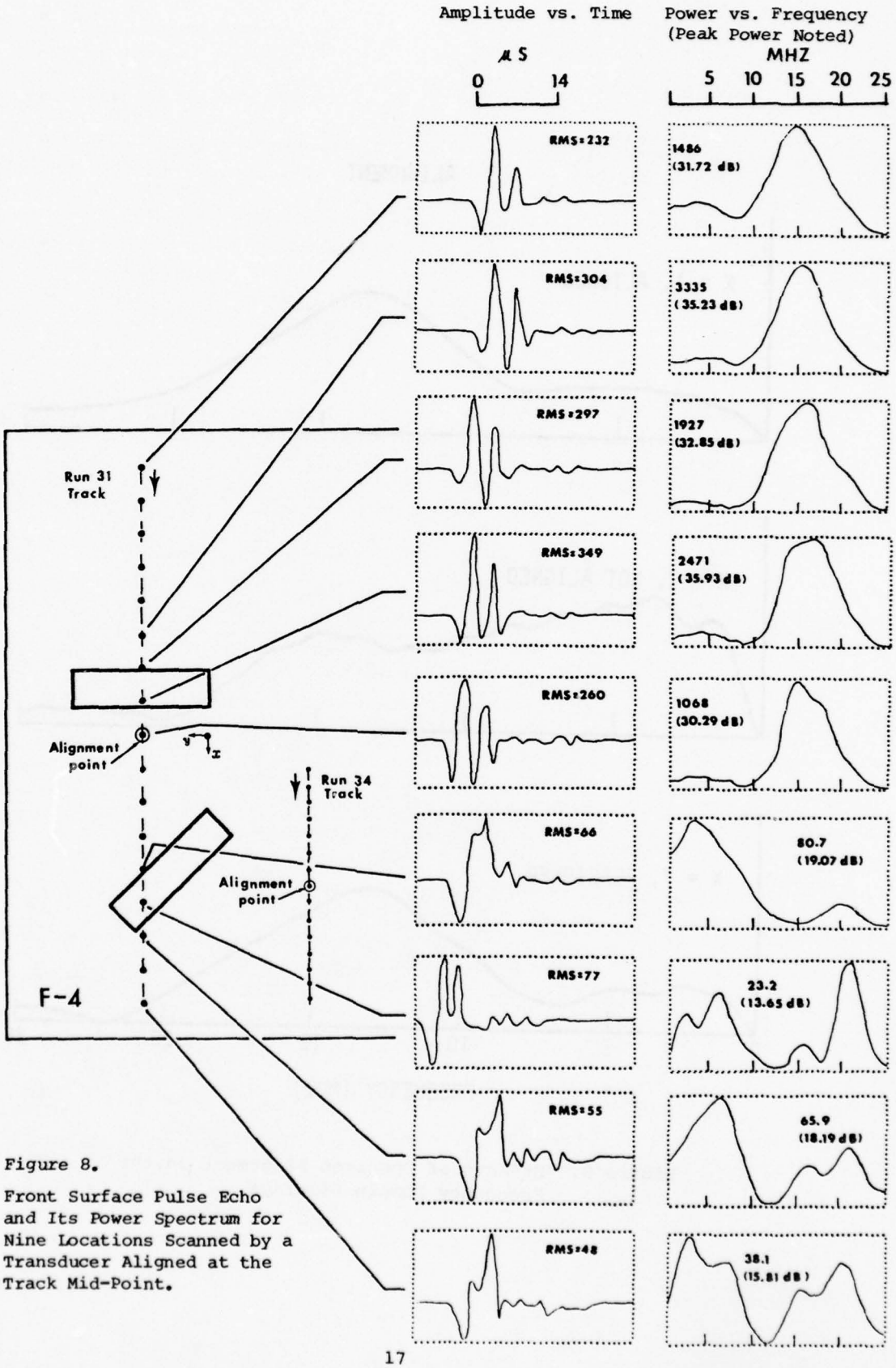

Figure 8.

Front Surface Pulse Echo and Its Power Spectrum for Nine Locations Scanned by a Transducer Aligned at the Track Mid-Point.

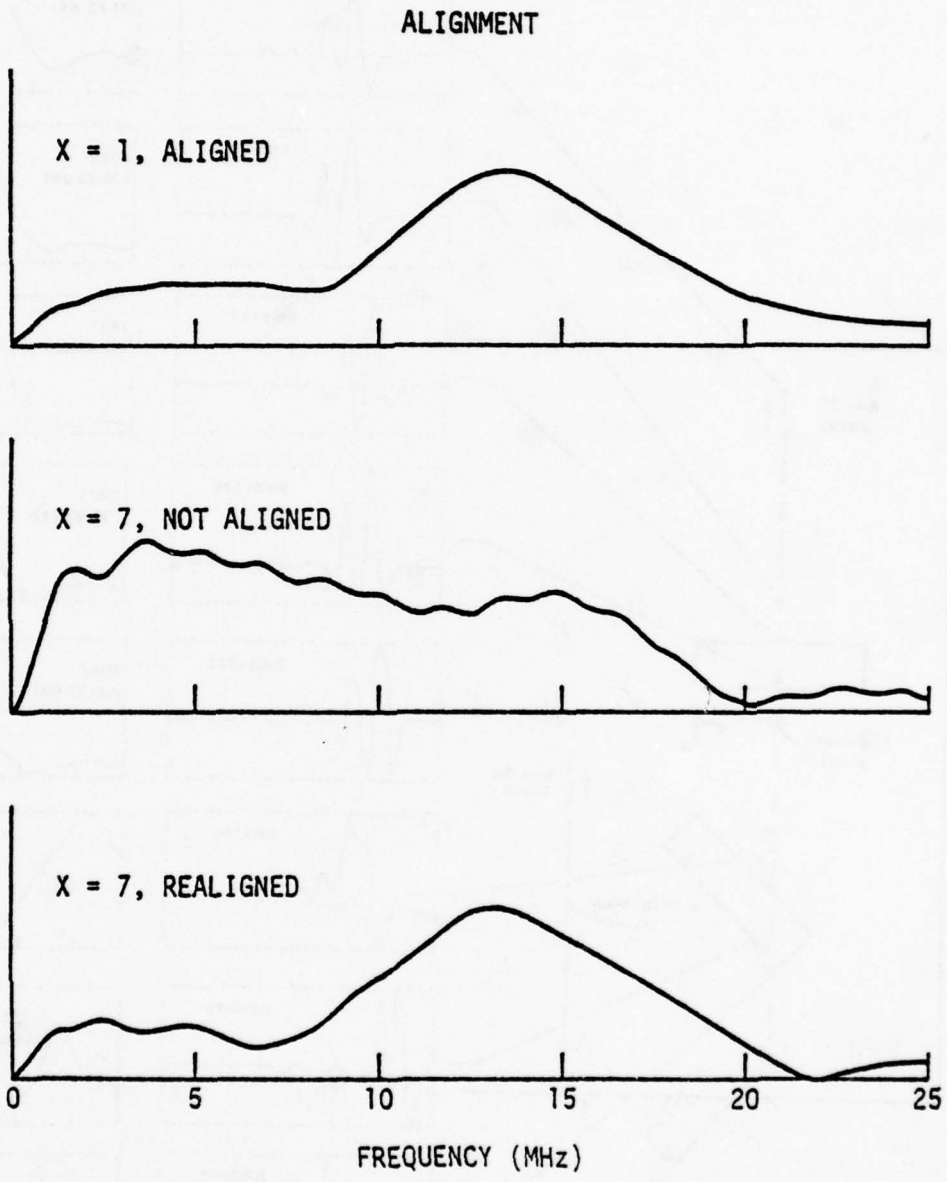

Figure 9. Effects of Specimen Alignment on the Frequency Domain Displays

The data base consists of 59 linear scans, each of which passes over one or two of the documented defects. Each scan consists of, typically, 5 to 10 RF waveforms acquired at equally-spaced intervals along a line parallel to either the X or Y axis of the part. The number of waveforms per scan was kept to a minimum consistent with the goal of providing data within, on the edge of, and outside of each discontinuity. The extent to which that goal was reached is described in Section 5.1, which discusses the assignment of a category to each waveform-layer combination.

Each waveform consists of 1,001 samples taken at 0.02μs intervals, for a total of 20μs. This therefore provides for frequency analysis from 50 kHz to 25 MHz. The ultrasonic transducer used provides useful data from about 1 to 20 MHz. This data base, containing one megabyte of data, was recorded on industry compatible 800 BPI EBCDIC 9-track magnetic tape.

Graphic documentation, consisting of two graphs of each waveform (a total of about 1,000 graphs) has also been generated. Figure 10 shows an example of this documentation which was provided for each point on the specimen.

Appendix A contains detailed descriptions of the scan paths, coordinate and labeling systems, and data-transmission formats.

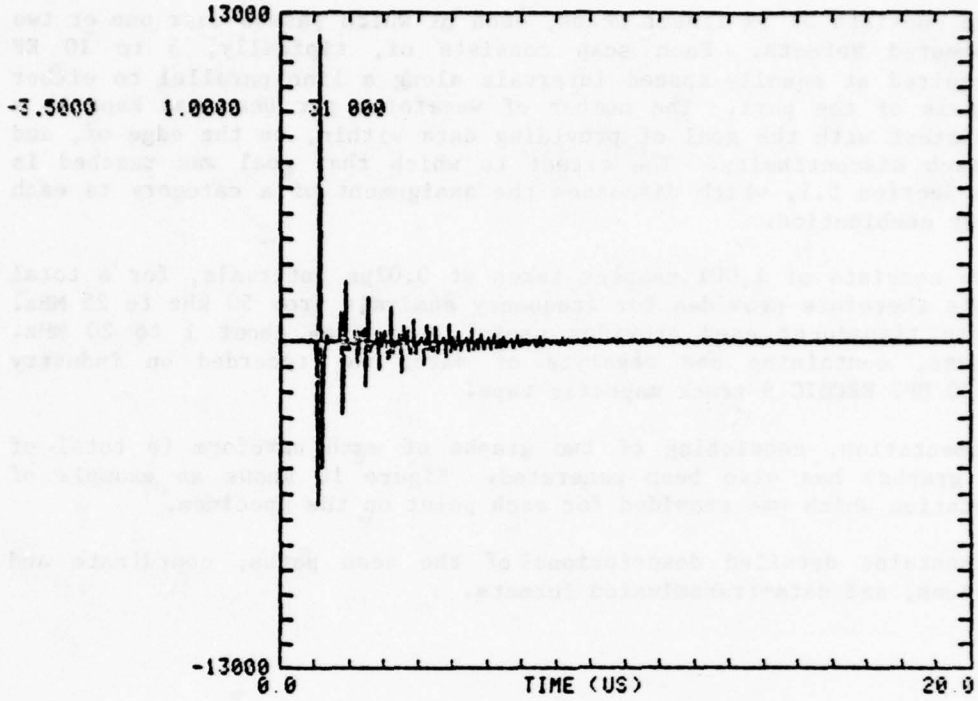

(a)

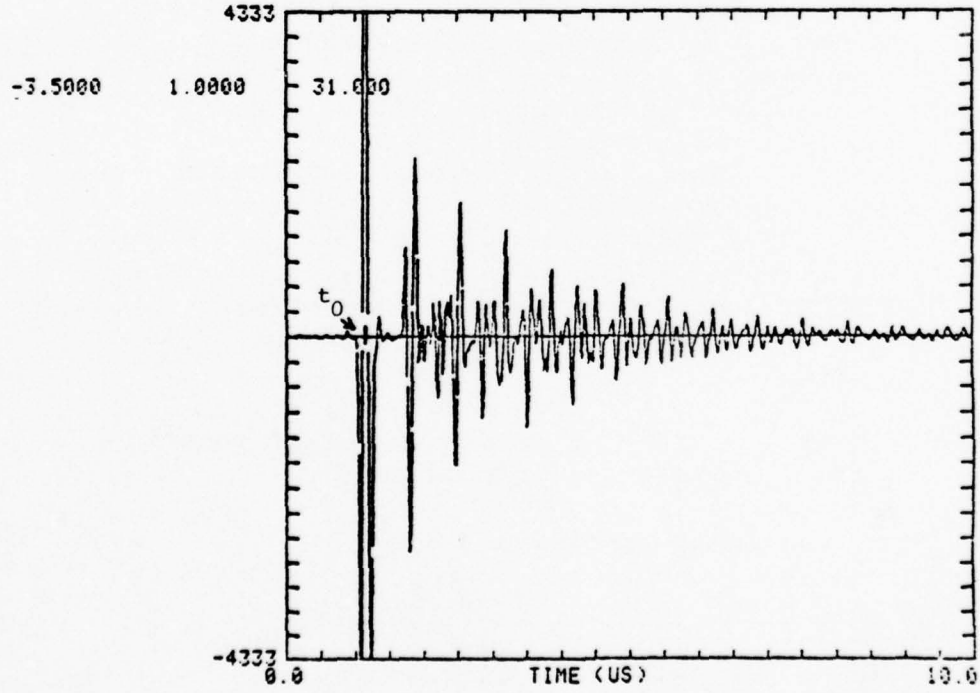

(b)

Figure 10. Typical Amplitude vs. Time Waveform Graphs Produced by the Computer from the Digital Data Recorded on Run 31 at Position X=3.5, Y=1. (a) General view of entire waveform. (b) High gain, detailed view of the early part of the waveform.

SECTION IV

SIGNAL PREPROCESSING AND EXTRACTION OF CANDIDATE FEATURES

4.1 OBJECTIVES

The problem addressed in this work was to identify consistently the types and sizes of bondline discontinuities lying at various depths in a multi-layered part, using a variety of real transducers that were only approximately normal to the surface of the part. Useful methods for nondestructive examination must be capable of compensation for or removing the effects of the conditions unique to a given inspection situation. Techniques that perform the compensation/normalization operations are described later in this section; they involve both time- and frequency-domain representations and result in the generation of waveforms that are independent of the principal inspection variables.

The next step in modeling is feature extraction. Features are characterizations of the defect classes of interest taken from whatever overall representations (e.g., waveforms) are available. Features should be capable of straightforward and reliable extraction (i.e., computation), be independent of each other, and, where possible, embody insights into the physical nature of the problem. The features used in the bondline characterization models are described in the following sections. Physical significance of certain features is noted during the discussions of those features.

4.2 TIME SIGNAL SEGMENTATION

The multi-adhesive layer nature of the samples and the fact that discontinuities can occur in one or more layers beneath any surface location on the samples mean that it is desirable to extract some features from the recorded time waveforms that are layer-specific. The goal is to make all defects of a given type look alike, regardless of the adhesive layers in which they occur. If that ideal can be realized, the problem will be simplified because recognition of a defect type will be independent of its location and depth. An effective approach is to divide the time waveform into segments, each of which contains information about a given adhesive layer.

The process of segmenting the signals takes advantage of knowledge of the construction of the samples -- knowledge that is likely to be available in nondestructive testing of actual adhesively-bonded structures. The four sample geometries -- F, B, T, and J (shown in Figure 2) -- were illuminated on their flat sides by the ultrasound transducer. (The F samples' flat sides were defined to be the 0.080 in. [80-mil] aluminum plates.) Thus, the F, B, and T samples all presented to the transducer the sequence of layers 80-mil aluminum, 5-to-8-mil adhesive, 40-mil aluminum, in that order; in parts of the B samples and all of the T samples, the additional layers were another 5-to-8-mil adhesive and a 63-mil aluminum. The J samples' layers (Figure 2) are of different thicknesses from those of the other three geometries; this creates a special case for the segmentation algorithm.

Because the incident waves are normal to the surface, the travel time of the ultrasound in the aluminum and adhesive layers of the samples can be computed readily. Using longitudinal velocities of 6.4 km/s and 1.17 km/s in aluminum and adhesive, respectively, we may construct the following table of one-way travel times in aluminum plates of various thicknesses:

Thickness, mils	Time, μs
25	0.1
40	0.16
50	0.2
63	0.25
80	0.32

The 5-to-8-mil adhesive has a one-way travel time of 0.11 to 0.17 μs.

The front-surface echo, always the largest peak in the time waveform (see Figure 10), provides a reference point t_0 for delineation of the layers of the sample. If, for example, the first layer of aluminum is 80 mils thick, an echo from its back surface should arrive 0.64 μs after the front-surface echo. The time waveform from inspection of an F sample (Figure 10) does, in fact, have its second peak at 0.64 μs after the front-surface echo. An echo from the back surface of the adhesive should arrive between 0.22 and 0.34 μs after the echo from the first plate, but is difficult to observe because of the persistence of of the earlier waveform. One may, nevertheless, establish a time window beginning at $t_0 + 0.64$ and ending somewhere between $t_0 + 0.88$ and $t_0 + 0.96$. The exact point is determined by an algorithm that considers phase relationships and durations relative to the front-surface echo. Figure 11 is another example of the identification of segments of a time waveform.

An ideal impulse is of zero duration. The real pulse provided by the transducer has finite duration and decays exponentially. This means that the start of an echo occurring too closely in time to a previous one will be difficult to discern. Such a situation always occurs with layers of adhesive, and occurs with the first layer of aluminum in the case only of the J samples. That first layer is less than one-third the thickness of the first metal layer of samples of the other geometries and its 0.2 μs round trip travel tim places it in the category of a layer of adhesive insofar as resolution of its back surface is concerned. This inherent limitation makes the use of phase relationships to assign exact endpoints very difficult and this is the reason that a special case exists for J samples.

The segmentation algorithms have been tested and evaluated by comparing their endpoint decisions to manually assigned endpoints. The high rate of agreement on a sample set of waveforms -- even with multiple-adhesive-layer samples -- gives great confidence that the algorithms are accurate.

Each waveform of the type shown (Figure 10) was submitted to the segmentation procedure. The resulting segments then were used in both the time- and frequency-domain feature extraction steps.

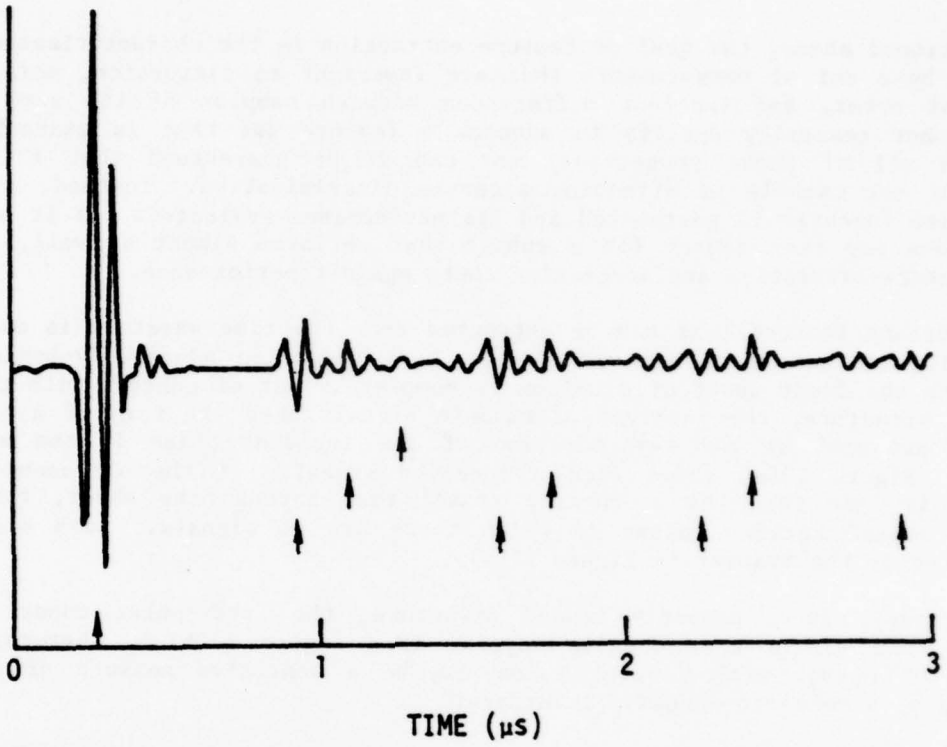

Level of Arrows	Meaning
First (Lowest)	Front surface echo
Second	Train of pulses traveling in the front plate, reflecting back and forth between the adhesive layer and front surface
Third	Set of signals arriving 165 ns after each member of the previous set; these may be pulses that have made one or more traverses of the adhesive layer and returned
Fourth (Highest)	Signal that is either a pulse that has passed through the back aluminum plate and returned, or pulse that has made several bounces in the adhesive layer

Figure 11. Time Domain Echoes from an Aluminum-Adhesive-Aluminum Sandwich (Sample F12)

4.3 FEATURE EXTRACTION: TIME DOMAIN

As mentioned above, the goal of feature extraction is the characterization of a sample by a set of measurements that are invariant to distortion, noise, measurement error, and inherent differences between samples of the same class. One cannot generally specify in advance a feature set that is guaranteed to possess all of those properties, nor can it be guaranteed that it is the smallest set capable of effecting accurate discrimination. Instead, a set of candidate features is postulated and its performance evaluated. If it performs well, one may then search for a subset that performs almost as well, trading off feature-extraction and processing costs against performance.

An important feature that can be extracted from the time waveform is useful in detecting regions of missing adhesive. In a defective adhesively-bonded part in which the front sheet of aluminum is completely out of contact with the rest of the structure, the received ultrasonic signal takes the form of a train of pulses produced by the reverberation of the incident pulse in the aluminum sheet. Figure 12(a) shows such a received signal. If the ultrasonic pulse length is less than the round-trip travel time through the sheet, there are "quiet zones" between pulses in which there are no signals. Such a zone is indicated by the bracket in Figure 12(a).

By contrast, in a properly bonded structure, the inter-pulse zones contain echoes from within the adhesive layer. (See Figure 12(b).) Therefore, the amount of energy within quiet zones can be a sensitive measure of lack of bonding at a metal-to-adhesive interface.

Figure 13(a) shows the normalized energy in the quiet zone shown in Figure 12 as the transducer was scanned over a 5 x 5 grid of positions in the vicinity of an adhesive cutout region of sample F9. A map of the region scanned is shown in Figure 13(b). Dots represent the transducer positions and the cutout region (shaded) is sketched in as it appears on the X-ray documentation. The ultrasound beam diameter is 1/2" (2 grid spaces). Note that the cutout is detectable even when it occupies only a fraction of the area of the beam. Therefore, a coarse raster of scan positions would still be able to find these void regions in a part. (See Section 5.1 for further discussion of that point.)

Feature x_{15} was defined as

$$x_{15} = \frac{\text{RMS value of segment}}{\text{RMS value of front-surface waveform}} + \text{depth correction}$$

and captures the quiet-zone information. Signals from second- and third-layer regions will be generally smaller than signals from the first layer because of the attenuation introduced by the intervening layers. The attenutation factor was estimated by fitting an exponential, ke^{d}, to data taken from layers at different depths known to have no discontinuities. The resulting equation was:

$$\hat{I}_N = 0.5012 \exp(-0.0259\ d)$$

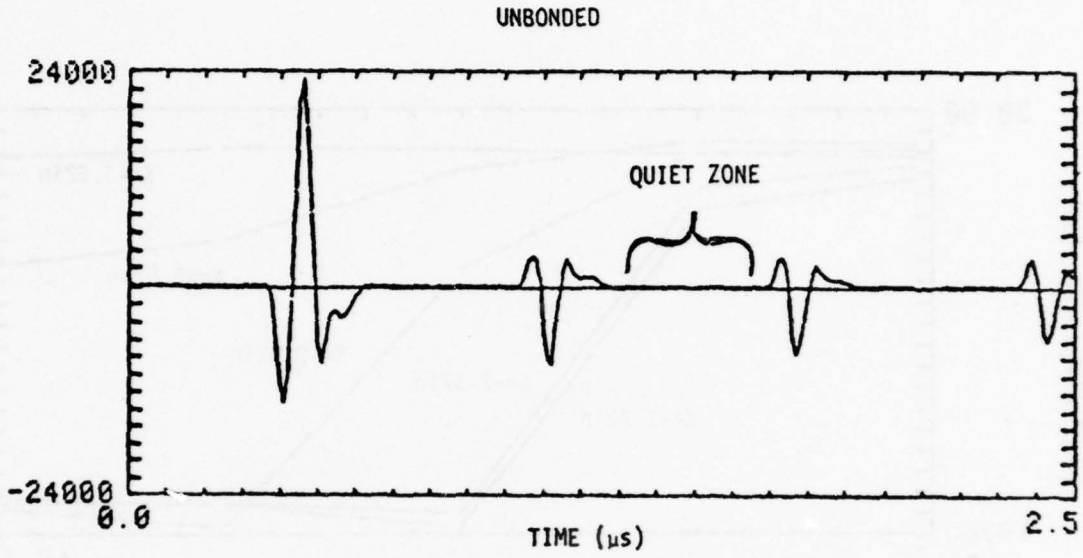

(a)

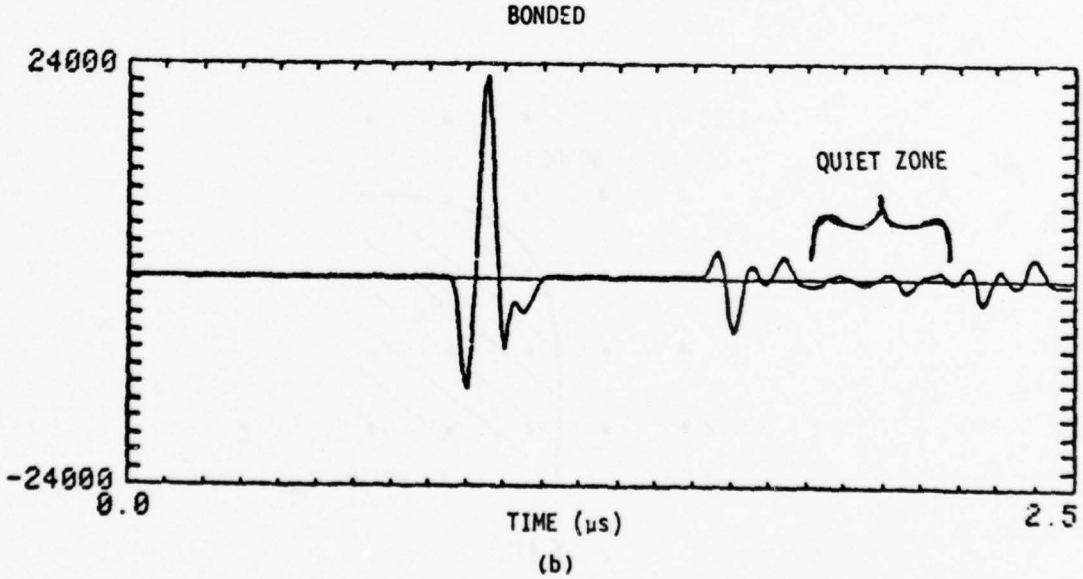

(b)

Figure 12. Examples of Quiet Zone in Unbonded and Bonded Specimens

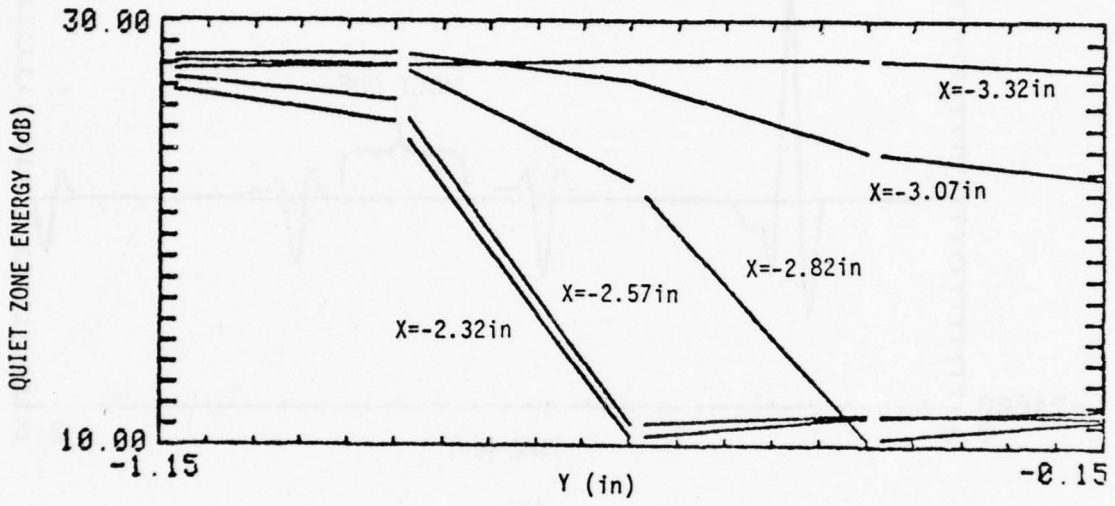

(a)

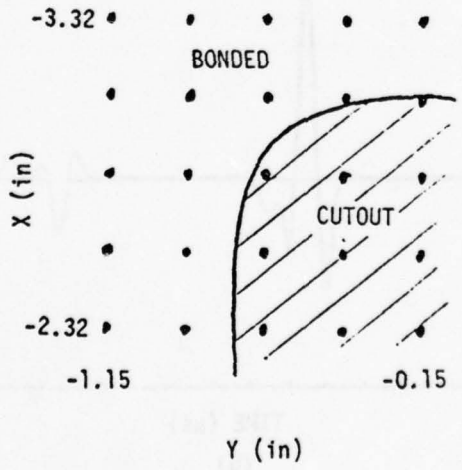

(b)

Figure 13. Variation of Energy in Quiet Zone with Bond Integrity

where $\hat{I}_N$ is the estimated intensity of the reflected signal and d is the layer depth in mils (thousandths of an inch). A correction factor was thus computed for each layer of each of the geometries as $1-\hat{I}_N$ and applied to each measured RMS ratio.

4.4 FEATURE EXTRACTION: FREQUENCY DOMAIN

4.4.1 Self-Normalization and Deconvolution

A self-normalization process was devised in this project in an attempt to remove the effects of intervening layers from the time signal that represented a given layer. This was achieved by successive deconvolution. Thus, the front-surface signal (that characterizes the transducer) is deconvolved from the raw first-adhesive signal to yield a time signal that is characteristic of that adhesive only. (The assumption is employed that the aluminum contributes nothing to the signal; this is reasonable both from theoretical arguments [small grain structure of aluminum] and from actual scans of plain aluminum sheets.) Then the raw first-adhesive time signal (that contains information not only about the first adhesive, but also about the transducer) is deconvolved from the time segment of the second adhesive, and so on, with each layer's signal being deconvolved from the signal from the next deeper layer. The theory of deconvolution is well documented (References 2 and 3 are good examples), and we note here only that to deconvolve signal A from signal B is to find the inverse Fourier transform of the ratio of the Fourier transform of B to the Fourier transform of A. Similarly, the power spectrum of the deconvolved signal is the ratio of the power spectrum of B to the power spectrum of A.

The time-waveform segments described in Section 4.2 were used in the deconvolution step to yield power spectra that were characteristic just of the bond lines. Candidate features were then extracted from the layer-specific spectra.

4.4.2 Layer-Specific Features

The following features were extracted from the quotient power spectrum for each segment.

Let $H(\omega_i)$ be the value of the power spectrum at frequency ω_i and

$$H_T = \sum_{i=1}^{N} H(\omega_i),$$

where N is the number of points in each spectrum (typically 32).

Then the first 12 features are:

x_1 = the location of the first point in $H(\omega)$ such that:

$$\sum_{i=1}^{x_1} H(\omega_i) \geq 0.1\ H_T$$

i.e., the 10-percent point.

Similarly:

x_2 = the 25-percent point

x_3 = the 50-percent point

x_4 = the 75-percent point

x_5 = the 90-percent point

Also:

$$x_6 = \frac{1}{H_T} \sum_{i=1}^{N} \omega_i H(\omega_i) \qquad \text{(first moment)}$$

$$x_7 = \frac{1}{H_T} \sum_{i=1}^{N} \omega_i^2 H(\omega_i) \qquad \text{(second moment)}$$

$$x_8 = H_T$$

$$x_9 = \frac{1}{H_T} \sum_{i=1}^{8} H(\omega_i)$$

$$x_{10} = \frac{1}{H_T} \sum_{i=9}^{16} H(\omega_i)$$

$$x_{11} = \frac{1}{H_T} \sum_{i=17}^{24} H(\omega_i)$$

$$x_{12} = \frac{1}{H_T} \sum_{i=25}^{32} H(\omega_i)$$

Thus, x_9 is the proportion of power in the quotient spectrum between 0 and 6.25 MHz, x_{10} the proportion between 6.25 MHz and 12.5 MHz, x_{11} the proportion between 12.5 MHz and 18.75 MHz, and x_{12} the proportion between 18.75 MHz and 25 MHz, the Nyquist frequency. All limits of summation are shown for 32-point segment spectra, the most common case. The four bins provide additional shape information for the spectrum.

Additionally:

x_{13} = location in frequency of the peak of the quotient spectrum

$$x_{14} = \frac{\sum_{i=x_{13}+1}^{N} H(\omega_i)}{\sum_{i=1}^{x_{13}-1} H(\omega_i)}$$

Features x_1-x_5 (percentage points), and x_9-x_{14} (bins and high/low ratio) all describe shape characteristics of a power spectrum. Subtle changes in spectral shape that are induced by discontinuities in an adhesive layer can be detected by changes in one or more of the shape features. Figure 14 provides a graphical interpretation of those features.

Feature x_{15} was described in Section 4.3 above.

It is likely that the entire 1,001-point waveform representative of the whole adhesive sandwich (and described in Section 3.2.4) also will contain useful information. To capture this, while retaining transducer independence and minimizing computational load, the power spectrum of that entire waveform (denoted $E(\omega_i)$) was computed and certain features were extracted from it. The ratios of those features to the same features extracted from the spectra of the front-surface waveforms provided eight additional features. Denoting the front-surface spectra $F(\omega_i)$ we define

$$x_{16} = \frac{\text{10-percent point of } E(\omega)}{\text{10-percent point of } F(\omega)}$$

where the percentage points are defined individually as for x_1.

Similarly:

x_{17} = ratio of 25-percent points

x_{18} = ratio of 50-percent points

x_{19} = ratio of 75-percent points

x_{20} = ratio of 90-percent points.

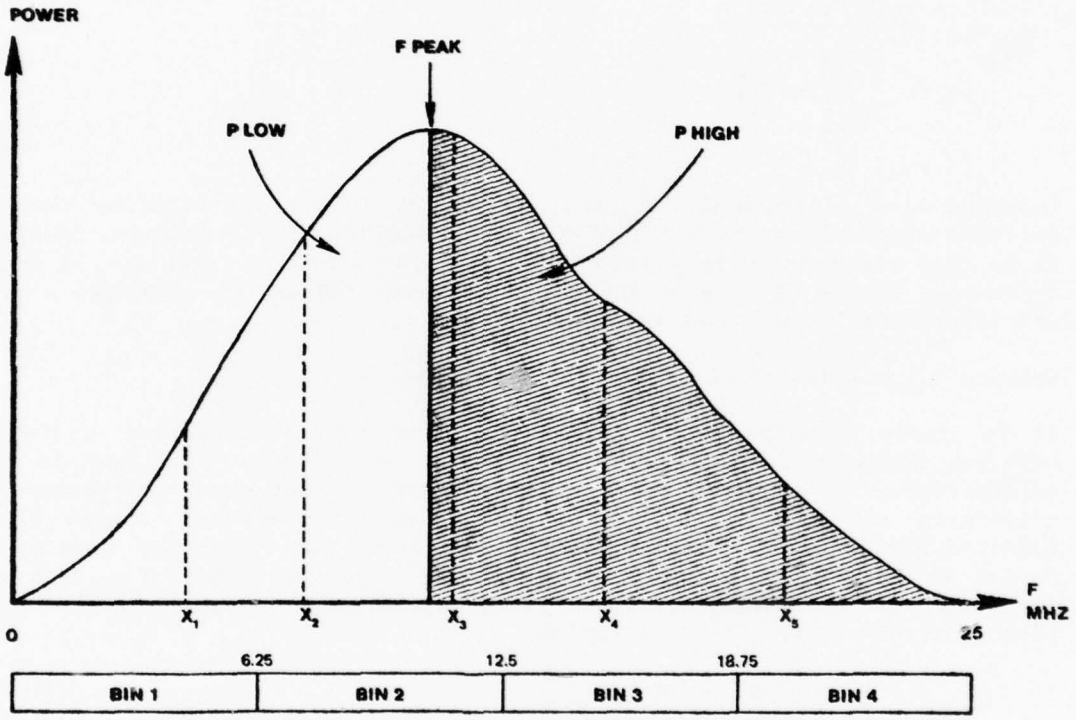

Figure 14. Definitions of Selected Spectral Shape Features

Also,

x_{21} = ratio of first moments, defined individually as for x_6

x_{22} = ratio of second moments, defined individually as for x_7

x_{23} = ratio of sums, defined individually as for x_8

4.5 ELIMINATION OF HIGHLY CORRELATED FEATURES

The set of 23 candidate features defined in the previous sections and extracted from each of the 1124 bondline locations was examined for multiple correlations. Groups of highly correlated variables each may be represented by just one of their respective number, with the benefits of tighter estimates of model coefficients, reduced computational load, and reduced sensitivity of model structure to particular sets of sample data.

The reduced set, which was used as the candidate set in all of the modeling runs described in later sections, was:

x_2, x_7, x_8, x_{10}, x_{11}, x_{13}, x_{14}, x_{15}, x_{16}, x_{17}, x_{18}, x_{19}, x_{21}, x_{22}, x_{23}.

Not all of the 15 variables listed above were required by the ALN models; a different subset was selected by each model as part of the modeling process. Each ALN classifier's data requirements are detailed in the next few sections.

SECTION V

ADAPTIVE LEARNING NETWORK SYNTHESIS FOR DEFECT CLASSIFICATION

5.1 ASSIGNMENT OF DEFECT TYPES FOR DOCUMENTED SAMPLES

As mentioned in Section 3.1.3, the transducer paths chosen for scanning the samples were intended to include the full range of types of bondline discontinuities, as inferred from the documentation. The inexact nature of the bonding/testing process evident in the documentation gave rise to a number of ambiguities, categorized as follows.

1. Intended discontinuity partially or completely missing

   The layout sheet (see, e.g., Figure 5) and a photograph of the metal plates made before bonding indicate what kinds of defects were desired at various locations on each sample. In some cases of intended adhesive cutout, for example, the adhesive surrounding the region of cutout oozed into the void when the bond was made. The extent to which the void was filled could not always be determined accurately from the X-ray and C-scan. Thus a transducer track that was believed to have generated a certain number of points from a region of cutout may have yielded fewer; that fact would have been unknown until much later in the course of work, when some of the samples were tested destructively. Variable bondline thickness (VBT) was a class of imperfection that appeared to have been created only rarely. Visual inspection of the perimeter of the bondline at the edges of the parts often revealed no evidence of VBT where it was claimed; X-rays and C-scans, although used primarily to detect rather than reject VBT, did so infrequently where expected.

2. Unintended discontinuity present

   Many regions of porosity and microporosity that were present upon destructive examination (and some of which in retrospect could be observed on the X-rays) were not apparent in the original documentation.

3. Region of discontinuity too small or incompletely scanned

   The field of view of the transducer had an area of approximately 0.2 sq. in. Many of the regions of discontinuity were either smaller than that (e.g., some pieces of release film), not contiguous over an area that large (e.g., porosities), or not close enough to the transducer track to fall fully within its field of view.

The first two ambiguity types resulted in some incorrect assignments of class labels to points along transducer tracks. About half of those errors were corrected when some samples were split apart and the adhesive layers examined as part of that destructive testing. It was then possible to compare assigned classes to those deduced from examination. ("Deduced" because the splitting did distort the adhesive in some samples; it was usually possible to decide whether an observed discontinuity had been present before splitting.)

The third ambiguity type poses a different kind of problem. In that case the signal received by the transducer represents -- for a single layer, i.e., after segmentation -- more than one category of bond. If, for example, the transducer were centered above the actual edge of an adhesive cutout in a given layer, the response from that layer at that point on the transducer track would be due partly to a continuous bond and partly to a discontinuous one. The resolution of the transducer guarantees the occurrence of that kind of a response. The response clearly is not a good representation of either category, yet cannot be ignored because of the large number of responses of this mixed kind in the data base. The ALN design (training) procedure (described in the next section) requires a set of unambiguously-labeled examples of each category of bondline that represents the variety of signals expected.

To accommodate this kind of ambiguity a new category was defined: transition. It was assigned whenever the transducer was positioned so that its (segmented) response from a given layer represented more than one kind of bondline condition. Examination of the split-apart samples led to reassignment of the transition label in some cases, just as was done for the first two types of ambiguities. Of the 1124 observations, 620 were verified by inspection of photographs of the split-apart samples.

Table 1 indicates the final number of observations available for each type of bondline category (i.e., after all ambiguities had been resolved to the extent permitted by documentation and examination) and for each layer of the multilayer samples. The subscript denotes the layer, with 1 used for the layer closest to the flat side. The table also defines the abbreviations used for bond line conditions.

5.2 TRAINING OF ALN's

Nonlinear combinations of the features described above were used to discriminate successfully among the bondline categories. Adaptive Learning Networks automatically construct from the data a polynomial, that is, that nonlinear function. Given a set of observations, the procedure finds the smallest set of features necessary for accurate discrimination, and measures accuracy with a set of data that was not used in the design stage.

A two-step approach was used for this problem: first, determine whether a given observation of the bondline was continuous, discontinuous, or transition; second, if it was classified as discontinuous, determine the type of discontinuity. Despite the assignment of the partial caul pressure label (supposedly representing variable bondline thickness) to 36 samples as shown in Table 1, sufficient doubt remained about the success of achieving VBT during sample preparation that the PCP/VBT set of observations was deleted from the data set before ALN training began.

TABLE 1

OBSERVATIONS FROM DOCUMENTED SAMPLES,
BY BONDLINE CATEGORY, GEOMETRY, AND
LAYER OF OCCURRENCE

BONDLINE CATEGORY & ABBREVIATION	GEOMETRY AND LAYER								TOTAL
	F	B_1	B_2	T_1	T_2	J_1	J_2	J_3	
A. CONTINUOUS: NO DEFECT (ND)	104	44	33	57	53	158	109	102	660
B. DISCONTINUOUS (DEF):									
(1) Adhesive Cutout (AC)	13	1	0	6	2	2	4	7	35
(2) Partial Caul Pressure (PCP)	27	6	1	0	0	0	2	0	36
(3) Porosity (POR)	39	15	0	2	1	0	3	0	60
(4) Release Film (RF)	2	3	0	1	2	0	1	1	10
C. TRANSITION (TR)	79	32	8	37	31	28	69	39	323
TOTAL	264	101	42	103	89	188	188	149	1124

5.2.1 ND/DEF/TR Discrimination

Three-way discrimination is carried out by three two-way classifiers: ND/DEF, ND/TR, and DEF/TR. Features for a given observation are submitted simultaneously to each of the three; if two of the three decide the same class, that is then the overall decision. The only alternative is a tie -- one "vote" for each class. In that case a tie-breaker is employed that measures the confidence of each of the three classifiers in its respective vote; the classifier with the highest is then allowed to decide. The overall structure of the three-way decision is shown in Figure 15, and the details of the component classifiers are shown in Figures 16, 17, and 18. Two features -- x_8 and x_{23} -- were selected by all three networks. Those features are the total area under the power spectrum for the segment, and ratio of the total power for the entire waveform to that for the front surface, respectively. Thus there is one absolute measurement and one relative measurement. Section 5.3 discusses the significance of those features and the others used in the networks.

The effectiveness of the overall structure of Figure 15 is also discussed in Section 5.3.

5.2.2 Defect Type Discrimination

With the elimination of PCP/VBT from the data base there remain three types of bondline discontinuities of interest: adhesive cutout (AC), porosity (POR), and release film (RF). This discrimination was itself a two-step process: first separate RF from the set of POR and AC; then separate the latter into its two components. Figures 15, 19 and 20 show, respectively, the overall structure and the individual nets.

The next section discusses the results obtained with the defect-type classifier structure.

5.3 RESULTS

The individual classifiers shown in Figures 16, 17, 18, 19, and 20 were combined as shown in Figure 15 and the overall structure evaluated by submitting to it the set of 1124 feature vectors from the documented samples. Approximately 20 percent of the feature vectors submitted to each classifier were completely new to it; i.e., had not been used in training (design) phases.

The performance of the overall structure is summarized in the tables below, which indicate the true classes of the waveforms and those classes assigned by the classifier structure, and for each combination the number and percentage (of the true class) of waveforms so described.

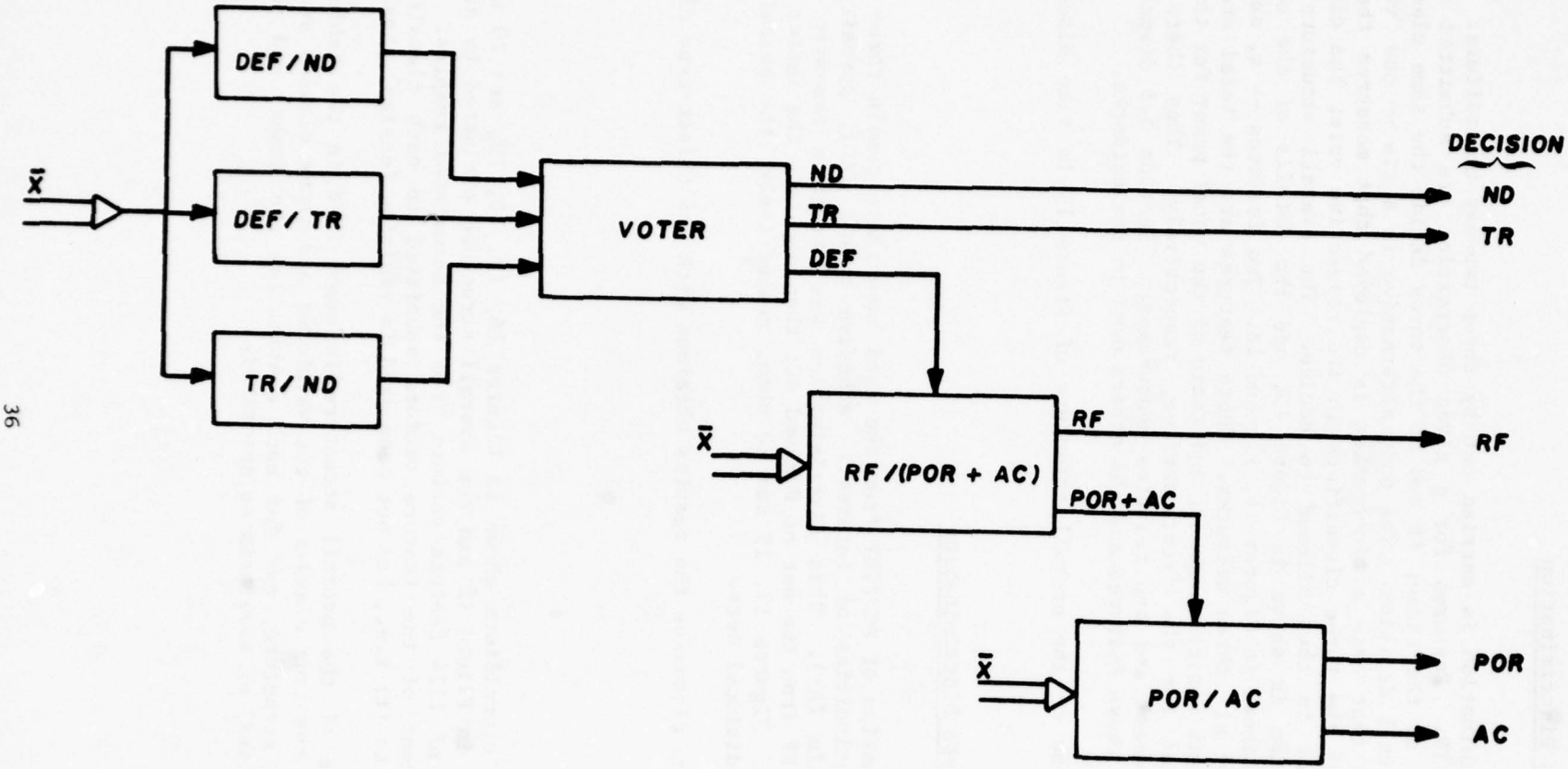

Figure 15. Structure of Overall Classifier

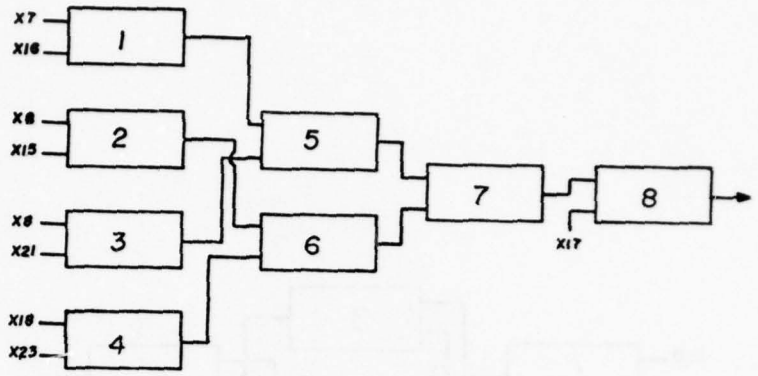

Figure 16. Defect/Non-Defect Descrimination Network

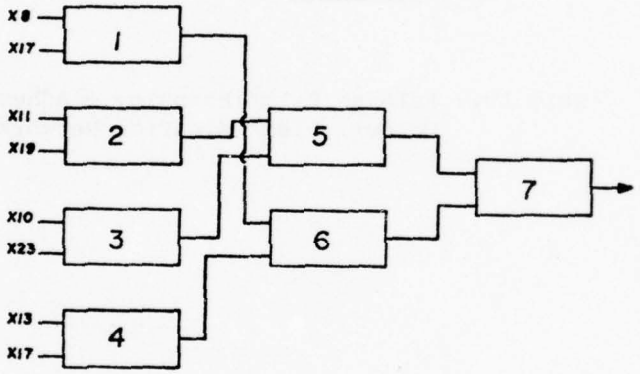

Figure 17. Transition/Non-Defect Discrimination Network

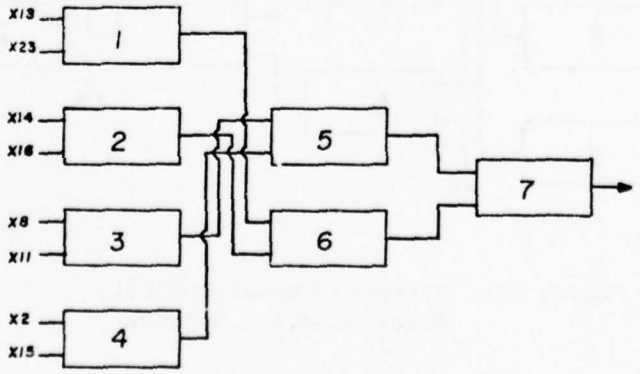

Figure 18. Defect/Transition Discrimination Netwcrk

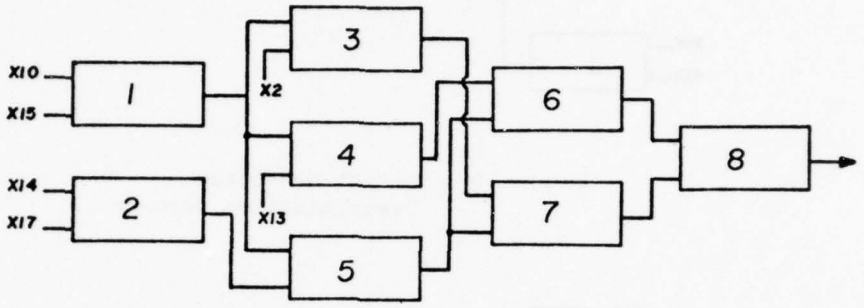

Figure 19. Release Film/(Porosity + Adhesive Cutout) Discrimination Network

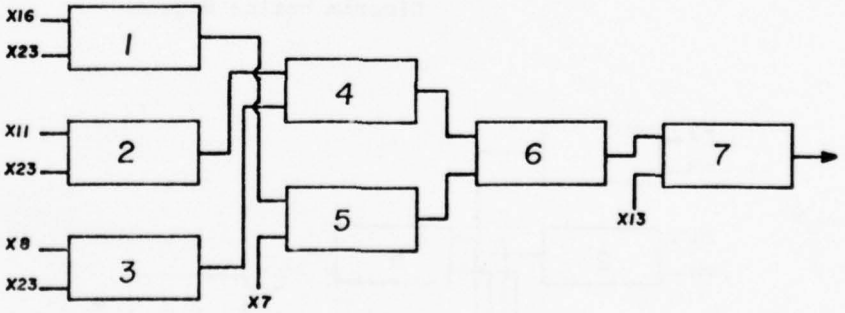

Figure 20. Adhesive Cutout/Porosity Discrimination Network

The results of the classification must be interpreted in light of the transition category defined in Section 5.1. For all but one of the samples, the transducer tracks did not provide an opportunity to explore the vicinity of a suspected discontinuity; it is almost certain that the defects giving rise to the transitions would have been detected had the transducer been capable of motion in all directions. (Note that this limitation was due to the need to limit the amount of scanning performed and data collected; an instrument that incorporated the feature-extraction and classification algorithms described earlier would not have such a limitation, as it would provide real-time discrimination.) Figures 18 and 19 present the exception and an example of all others, respectively. Sample F9 contains several scans that achieved excellent coverage of known defects. Noting the point-by-point classifications that were made for those scans (Fig. 18), we can conclude that a transition call serves as an alert: in a real-time application we would then begin scanning in the neighborhood, looking for a region of definite discontinuity.

It is reasonable to conclude that the proportions of transitions in both true classes and the decisions are much greater than would be the case in real-time testing. This is because an operator of a real-time system would not continue scanning along a predetermined path after an alert was received but would proceed as described in the previous paragraph.

The performance results should therefore incorporate the reasoning above and reflect the following facts that would affect design of a real-time instrument: (1) far fewer true transition points would be encountered in practice, and (2) far fewer transition decisions would be made in practice. The matrix that exists after deletion of the transitions is:

TABLE 2:

ALN CLASSIFIER PERFORMANCE FOR
NON-DEFECT VS. DEFECT DECISION

TRUE CLASS	NUMBER CLASSIFIED AS ND	DEF
ND	397(80%)	102(20%)
DEF	17(16%)	89(84%)

The false alarm rate -- the fraction of non-defects called defect -- is 20 percent and the false dismissal rate -- the number of defects called non-defects -- is 16 percent; overall accuracy is 80 percent.

Of those classified as defect above and after the exclusion of the PCP/VBT waveforms (see Section 5.2), the assignment of defect types yielded the following table.

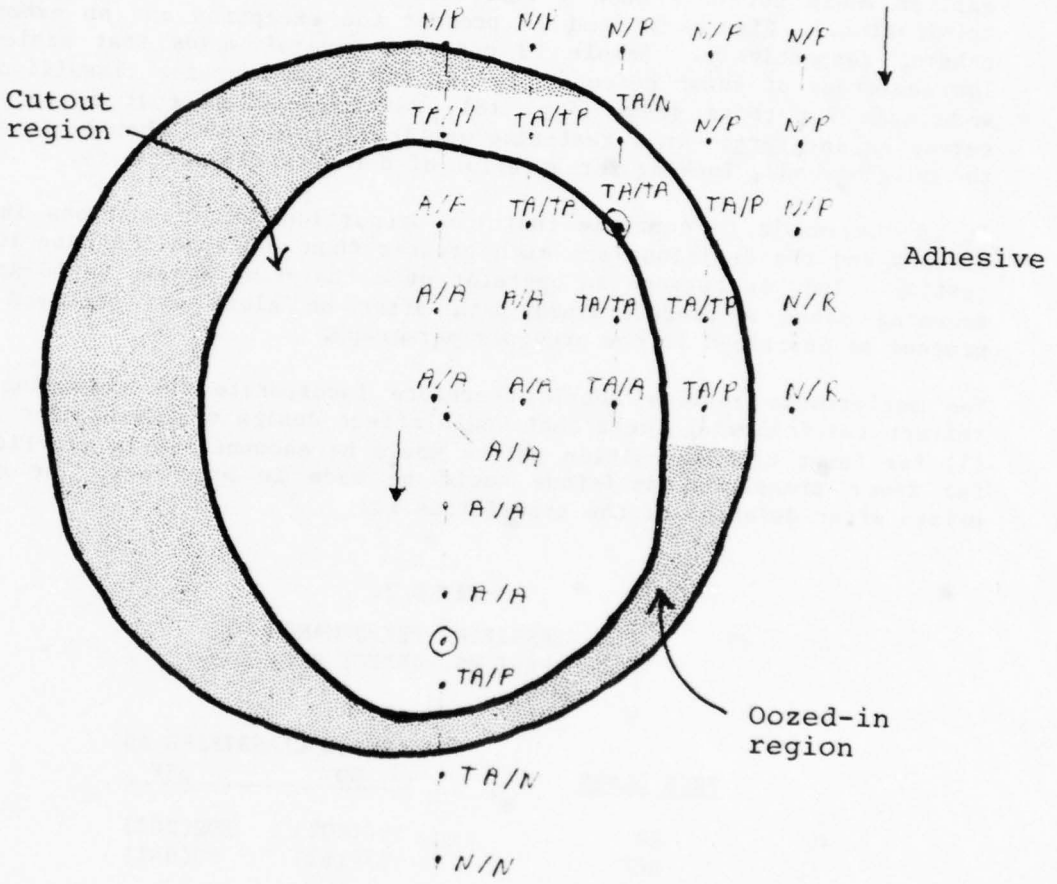

Figure 21. Point-By-Point Classifications Over a Large Contiguous Region

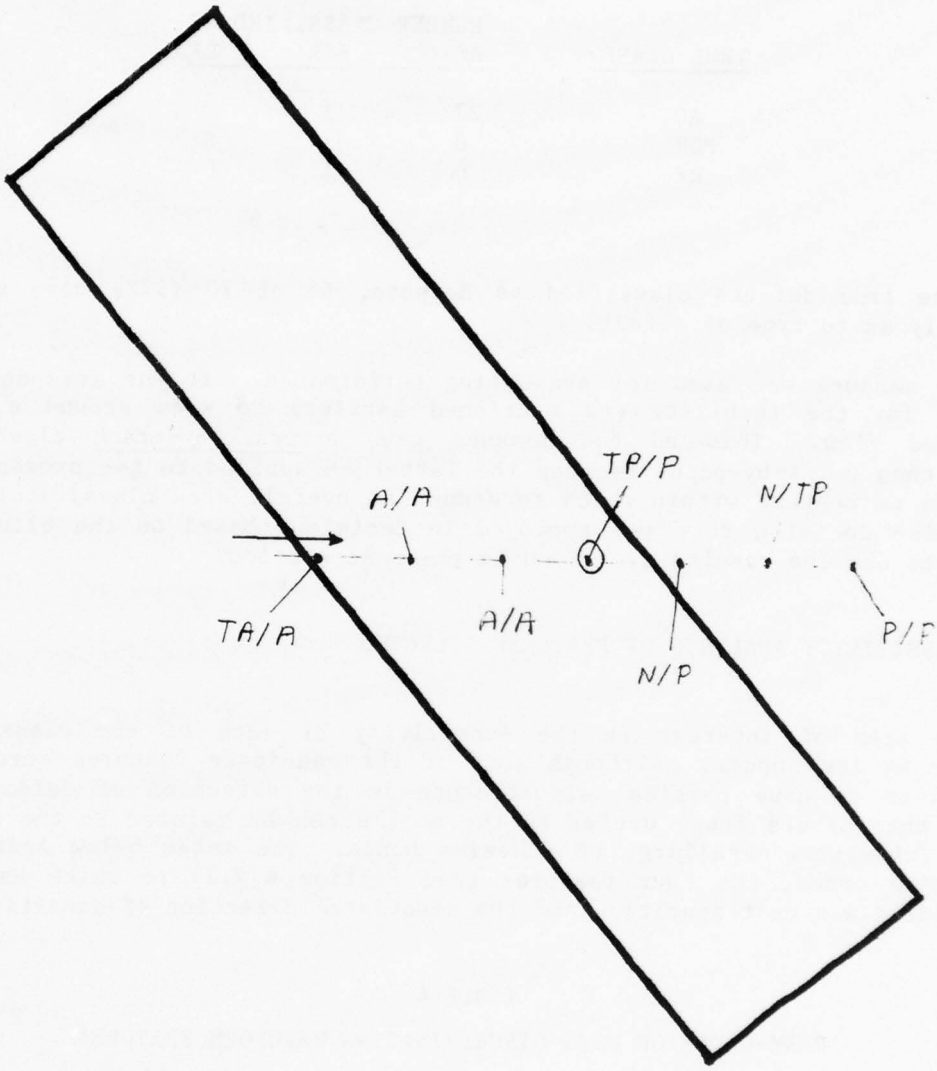

Figure 22. Straight-Line Path -- The Typical Scanning Procedure Results in Numerous Transition Points

TABLE 3

ALN CLASSIFIER PERFORMANCE FOR DEFECT DECISIONS

TRUE CLASS	NUMBER CLASSIFIED AS AC	POR	RF
AC	27	1	0
POR	0	41	0
RF	0	1	0

Of those true defects classified as defects, 68 of 70 (97%) were classified correctly as to type of defect.

Another measure was used for evaluating performance. It was intended to compensate for the inability (as mentioned earlier) to scan around a point of suspected flaw. This ad hoc measure gave a track-by-track classification rather than point-by-point because the latter -- applied to the present data -- provides no context within which to deduce an overall area classification. The track-wise decision rule was employed in decisions based on the blind evaluation data and the results are given in the next section.

5.4 SENSITIVITY ANALYSIS OF FEATURES SELECTED

Another area of interest is the sensitivity of each of the classifiers to changes in its inputs. Although some of the candidate features were believed in advance to have physical significance in the detection of defects, it is likely that others found useful in the models can be related to the underlying physics/chemistry/metallurgy of adhesive bonds. The table below indicates, in decreasing order, the four features (see Section 4.4.2) to which each of the five models was most sensitive and the associated direction of sensitivity.

TABLE 4

RANK-ORDER OF MOST DISCRIMINATING WAVEFORM FEATURES

TR/ND		DEF/ND		DEF/TR		AC/POR		RF/(POR+AC)	
Feature	Sign	Feature	Sign	Feature	Sign	Feature	Sign	Feature	Sign
x	-	x	-	x	-	x	+	x	-
x	-	x	+	x	-	x	+	x	-
x	+	x	-	x	-	x	-	x	+
x	-	x	-	x	-	x	+	x	+

In each case the polarity is to be interpreted as the direction in which the indicated feature would have to change in order to make the classifier's output tend toward the class whose abbreviation appears before the slash that heads the column. If x_{15} (the RMS ratio) increases, for example, the output of the RF/(POR + AC) classifier tends to look more like release film. This is consistent with the quiet-zone interpretation of Section 4.3.

Other observations based on the sensitivities point to hypotheses that should be pursued further. Feature x_{17} is the ratio of the location of the 25-percent point of the spectrum of the entire waveform to the location of that point in the spectrum of the front-surface waveform. The smaller that value is, in general, the greater is the low-frequency content of the overall signal as compared to that of the front-surface signal. Thus as the ratio decreases, the classifiers TR/ND and DEF/ND tend to decide TR and DEF, respectively. Equivalently, the greater the high-frequency content, the more like no-defect the classifications appear.

A measurement related to the quiet zone energy is x_8 (the total power in a segment's signal); it appears in the DEF/ND and DEF/TR classifiers and as it decreases leads the classifiers to indicate defect. This is plausible on physical grounds since a defective bond that is AC or POR will return less power from the bond line than a nondefective region.

Additional insights will result as the results above are studied, but the intuitive appeal of many of the features chosen increases confidence that the models are not spurious.

SECTION VI

APPLICATION OF CLASSIFIER TO UNDOCUMENTED SAMPLES

6.1 DATA ACQUISITION

A set of 20 samples (five of each geometry) for which no documentation had been supplied was to serve as a final and blind test of the classifier. The subcontractor (Rockwell) was given the documentation so that the number of scan tracks could be kept reasonably small. Without disclosing to Adaptronics the true nature of the bondline for each of the samples, Rockwell provided waveform data in a form identical to that used for scans of the documented samples. A total of 64 tracks were scanned and they accounted for 1,078 observations, once the layers were considered.

The experimental conditions had changed from those existing at the time of the documented scans in two respects (both believed to be minor); chief among them was a change in the damping of the transducer's pulser-receiver. This meant that the number of sample points in the front-surface segments changed, as did the numbers of points in the remaining segments of the waveforms. The effect on the segmentation algorithm was minor, however. Comparison of manually-identified endpoints with computer-chosen ones indicated that the segmentation algorithm is sufficiently general to tolerate small changes in damping.

6.2 FEATURE EXTRACTION

The same algorithms used to remove the effects of the transducer and intervening layers from the documented waveform segments were used again with the undocumented data. Features were extracted from the power spectra from the undocumented samples in exactly the same way as for the documented samples. The resulting sets of 23 features were compared to those from the earlier data, and no anomalous values were found. The features were used in the classifiers developed on the documented data, and point-by-point signal interpretations were made for the undocumented tracks. Those interpretations were transmitted to AFML to establish the blind nature of the test; Rockwell then supplied the documentation packages to Adaptronics.

6.3 RESULTS

As shown in Figures 21 and 22, the point-by-point waveform segments fell into tracks. The classifier scheme (Figure 15) rendered a decision for each of the 1,078 points contained in all of the tracks scanned.

Each track was then divided into one or more regions. Each region was determined by examining visually whether the points in that region were within a segment of ND, TR, or DEF. If ND, the accuracy was perfect if an ND call was given. If TR, the accuracy was perfect if at least one call in the track region was TR, thereby providing an "alert" that a defective region was nearby. If DEF, the accuracy was judged perfect if the call was DEF. In the latter case, in addition, the accuracy was further tested by determining which of the three DEF types was called: AC, POR, or RF.

Dividing each track into regions was an attempt to mimic the actual field NDE conditions; that is, the inspector is only interested in whether defects exist and where in a part. The number of point-by-point decisions is not really relevant, only the output that a certain defect type exists in a given location. Due to cost constraints, a sparse number of waveforms was recorded and analyzed per track. This meant that there were only a few pulse-echoes per region upon which to base a decision. This lack of contextual information -- i.e., a large set of computer-generated decisions to be examined in a second-stage decision logic -- means that the results reported below are quite conservative; more echoes per part would lead to better accuracy rates.

The two-way ND versus DEF results are given in Table 5.

TABLE 5

ALN CLASSIFIER PERFORMANCE FOR NON-DEFECT VS. DEFECT REGION DECISIONS ON EVALUATION DATA

TRUE CLASS	CLASSIFIED AS ND	DEF
ND	47(81%)	11(19%)
DEF	2(2%)	87(98%)

The overall accuracy was 91% (136/149). The false dismissal rate (DEF called ND) was 2% (2/89); the false alarm rate (ND called DEF) was 19% (11/58). It is very encouraging that the region accuracies for the blind evaluation data (Table 5) are very close to the point-by-point accuracies (Table 2, Section 5.3).

The detected 87 defects were then further classified into the three DEF classes with the following results:

TABLE 6

ALN CLASSIFIER PERFORMANCE FOR DEFECT REGION DECISIONS ON EVALUATION DATA

TRUE CLASS	CLASSIFIED AS AC	POR	RF
AC	21(88%)	2(8%)	1(4%)
POR	2(4%)	49(92%)	2(4%)
RF	0(0%)	0(0%)	10(100%)

The overall accuracy was 92% (80/87).

The ND versus DEF discrimination in Table 5 was further analyzed regarding the accuracy of the ALN classifier with respect to part geometry and layer. The results are given in Table 7.

TABLE 7

ALN CLASSIFIER PERFORMANCE FOR NON-DEFECT VS. DEFECT DECISIONS AS A FUNCTION OF PART GEOMETRY AND LAYER IN THE MULTI-LAYER STRUCTURE

Per Geometry	Per Layer
F : 87.5%	L1 : 89.5%
B : 86.5%	L2 : 83.7%
T : 87.1%	L3 : 83.3%
J : 89.5%	

It can be seen that the classifier is quite insensitive to differences in part geometry and layer.

SECTION VII

CONCLUSIONS

It has been shown that it is feasible and practical to use ultrasound to detect and classify defects and flaws in multiple-layer adhesively bonded structures, regardless of the layers in which they lie. The method is, by design, insensitive to moderate variations in transducer orientation and to construction geometry. The accuracies on the blind evaluation test compare very well with the data used to train the ALN classifier system indicating that the system can be expected to perform comparably under future, similar NDE conditions.

Parameters are extracted from the ultrasound waveforms and their power spectra; nonlinear functions of the parameters are implemented by Adaptive Learning Networks and were quite successful at discrimination among bond types and defect types.

An estimate of 87 to 92 percent as the accuracy of a real-time system embodying the techniques presented here is realistic and attainable for three-layer samples.

Further work is needed to lower the 19% false-alarm rate. More UT data should be collected so that the possibility of using multiple-point (contextual) information from contiguous scans can be investigated. It is believed that this investigation would lead to a significant lowering of the false-alarm rate to a level consistent with the requirements on field systems (i.e., less than 10%).

SECTION VIII

RECOMMENDATIONS FOR FUTURE WORK

Microprocessors and related new computing hardware now make possible the development of a portable scanning and data analysis instrument that incorporates the techniques presented here. In the hands of an operator the instrument could be used to locate defects and classify them in real-time. The interactive nature of the process would eliminate many of the transition decisions because the operator would have the freedom to explore suspicious indications regardless of the directions in which they lie.

However, in view of the limited data set evaluated under this program, a more extensive defect classification program is needed prior to the development of a field unit. Such a program would include the data set and remaining samples from the present program and additional samples incorporating defects found to be critical from the PABST program, i.e., edge disbonds, edge cracks, etc.

APPENDIX A

DATA FORMAT

AND

TRANSMISSION SPECIFICATIONS

APPENDIX A

A.1 DATA FORMATS

Data generated in this project are available on industry compatible 9-track 800 BPI magnetic tape in an unlabeled EBCDIC 80-column card image format, 10 card images per block. The data are organized in files, each of which contains one or more records. Each record contains one time domain or frequency domain waveform, and each file contains the records associated with a scan under a particular set of experimental conditions.

It is best to think of the data in two different representations (or formats): (1) the multiple record format, which is a large two-dimensional array suitable for use by data processing programs within a computer, and (2) the card image format, in which a multiple record file is reformatted to fit within the restrictions of an 80-column card image format.

The multiple record format is shown in Table A.1. Each record (i.e., each row) consists of a parameter count (2), the two parameters which distinguish one record from another (x and y position), the data count (N_D), and finally the waveform (in either time domain or frequency domain).

The card image format is described in Table A.2. To produce a card image file, a multiple record file is converted to a vector (of length $N_{TOT} + 1$) by reading off its elements left to right, then top to bottom (this is the APL function "RAVEL"). This vector is then entered, five elements at a time, in the right-hand 60 columns of as many data data cards as are needed to contain the file. The set of data cards is preceded by a set of comment cards describing the experimental conditions pertaining to the file.

In addition to the comment cards preceding each file, there is a set of "standard comment cards" containing information applying to the entire project and default values of some of the file comments. The standard comment cards form a single data-less file.

Tables A.3 and A.4 list the comments to be included with each file and in the standard set.

A.2 RUNS MADE

Table A.5 describes the ultrasound scanning runs made on the documented samples, including assessments of the kinds of defects present. The coordinate system within which the tracks are defined is illustrated in Figure A.1.

TABLE A.1
MULTIPLE RECORD FILE

TIME DOMAIN FILES:

N_{TOT}	2	X	Y	N_D	N_D TIME DOMAIN VALUES

← 1 RECORD

X,Y = POSITION RELATIVE TO STANDARD COORDINATE SYSTEM

N_{TOT} = (ND + 4) x NUMBER OF RECORDS (ROWS) = AREA OF FILE

N_D = NUMBER OF TIME DOMAIN POINTS

FREQUENCY DOMAIN FILES:

REPLACE

N_D	N_D TIME DOMAIN VALUES

BY

$-N_D$	N_D REALS	$-N_D$	N_D IMAGINARIES

TABLE A.2

CARD IMAGE FORMAT

The card images are of two types:

Card Type 1 = Comment Card

Card Type 3 = Data Card

Comment Card:

Col.	Contents	Format
1-2	Card Type = 1	I2
3-5	Project #	I3
6-9	Run #	I4
10-14	Line #	I5
		6X
21-55	Comment	S35
56-80	Test Variable Value	E12.5

Data Card:

Col.	Contents	Format
1-2	Card Type = 3	I2
3-5	Project #	I3
6-9	Run #	I4
10-14	Line #	I5
		6X
21-80	Data	5E12.5

TABLE A.3

COMMENT CARDS TO BE INCLUDED WITH EACH FILE

Line #	Information	With Every Run	With Run If Different From Standard	Standard Value
10	Sample Number	X		
11	Flat Side Up?		X	Flat Side Up
12	Transducer: Manuf/Mod/Serial	X		
13	Distance	X		
14	Angle		X	0^{o}
15	Pulser: Manuf/Mod/Serial	X		
16	Plug-In		X	
17	Attenuation		X	0 dB
18	Buffer: Manuf/Mod/Serial	X		
19	Range	X		
20	Biomation: Range	X		
21	Sample Interval	X		
22	Averages		X	10
23	Water Temp		X	

TABLE A.4

STANDARD COMMENT CARDS

Line #	Information	Value
11	Flat Side Up?	Yes
14	Transducer Angle	0
16	Pulser Plug-In	
17	Attenuation	0 dB
22	Averages	10
23	Water Temp	

All other Biomation settings = 0

For each transducer: nominal frequency, diameter and damping

Statement of standard coordinate system

Statement of parameters in each record

TABLE A.5

ADHESIVE BOND RUN DESCRIPTIONS

PROJECT 2, RUNS 3-9, 31-37

RUN	NO. OF ADHESIVE LAYERS	DEFECT	SAMPLE	FLAT SIDE UP OR DOWN	X-SCAN (IN)	Y-SCAN (IN)
3	1	None	F4	UP	[-4,4] by ½	1
4	1	Porosity	F2	UP	[-4, 4] by ½	-.75
5	1	Circular Void	F9	UP	[-3.4, -2.4] by ¼	[-1.5, -0.15] by ¼
6	1	Cracklike Voids	F4	UP	[0.5, 4] by ¼	-1.5
7	1	Unbond, Far Side	F9	UP	[-3.2, -2.45] by 0.15	[1.35, 2.10] by 0.15
8	1	Bondline Thickness	F6	UP	[-1.5, -0.7] by 0.4	[-2, 1.5] by ¼
9	1	Unbond, Near Side	F9	DOWN	[-3.2, -2.45] by 0.15	[-2.10, -1.35] by 0.15
31	1	None	F4	UP	[-4, 4] by ½	1
32	1	Porosity	F2	UP	[-4, 4] by ½	-.75
33	1	Circular Void	F9	UP	[-3.4, -2.4] by ¼	[-1.5, -0.15] by ¼
34	1	Cracklike Voids	F4	UP	[0.5, 4] by ¼	-1.5
35	1	Unbond, Far Side	F9	UP	[-3.2, -2.45] by 0.15	[1.35, 2.10] by 0.15
36	1	Bondline Thickness	F6	UP	[-1.5, -0.7] by 0.4	[-2, 1.5] by ¼
37	1	Unbond, Near Side	F9	DOWN	[-3.2, -2.45] by 0.15	[-2.10, -1.35] by 0.15

TABLE A.5 (Cont.)

Description of Runs 41-99

RUN	NO OF ADHESIVE LAYERS	DEFECT	SAMPLE	FLAT SIDE UP OR DOWN	X-SCAN (IN)	Y-SCAN (IN)
41	1	(VB1)	F1	UP	-0.5	[.2,1] by - 1/4
42	1	(TB1) (PE1)	F2	UP	-2.5	[-3,-1] by 1/2
43	1	(LE1)	F4	UP	[1.125,2.375] by 1/4	-1.5
44	1	(VB1),slight (PE1)	F5	UP	-1.75	[0,-1.5] by -1/4
45	1	(TB1),2" diam. annulas of (P1) at Y = 1/4"	F5	UP	2.25	[0.75,-1.25] by -1/4
46	1	(LB1)	F8	UP	[-0.3,0.45] by 1/4	-2.75
47	1	3/8" diam.(VE1)	F9	UP	[2.1,2.7] by 0.1	-0.21
48	1	1.5" diam.(VB1)	F9	UP	[-2.25,-1] by 1/4	-0.21
49	1	1/4" diam.(VB1), 1/4"x3"(V1) at X=1.1", 1/4" diam. (DE1)	F10	UP	[-1.9,3.5] by 0.491	-1.0
50	1	(DB1)	F11	UP	[-0.5,0.75] by 1/4	-1.5

51	1	(tB1),(tE1)	F12	UP	[-2.75,2.25] by 1	-1.25
52	2	(TB1)	B1	UP	[-3.375,-2.125] by 1/4	1.95
53	1	(TB2)	B1	UP	1.73	[-2.75,-125] by 1/4
54	1	in joggle: (LB1),(LE1)	B1	UP	[0.1,1.35] by 1/4	-0.1
55	2	(DE1)	B2	UP	2	[0.75,1.75] by 1/4
56	1	(UB1)	B2	UP	2.75	[-1.75,-0.75] by 1/4
57	2,1	(TB2),(LM1) in joggle, (P1) from Y=1/2 to -1.75	B3	UP	1	[1.15,-2.35] by -1/4
58	2	(DB1),(DM2)	B5	UP	[-1.25,0.25] by 1/4	+1.5
59	2	(DB1)	B7	UP	[-1.75,-0.75] by 1/4	1.1
60	1	(TB2)	B7	UP	[2,3.5] by 1/4	1.35
61	1,2	(PB1) for Y 0, 1/8" wide (VE?)	B10	UP	3.6	[-1.15,0.85] by 1/4
62	1	(T1) at X=-0.5", (T1) at X=3"	B11	UP	[-2,4] by 1	-1.4
63	2,1	(VM1)	B15	UP	-1.5	[0.5,-2] by -1/4

64	2,1	almost complete(PM1) for 0 Y -1; insert at Y -1.1"	B15	UP	4.1	[0.5, -2] by -1/4
65	2,1	(DB2),(DM1)	T1	UP	-2	[-0.5,-1.75] by -1/4
66	2	(DB2),(DM1)	T1	UP	[-2,-1] by 1/4	-0.5
67	2	(VB1),(VE2)	T2	UP	[-2.6,0.4] by 1/2	0
68	2	(LM1),(LM2)	T2	UP	-3.5	[0,1] by 1/4
69	2	(VB2)	T3	UP	0.25	[0,-1] by -1/4
70	2,1	(VM1), probably not (VM2)	T3	UP	-2.25	[0.5,2] by 1/4
71	2	(VB1),(LM1)	T4	UP	[1.75,3.75] by 1/4	0.35
72	0,1,2 1,0	no defect	T4	UP	0	[-2.5,2.5] by 1/2
73	2	(VM?) at Y=0.25" (LM?) at Y=0.85"	T5	UP	0	[-0.25,1.25] by 1/4
74	2	(VB1),(VB2)	T6	UP	-0.875	[0,075] by 1/4
75	2	(VM2) at Y=-0.4", (LB1), (VM1) at Y=0.25"	T6	UP	-0.45	[-1,1] by 1/4

76	2	(UE?)	T7	UP	[1,3.5] by 1/2	0.5
77	2	(DM1) at X=-0.5" (DM2) at X=0"	T9	UP	[-1.25,0.5] by 1/4	-0.7
78	1	1/8" wide (DB1)	T10	UP	[2,3] by 1/4	-1.4
79	1	1/4" (DB1)	T10	UP	[-1,0] by 1/4	-0.85
80	2	(PB?) until X=1.4"	T11	UP	[1,2.5] by 1/4	0.5
81	2	(TB2)	J1	UP	[1.7,2.7] by 1/4	-1.3
82	2	0.070" wide(VB2)	J2	UP	[1.4,0.4] by -1/4	1.25
83	3	1/8" wide(VB2)	J2	UP	[-2,-3] by -1/4	-0.375
84	3	(VM1),(VM2),(DM2) (VM3)	J3	UP	[-1.5,1] by 0.1	-0.15
85	2 1/2	(L,M&E, 1 or 2)	J3	UP	[-0.5,1] by 1/4	-0.8
86	3	(VM3),(L,B&M, 1 or 2),(DM3)	J4	UP	[-3,0] by 1/4	0
87	3,2	(DM3),(VB&M3) (LB 1 or 2)	J4	UP	-1.8	[0,-1] by -0.2
88	3,2	(DM3),small(VB3)	J4	UP	-1.2	[0,-1] by -0.2
89	3	DB3	J5	UP	[-2.2,-1.2] by 1/4	0

90	3	DE1	J5	UP	[2,3] by 1/4	0
91	2,0	0.2"(VM2)	J5	UP	-0.375	[1.125,2.125] by 1/4
92	3	(VM1) at X=2", 1/4"(VM2) at -1.25", (VM2) at 1", (LM?) at 0.4"	J6	UP	[-3.25,2] by 1/4	0
93	3	(VM2) at Y=-1/4" +3/8"	J7	UP	0	[-0.75,1] by 1/4
94	2	1/4" wide(DB2)	J8	UP	[-1.75,-0.75] by 0.1	-1.5
95	2 1/2	(DM2),(DM3) 1/4" wide	J8	UP	[-2.5,-1.6] by 0.1	-0.85
96	3	1/4" wide(DB3)	J8	UP	[-2.25,-1.25] by 0.1	-0.5
97	3	1/4" diam(VB2)	J9	UP	[-2.6,-1.6] by 1/4	-0.25
98	2,3	B16(PM?) at Y=1.15" & -0.85"	J9	UP	0.4	[-1.55,-0.55] by 0.1
99	3,2	1/8"(VM3) at Y=1/8", (PM?) at Y=1/8"	J10	UP	0	[-0.5,1.7] by 0.1

TABLE A.6

NOTATION USED IN TABLE A.5

(D) = disbond caused by release film.
(L) = "leaves", i.e. quasi-linear collections of voids.
(P) = porosity.
(T) = bondline thickness variation due to positive caul pressure.
(t) = bondline thickness variation due to caul plate cutout.
(u) = ultrasonic indication of unknown origin.
(V) = void caused by adhesive cutout.
(B) = at beginning of linear scan.
(M) = at middle of linear scan.
(E) = at end of linear scan.
(1) = in first adhesive layer
(2) = in second adhesive layer.
(3) = in third adhesive layer.

Example: (PB2) means pososity at the beginning of the scan in adhesive layer 2.

The defects are assumed to be at least 1/2" across unless otherwise noted.

Brackets [] around two coordinate numbers designate the starting and stopping points of the scan.

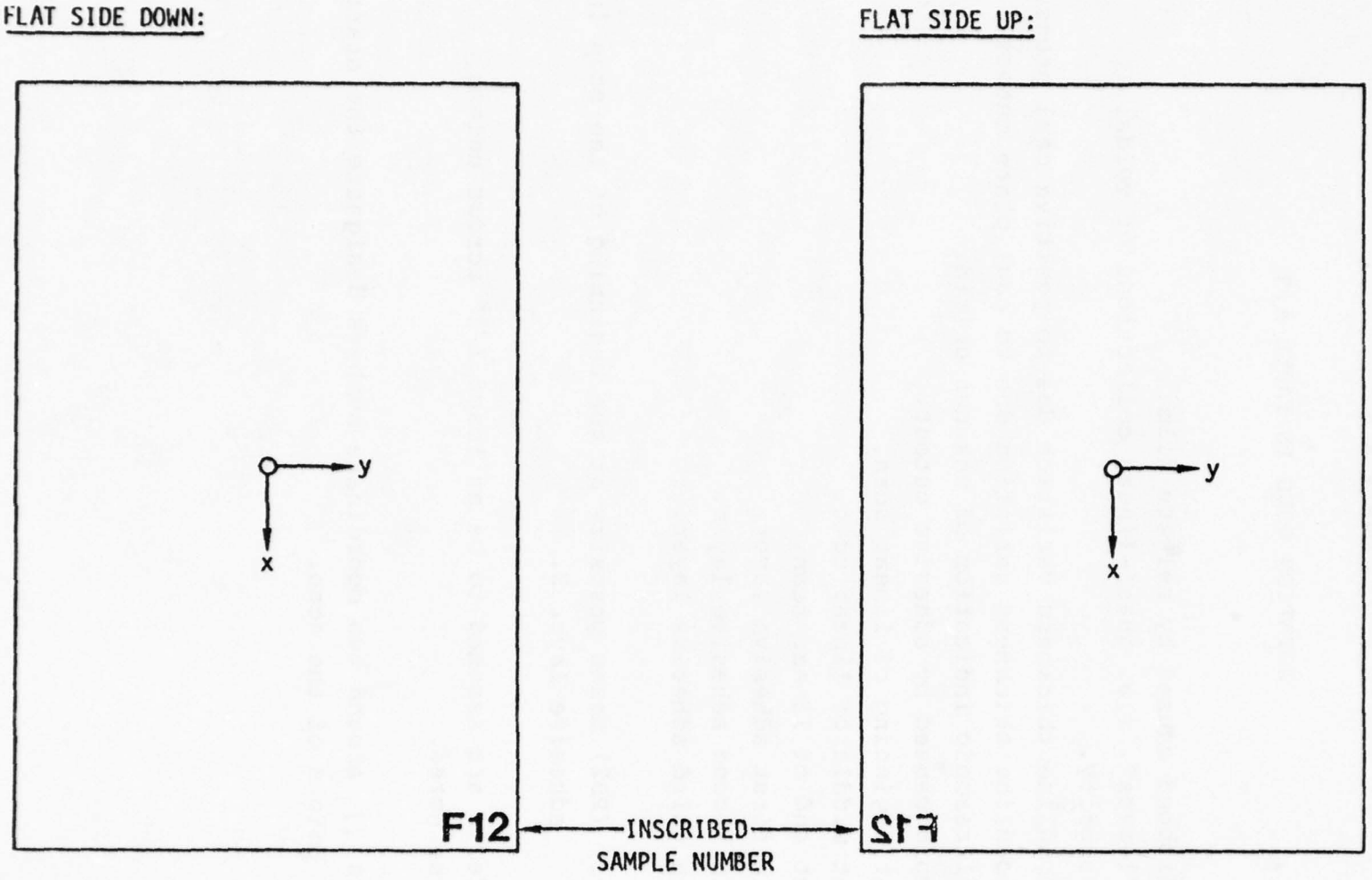

Figure A.1. Coordinate System Centered at Center of Sample and Referenced to Inscribed Sample Number

APPENDIX B

LAYOUT SHEETS CONTAINING

THE TRANSDUCER SCAN TRACKS

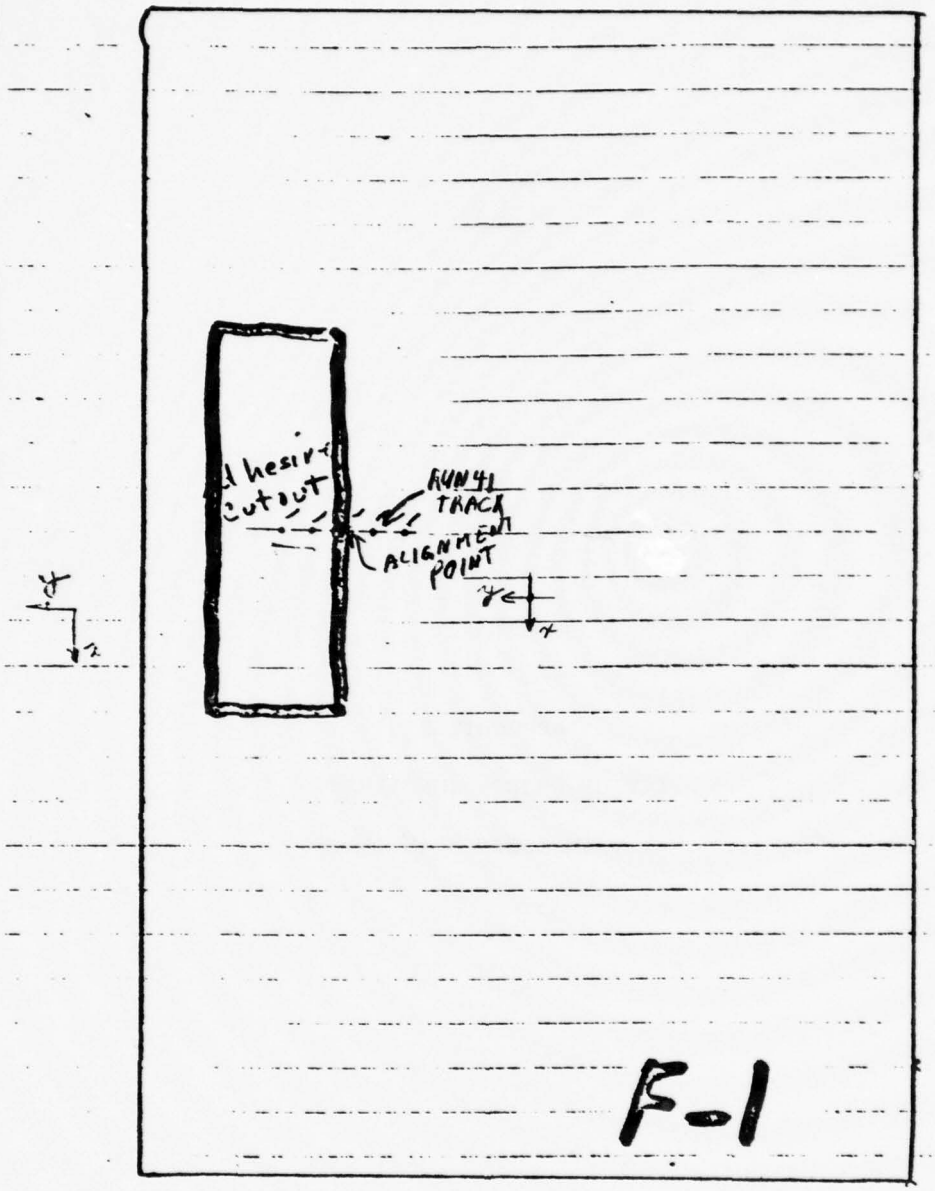

Figure B.1: Sample - F-1
Use - Classifier Design

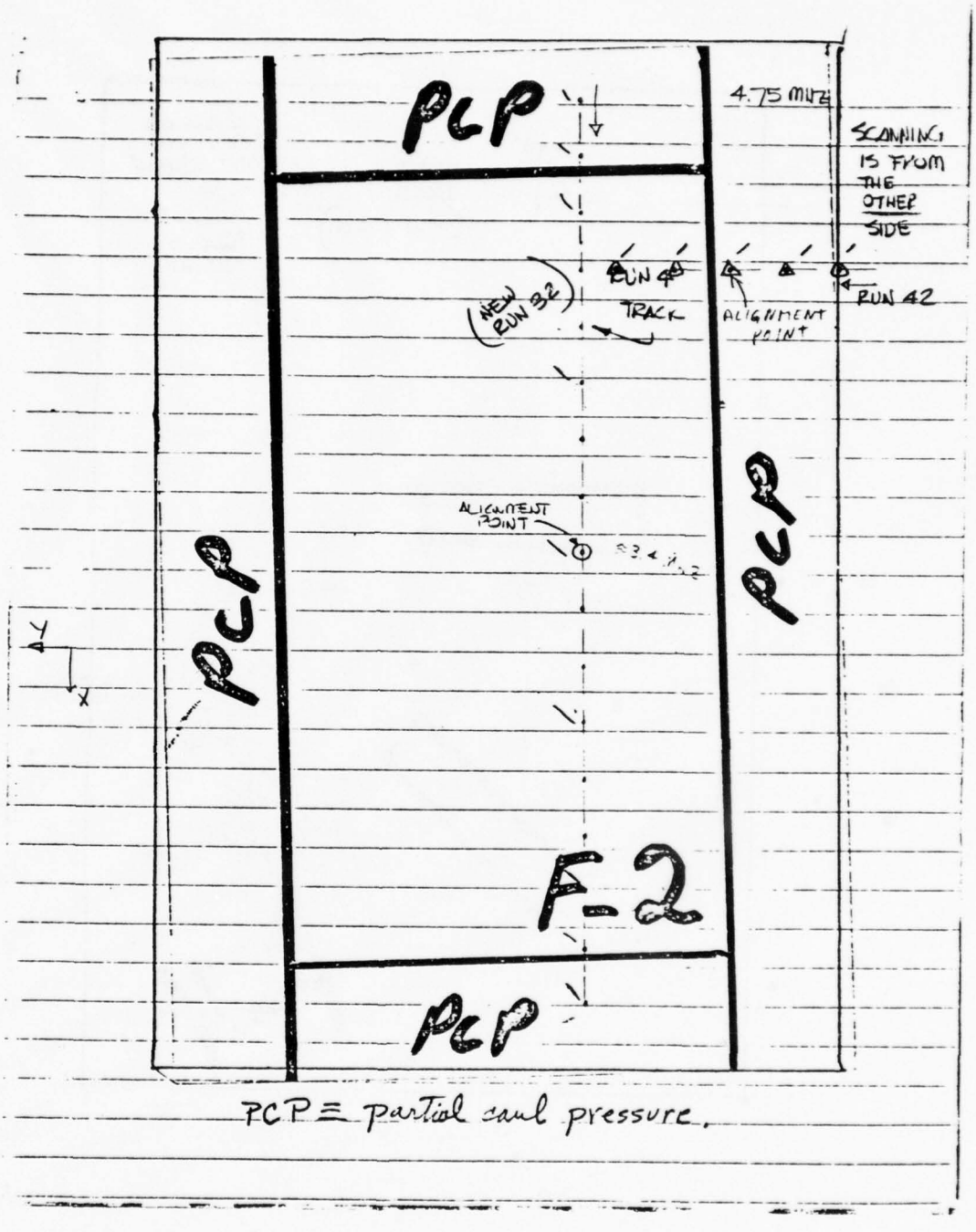

Figure B.2: Sample - F-2
Use - Classifier Design

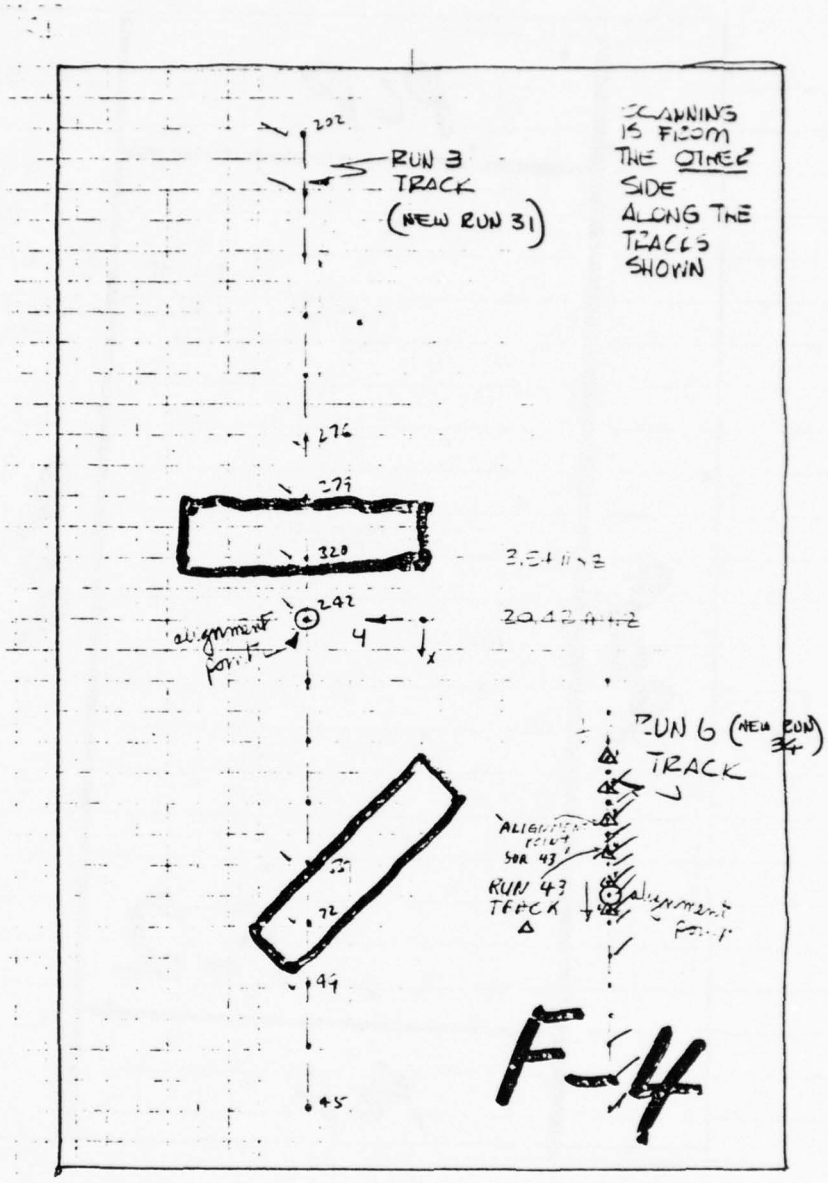

Figure B.3: Sample - F-4
Use - Classifier Design

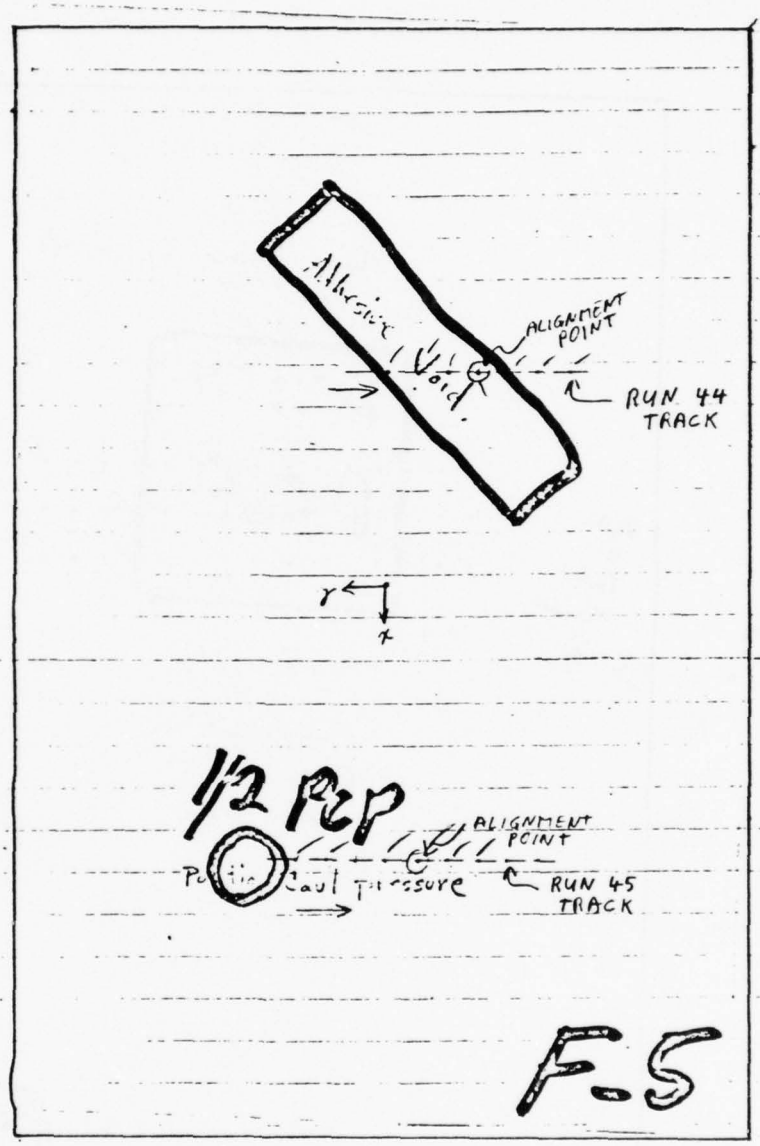

Figure B.4: Sample - F-5
Use - Classifier Design

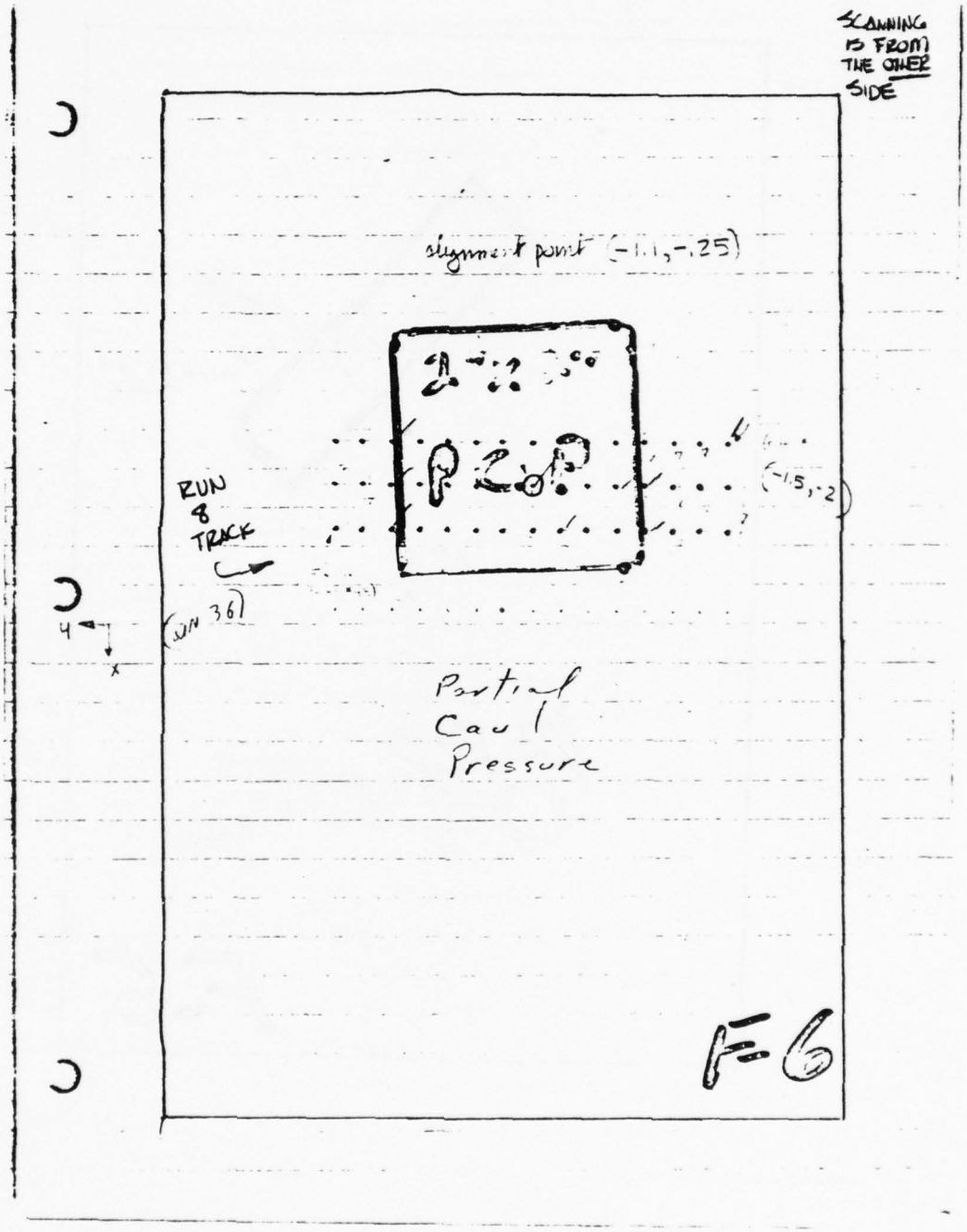

Figure B.5: Sample - F-6
Use - Classifier Design

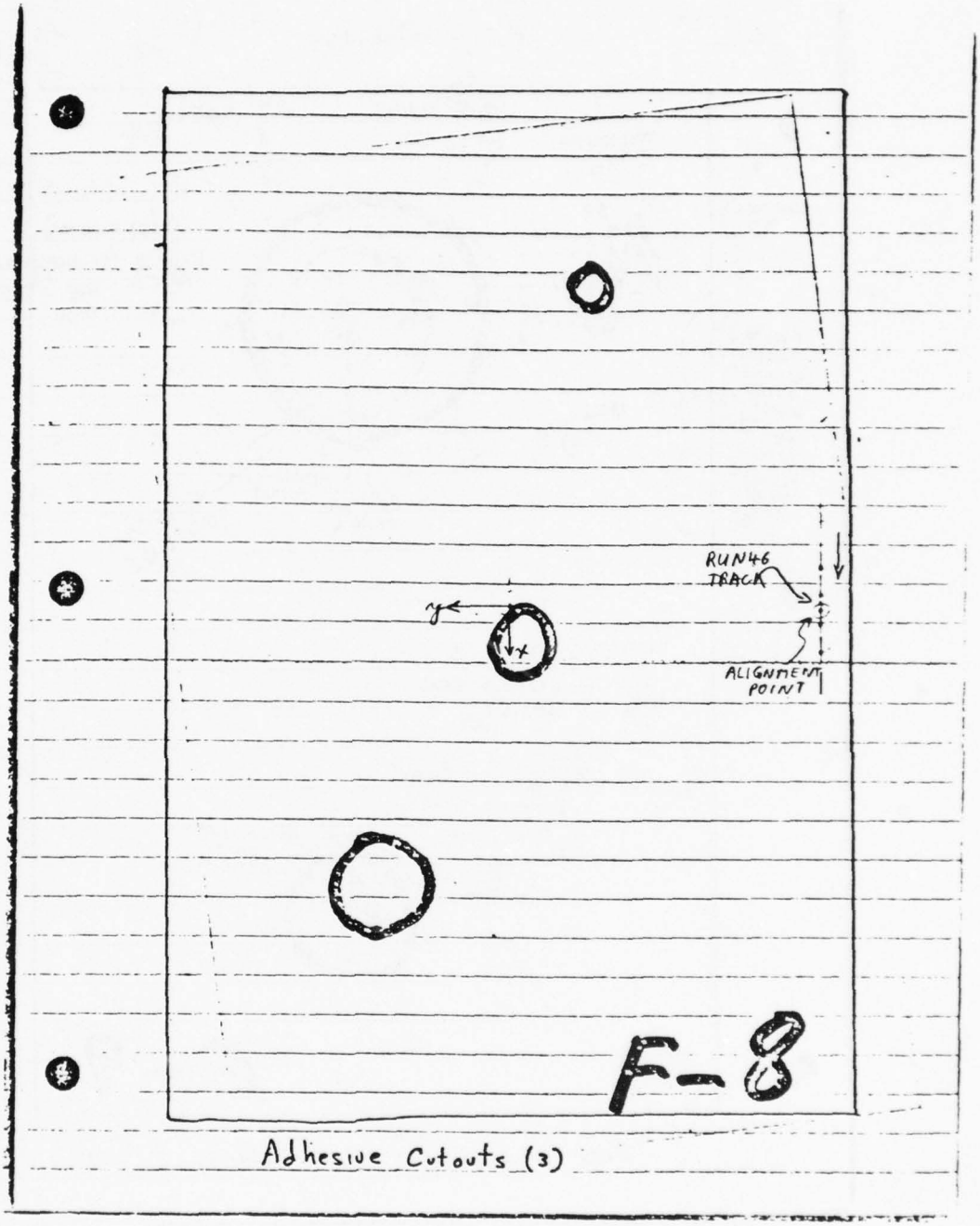

Figure B.6: Sample - F-8
Use - Classifier Design

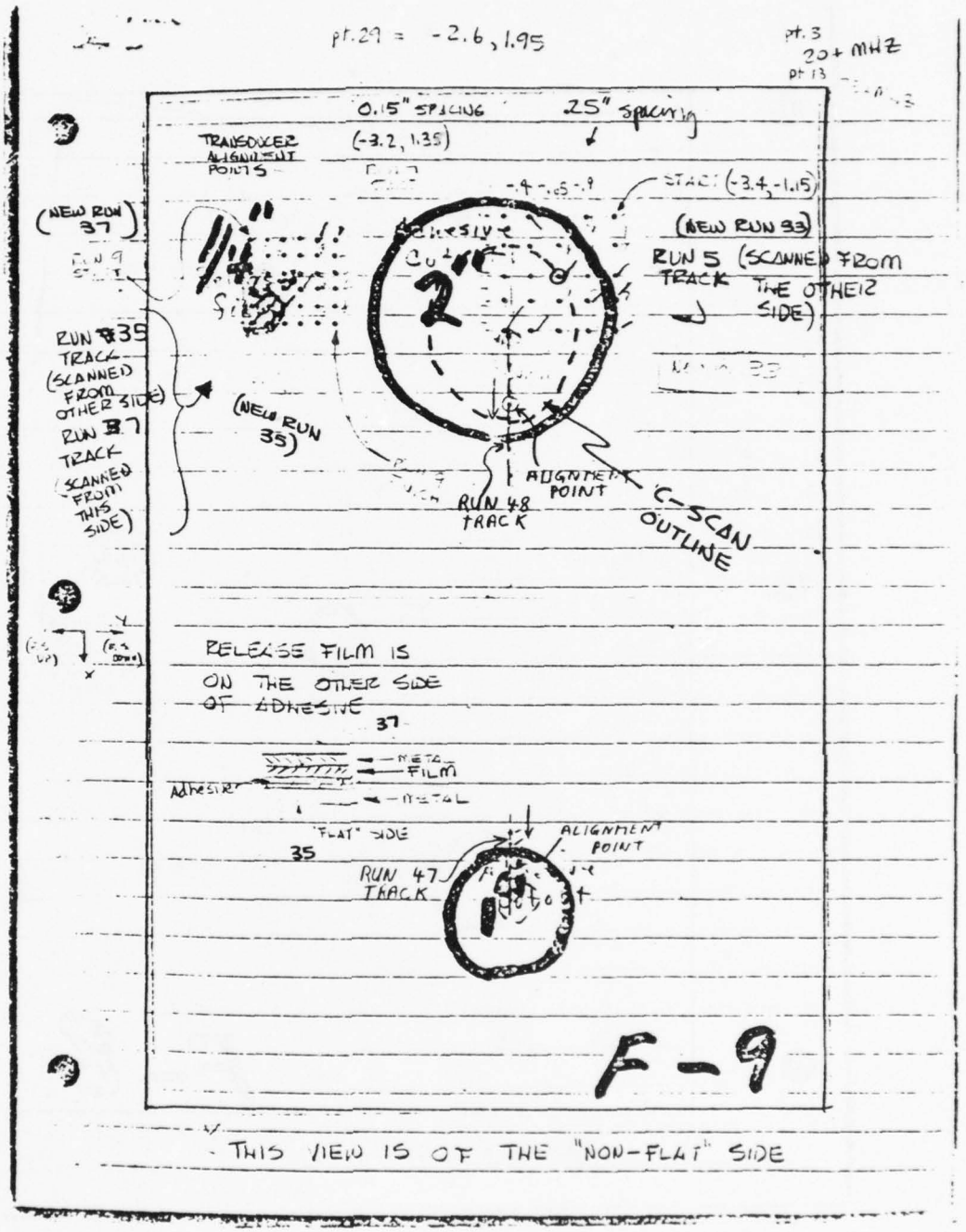

Figure B.7: Sample - F-9
Use - Classifier Design

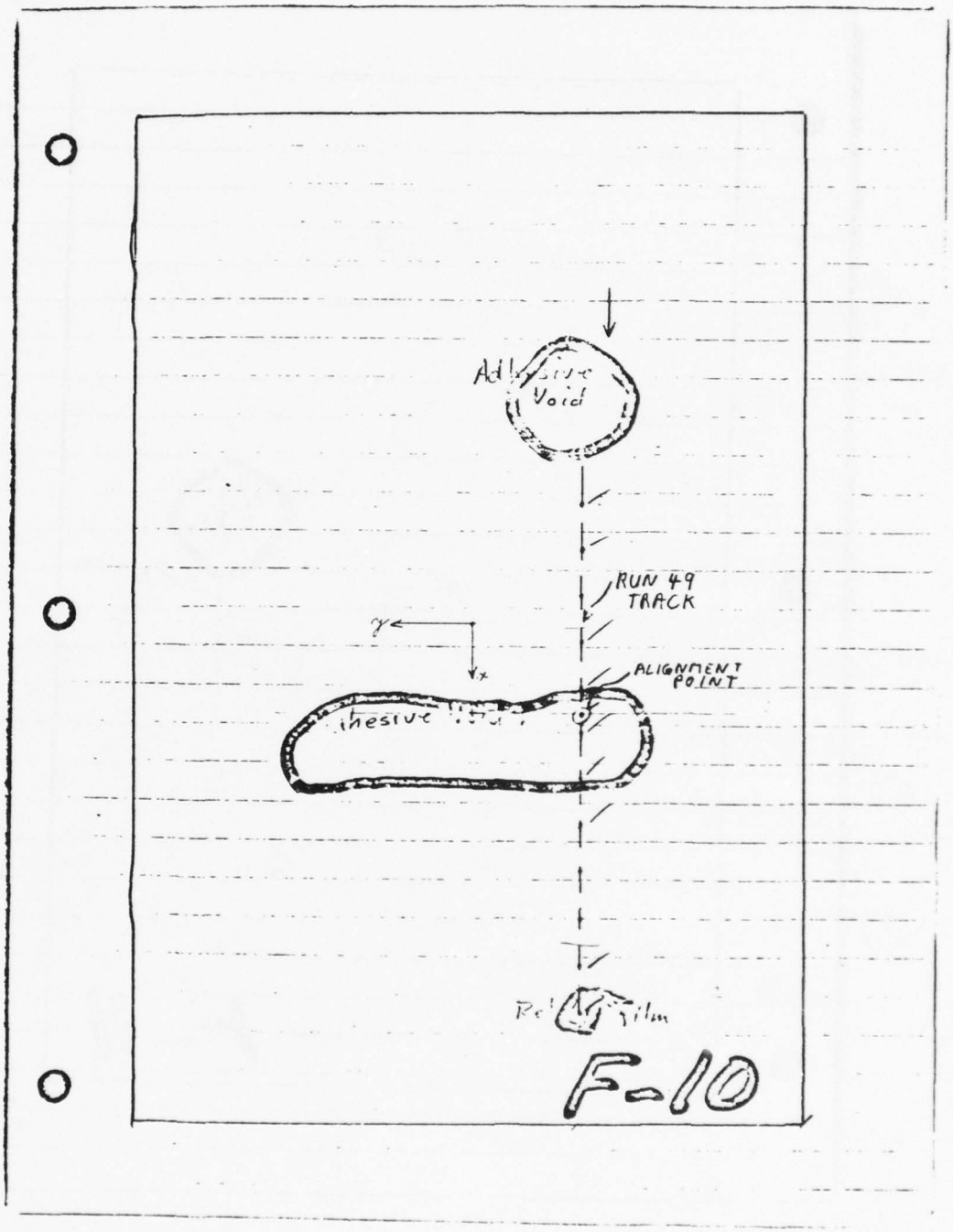

Figure B.8 Sample - F-10
Use - Classifier Design

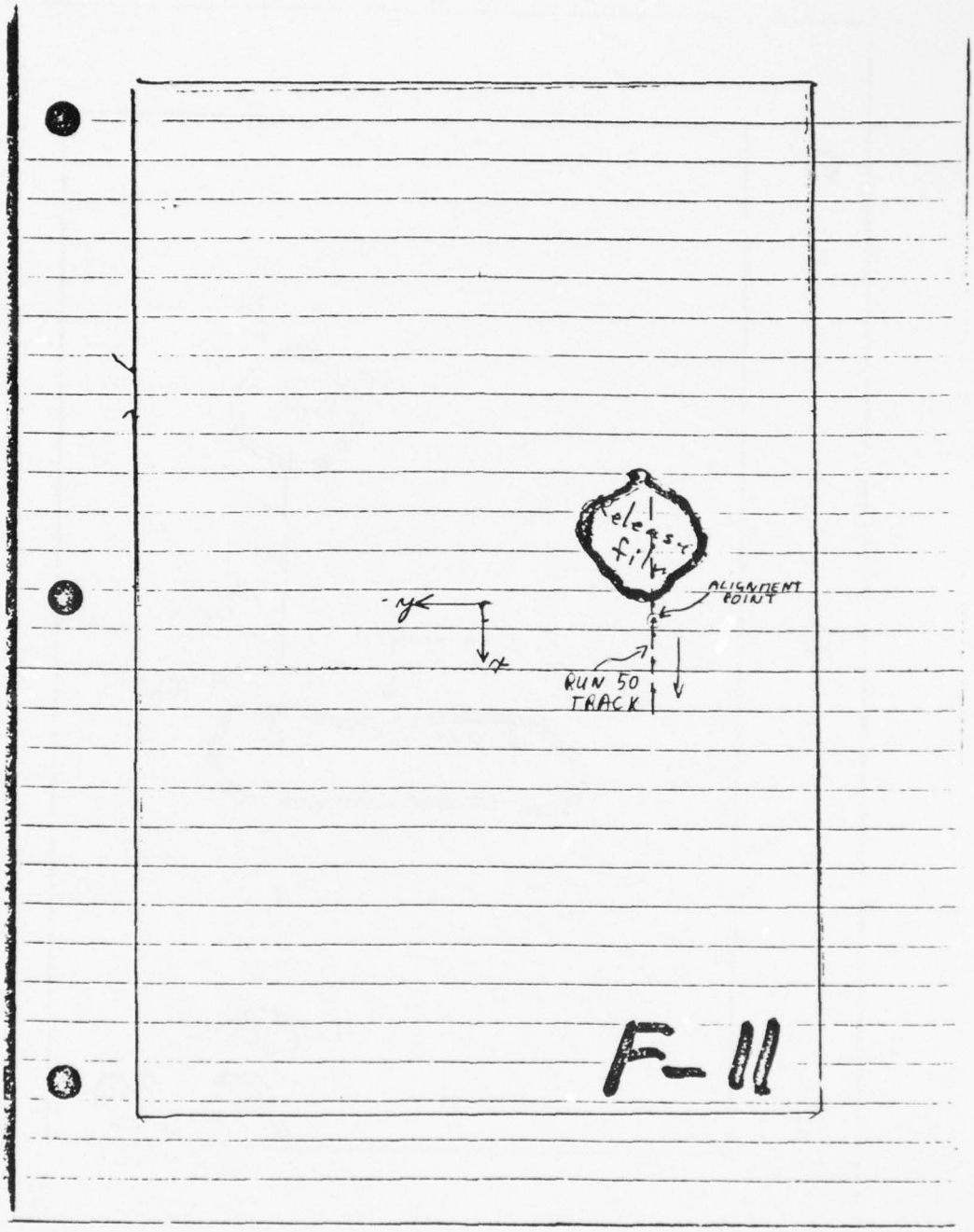

Figure B.9: Sample - F-11
Use - Classifier Design

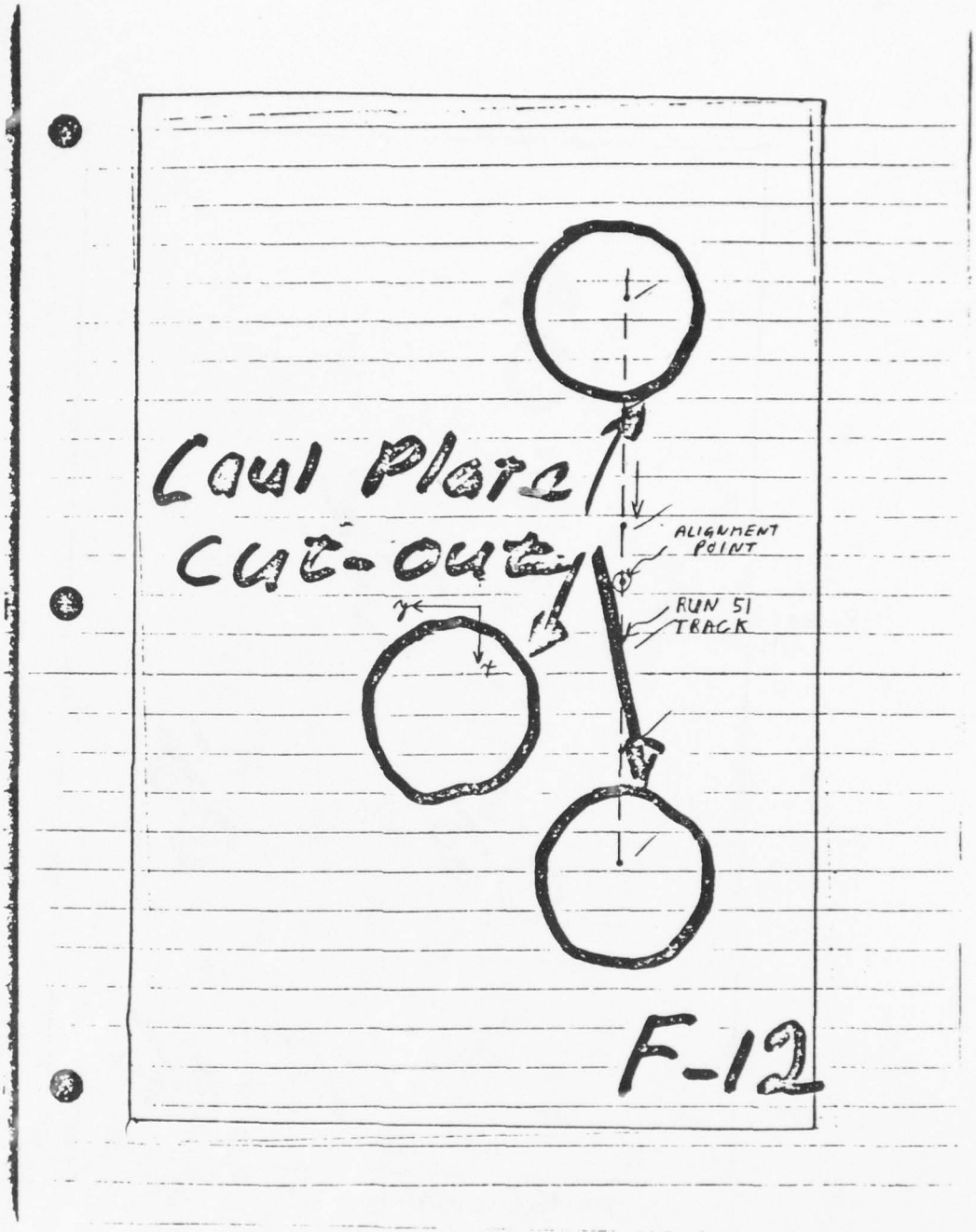

Figure B.10: Sample - F-12
Use - Classifier Design

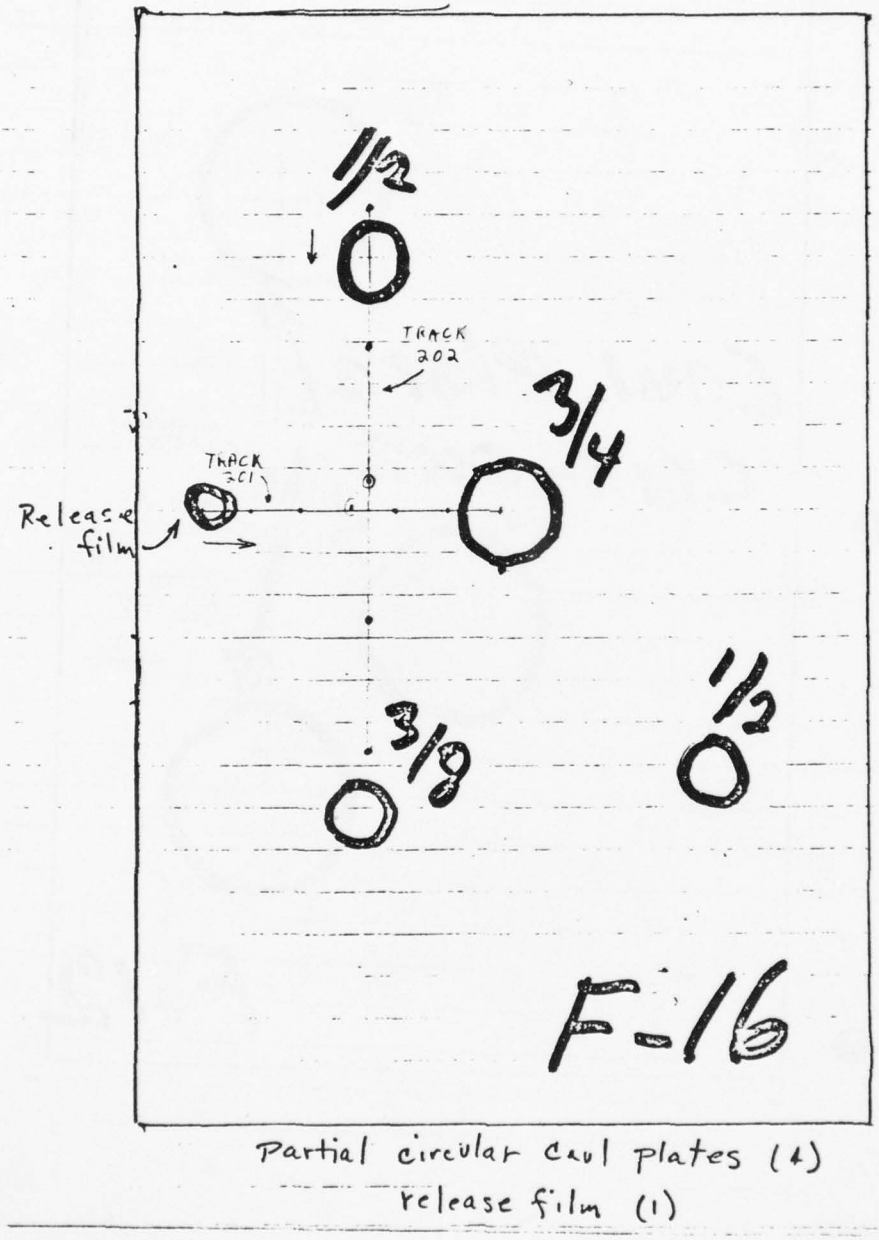

Figure B.11: Sample - F-16
Use - Classifier Evaluation

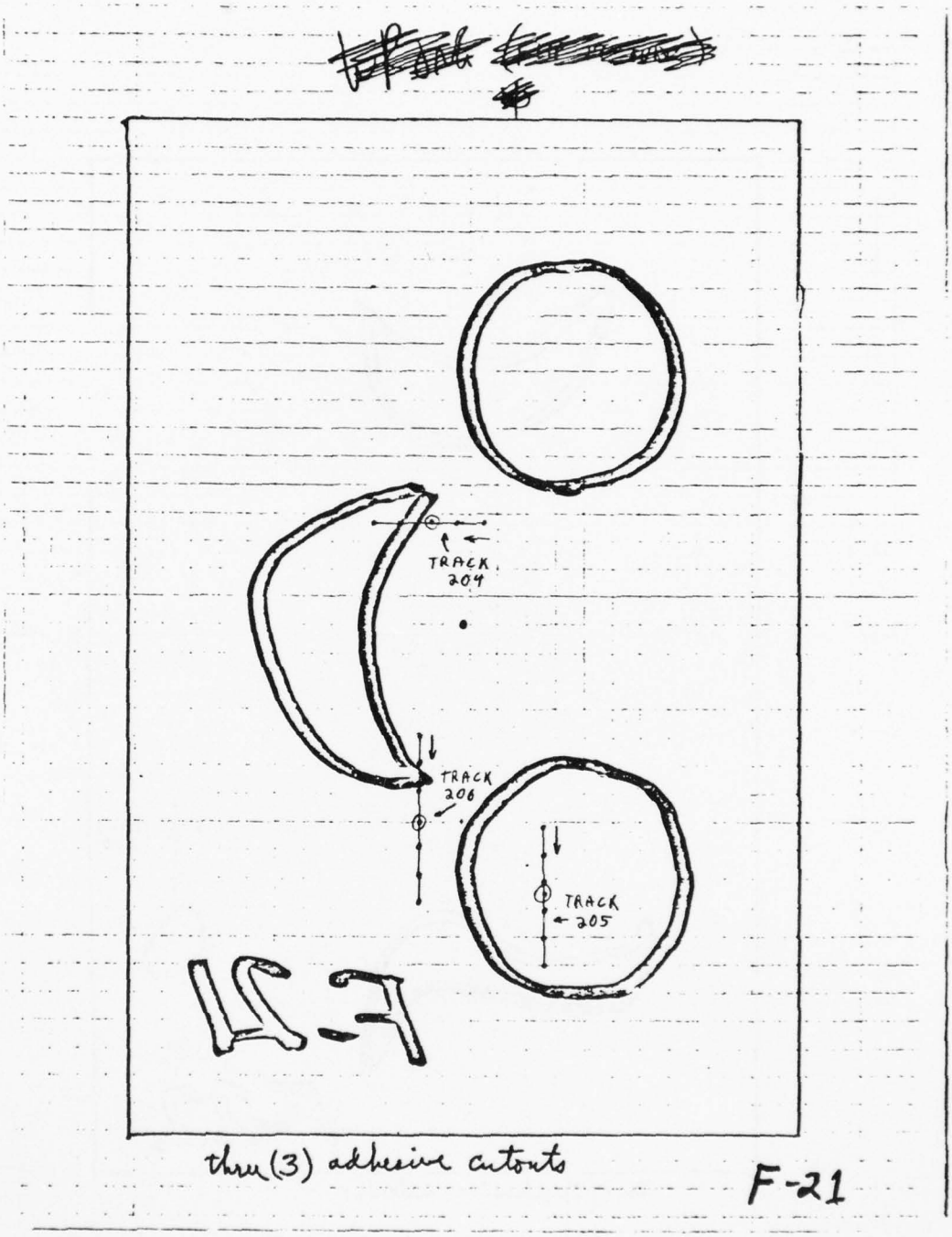

Figure B.12: Sample - F-21
Use - Classifier Evaluation

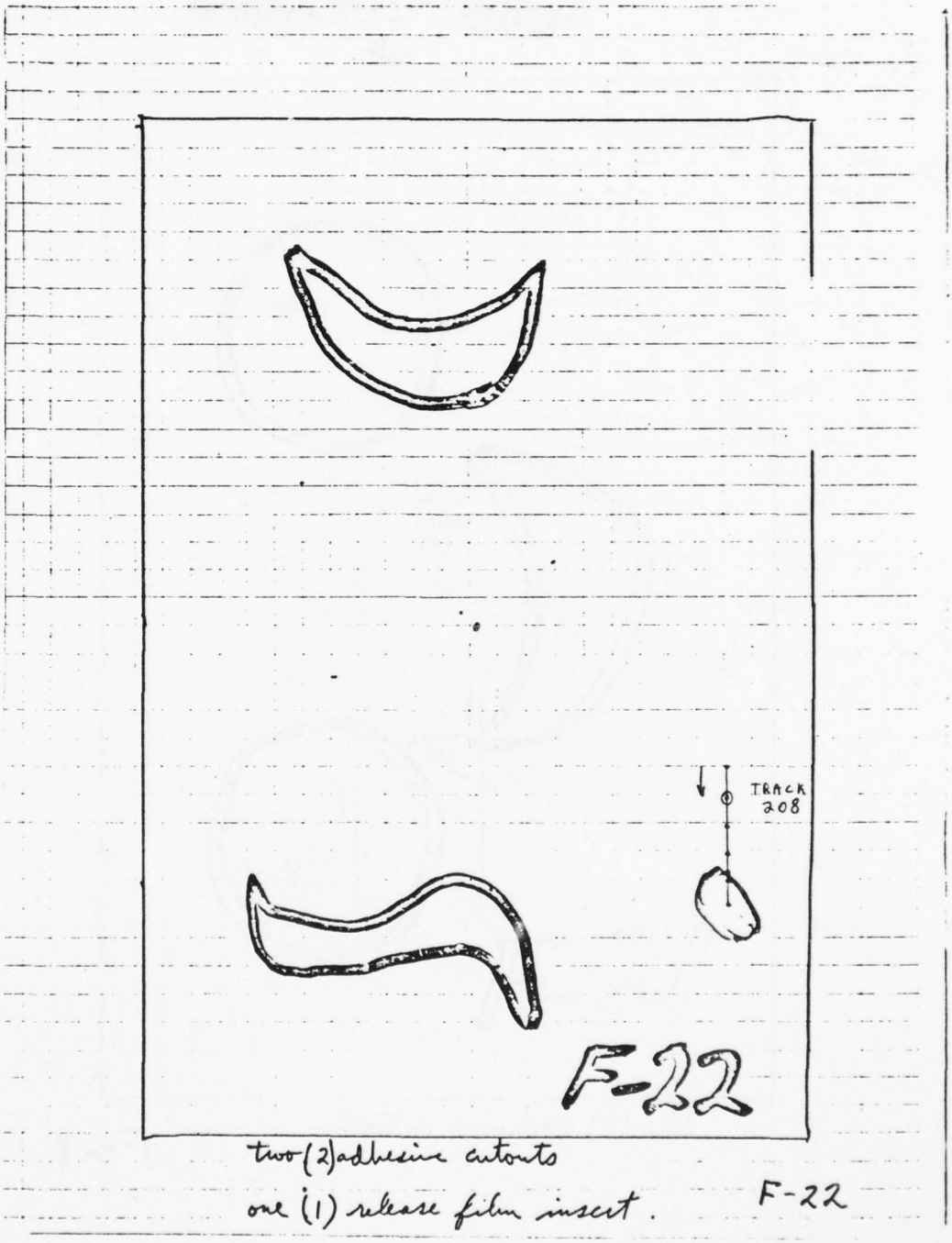

Figure B.13: Sample - F-22
Use - Classifier Evaluation

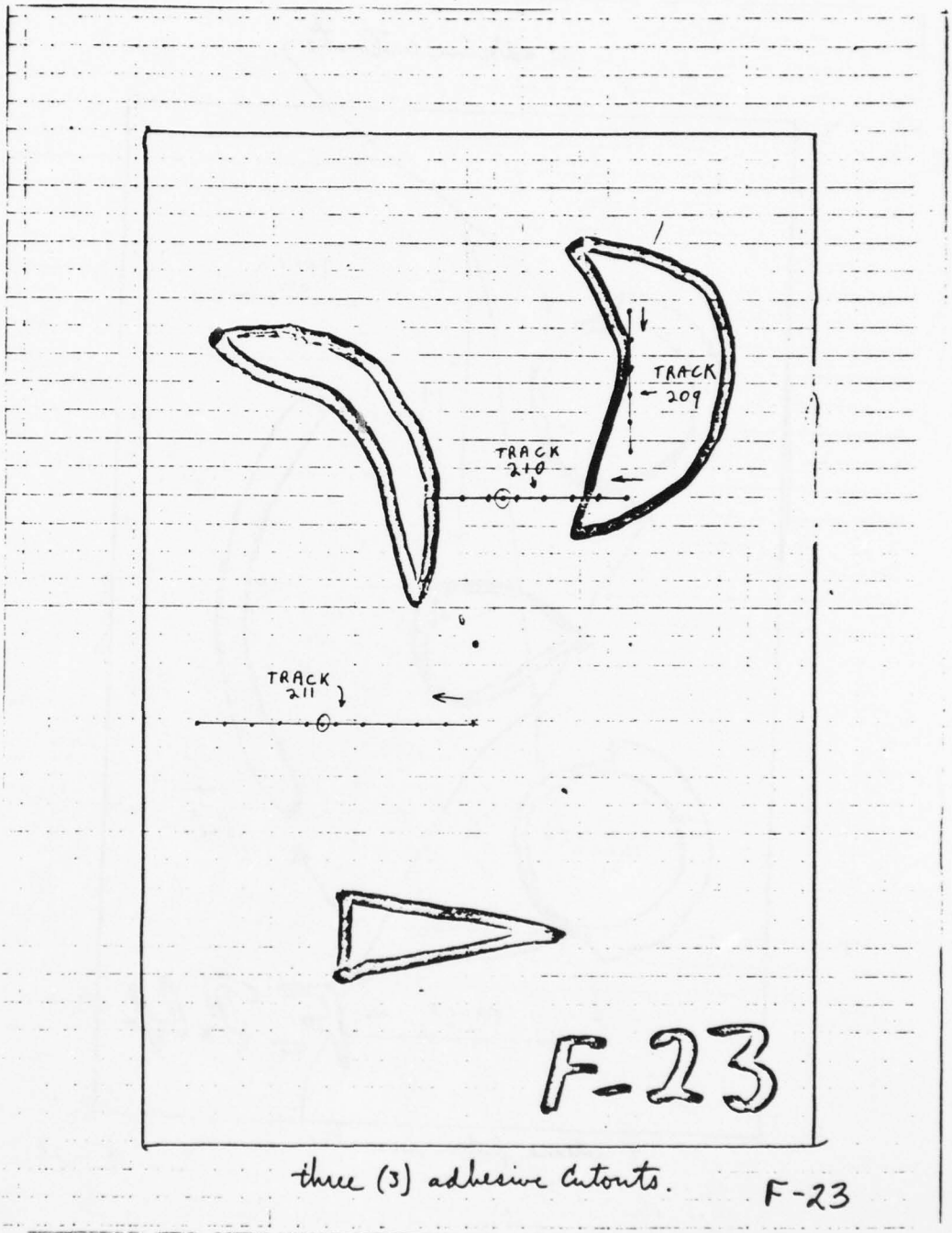

Figure B.14: Sample - F-23
Use - Classifier Evaluation

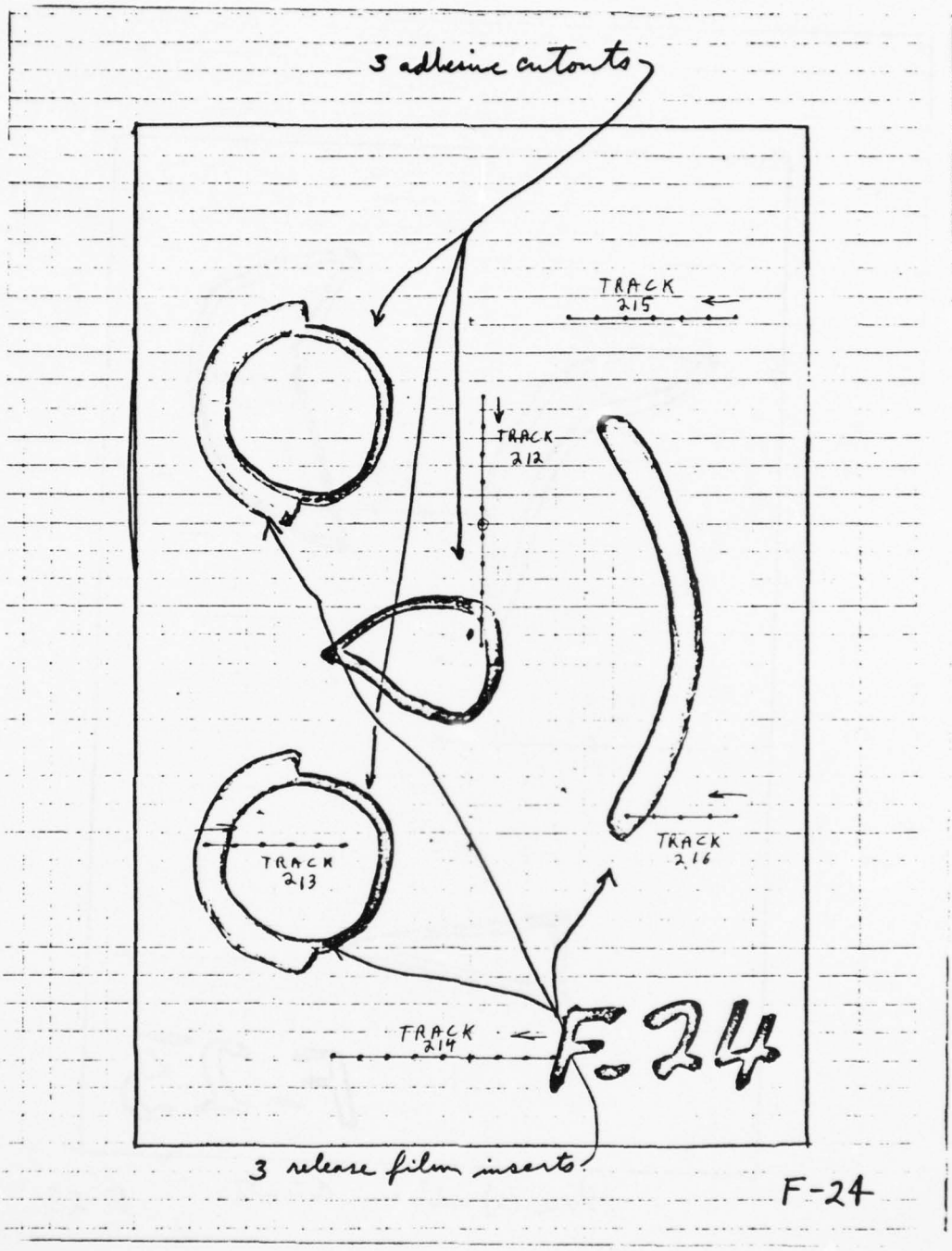

Figure B.15: Sample - F-24
Use - Classifier Evaluation

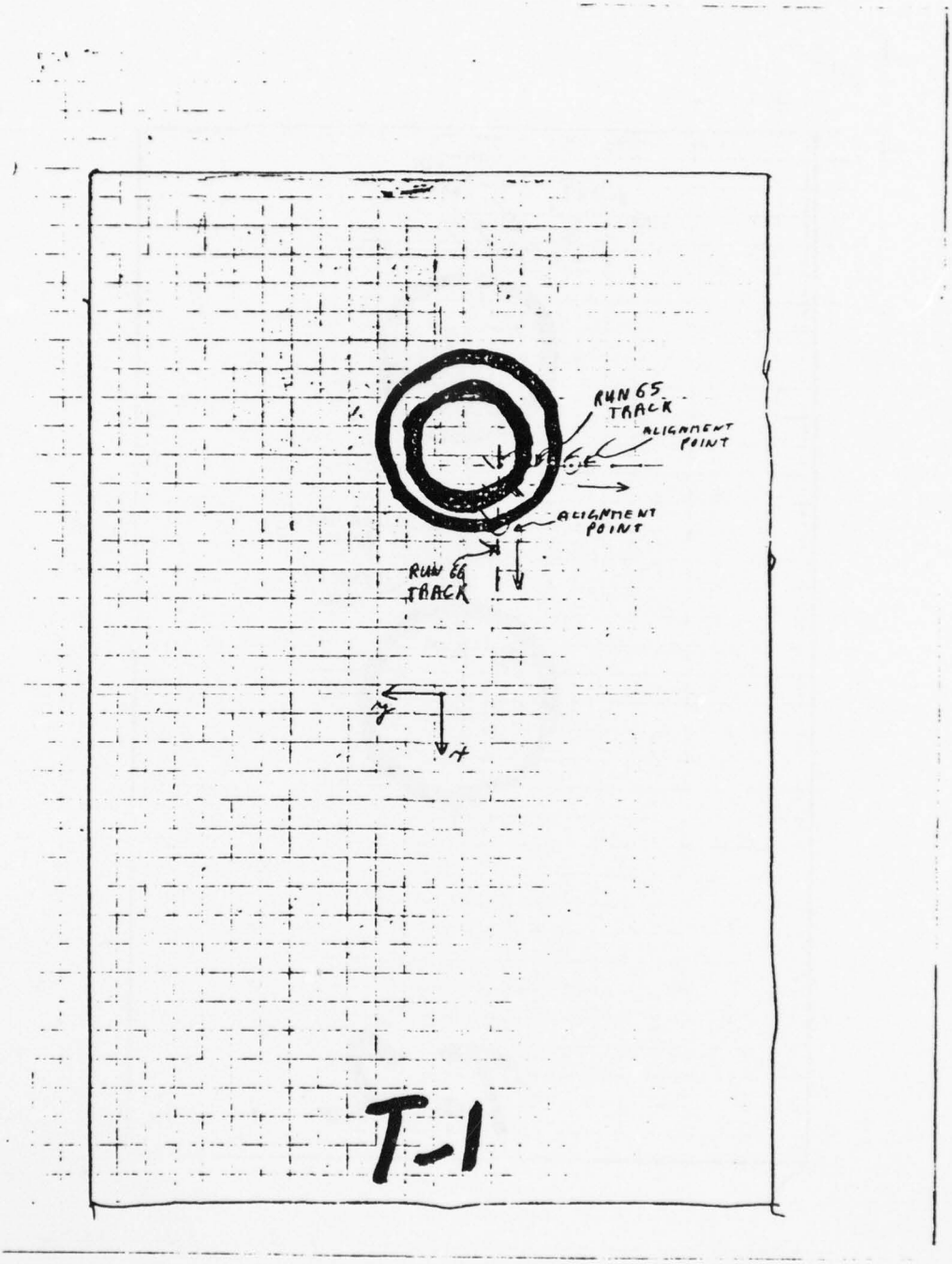

Figure B.16: Sample - T-1
Use - Classifier Design

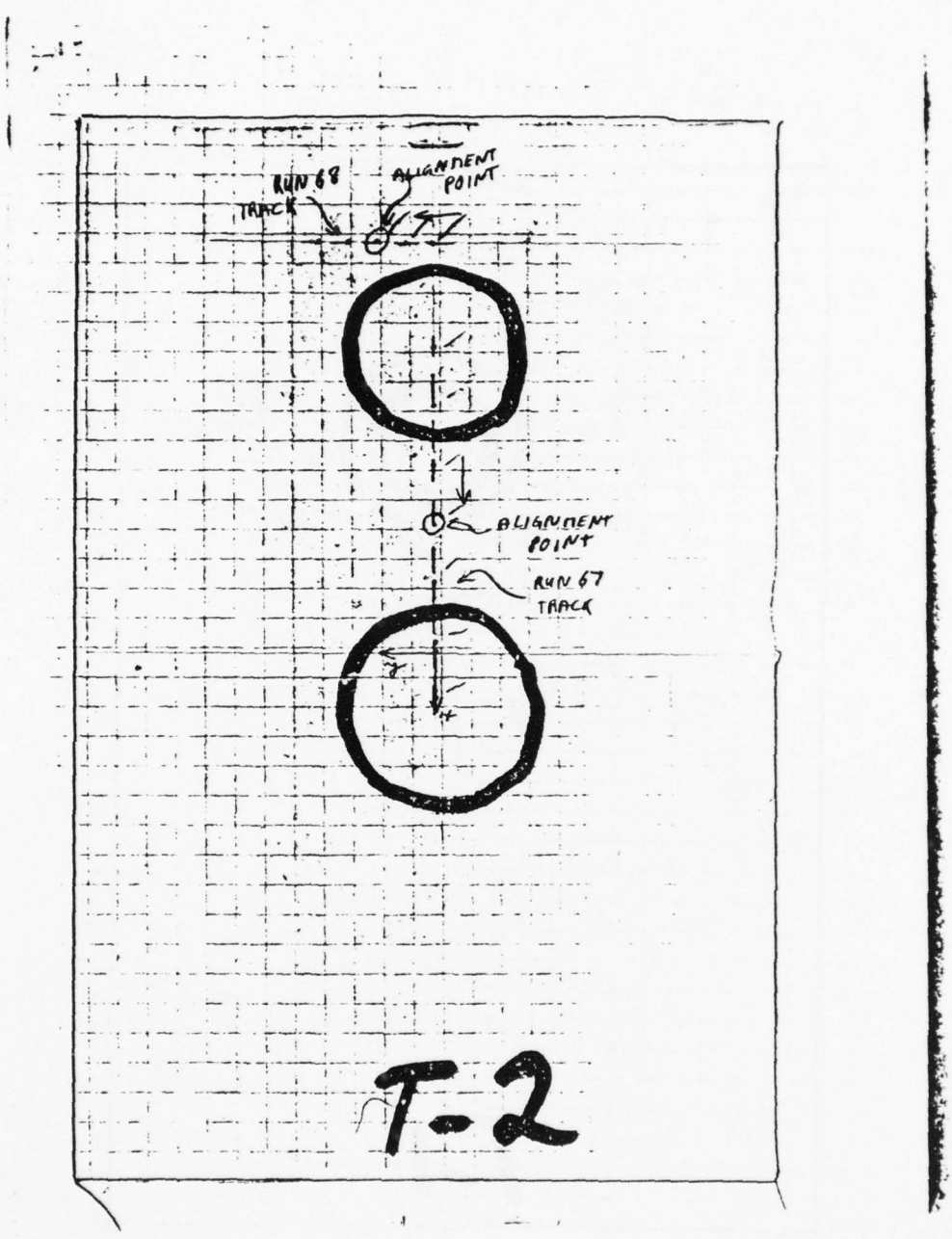

Figure B.17: Sample - T-2
Use - Classifier Design

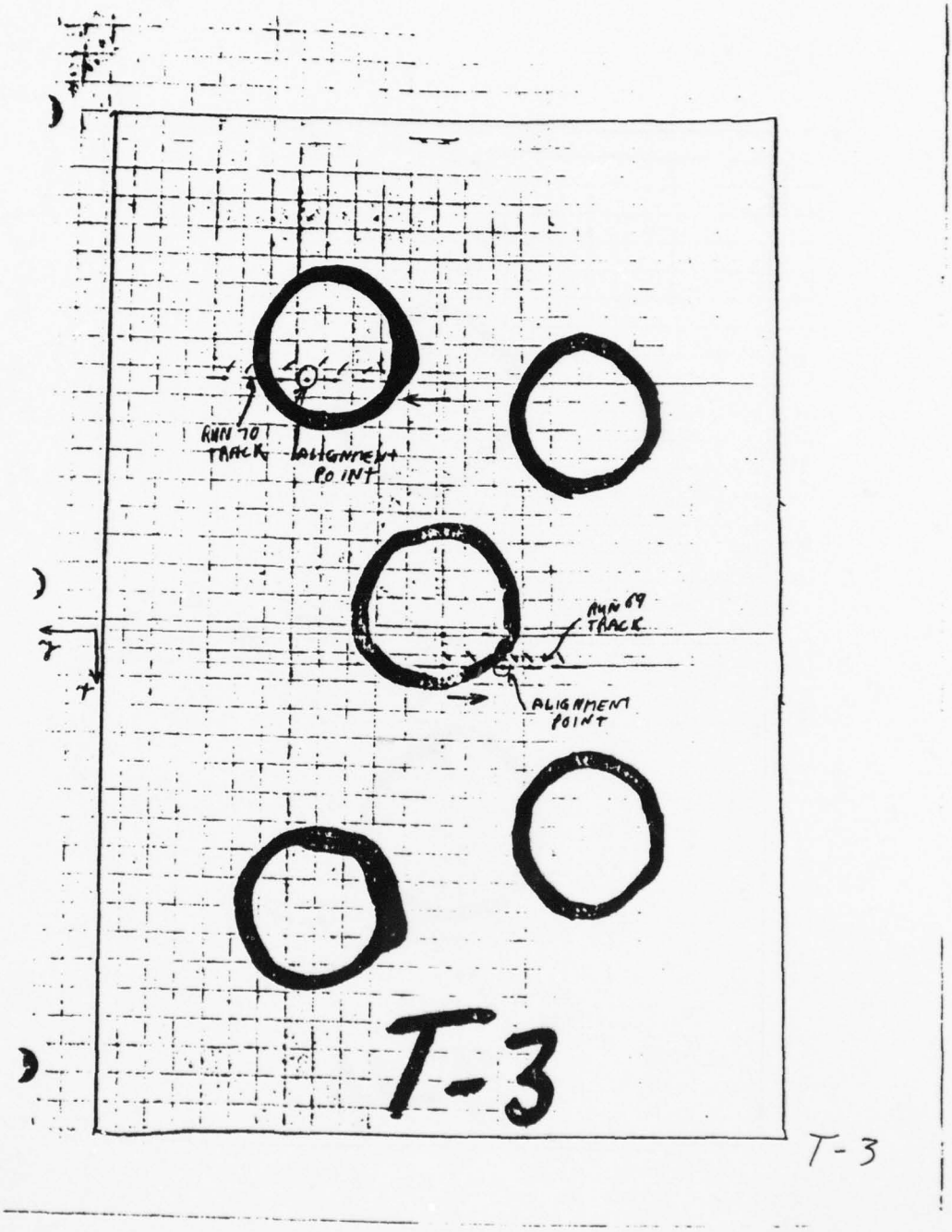

Figure B.18: Sample - T-3
Use - Classifier Design

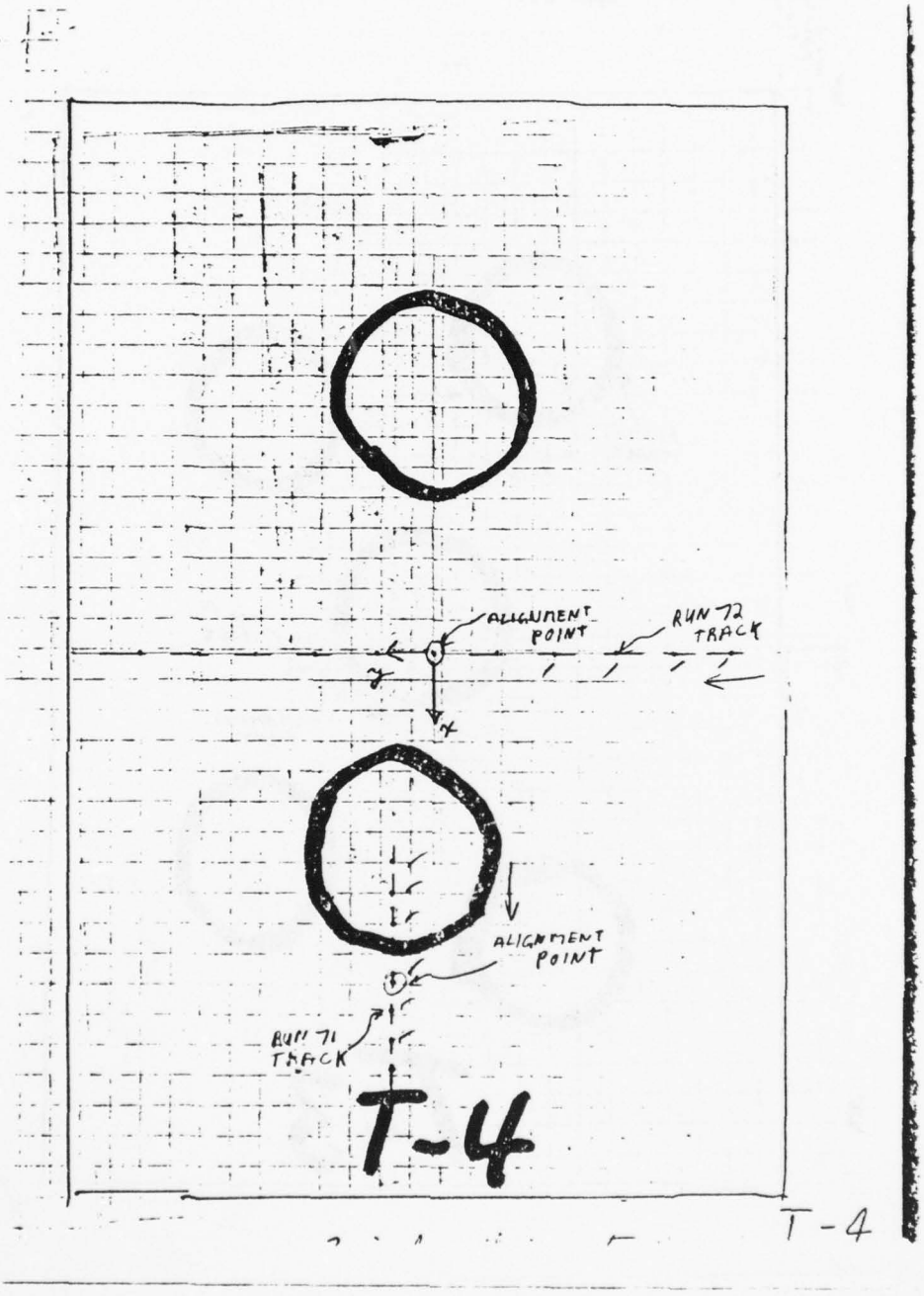

Figure B.19: Sample - T-4
Use - Classifier Design

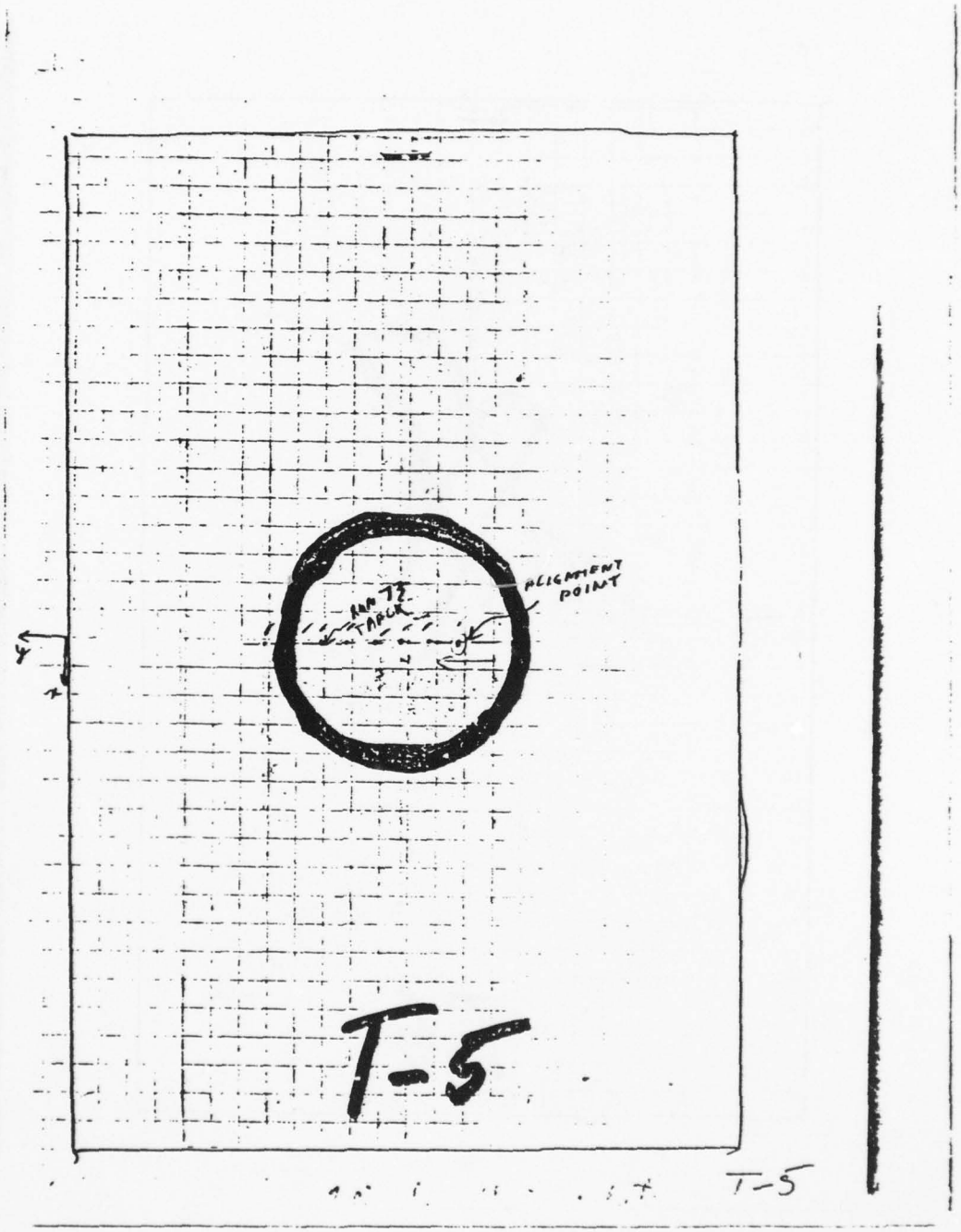

Figure B.20: Sample - T-5
Use - Classifier Design

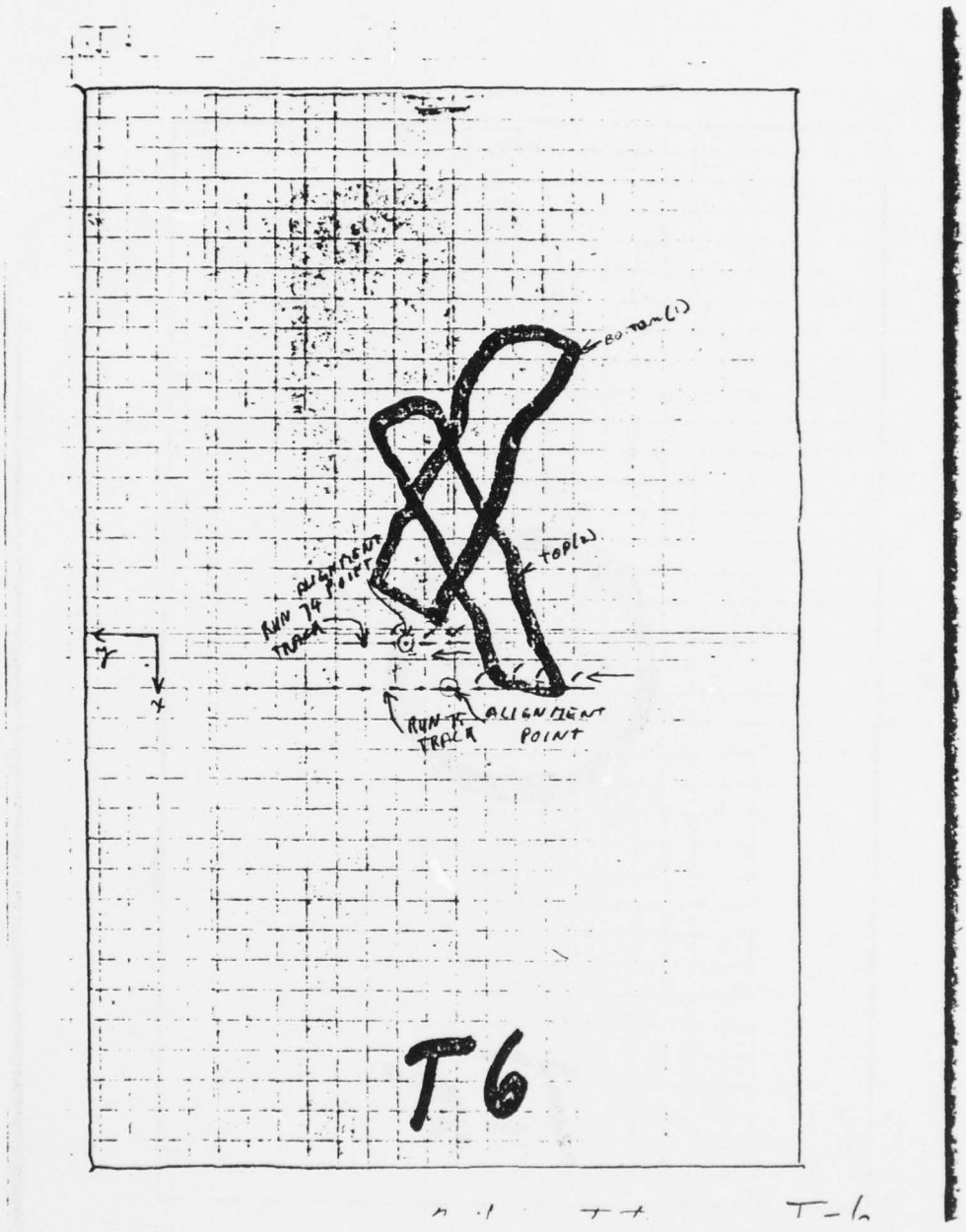

Figure B.21: Sample - T-6
Use - Classifier Design

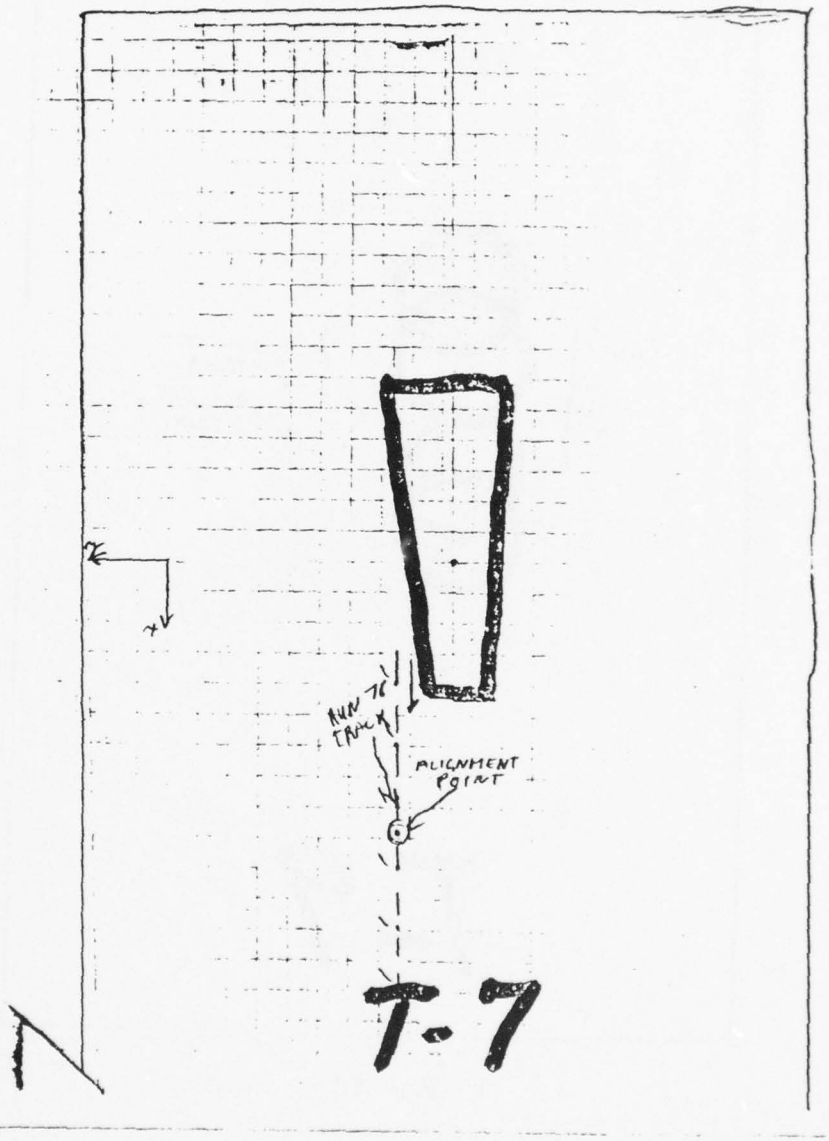

Figure B.22: Sample - T-7
Use - Classifier Design

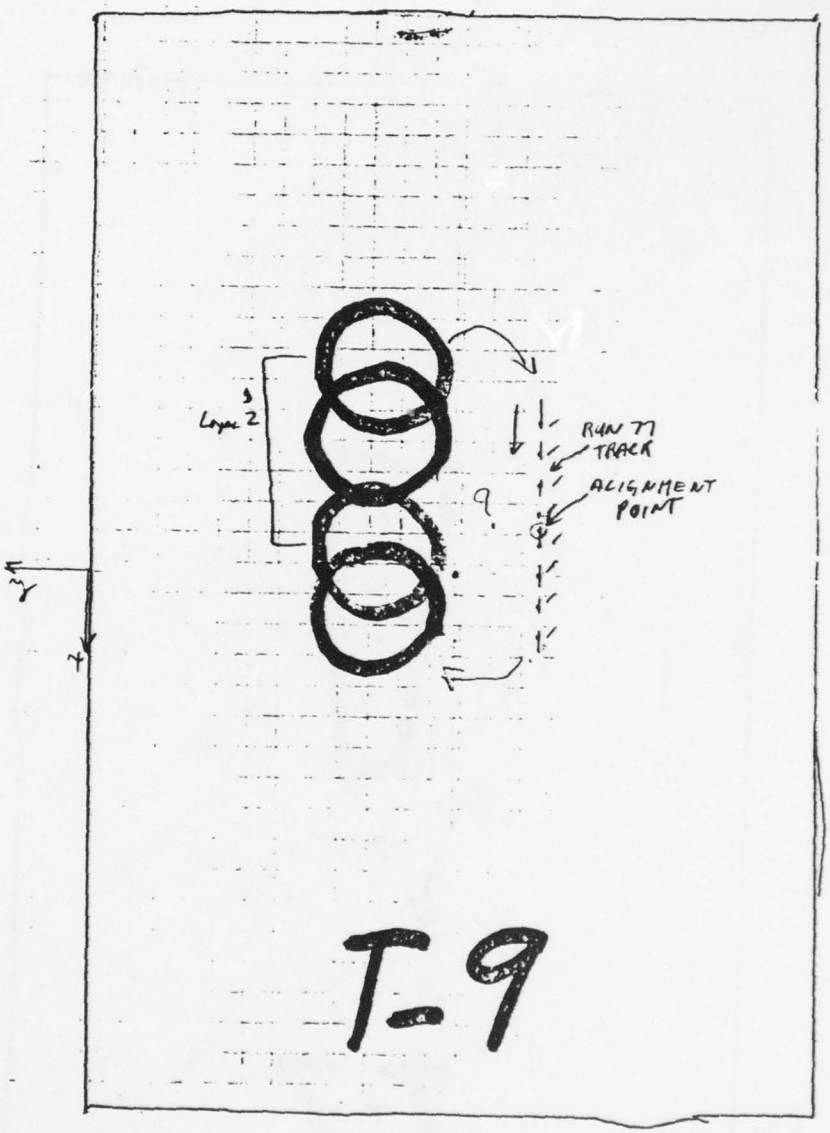

Figure B.23: Sample - T-9
Use - Classifier Design

AD-A072 724 ADAPTRONICS INC MCLEAN VA F/G 14/2
EXPLORATORY DEVELOPMENT OF ADHESIVE BOND FLAW DETECTION.(U)
DEC 78 M H LOEW, J M FITZGERALD F33615-76-C-5079
UNCLASSIFIED AFML-TR-78-206 NL

2 OF 2
ADA
072724

END
DATE
FILMED
9-79
DDC

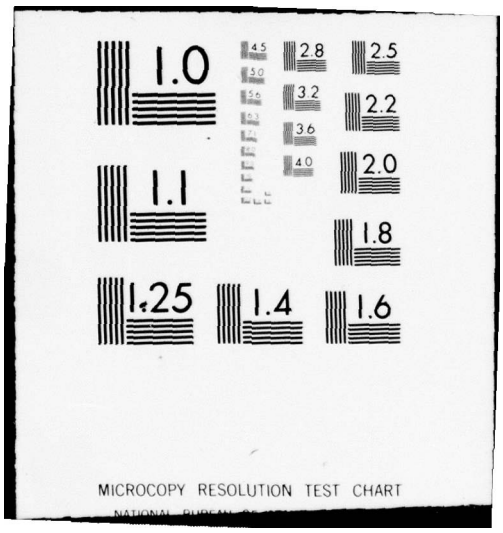
1.0
1.1
1.25
1.4
1.6
1.8
2.0
2.2
2.5
2.8
3.2
3.6
4.0
4.5
5.0
5.6
6.3
MICROCOPY RESOLUTION TEST CHART

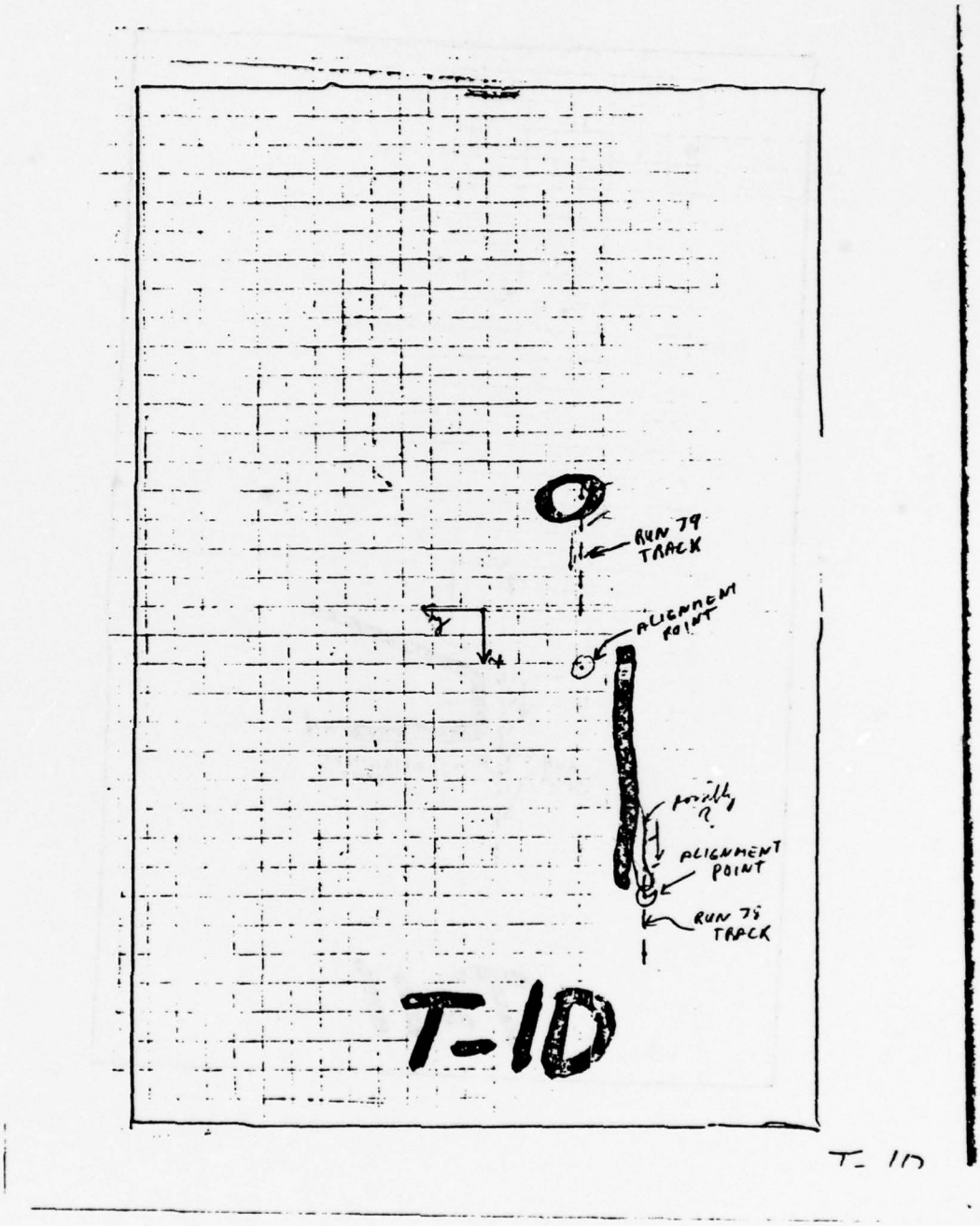

Figure B.24: Sample - T-10
Use - Classifier Design

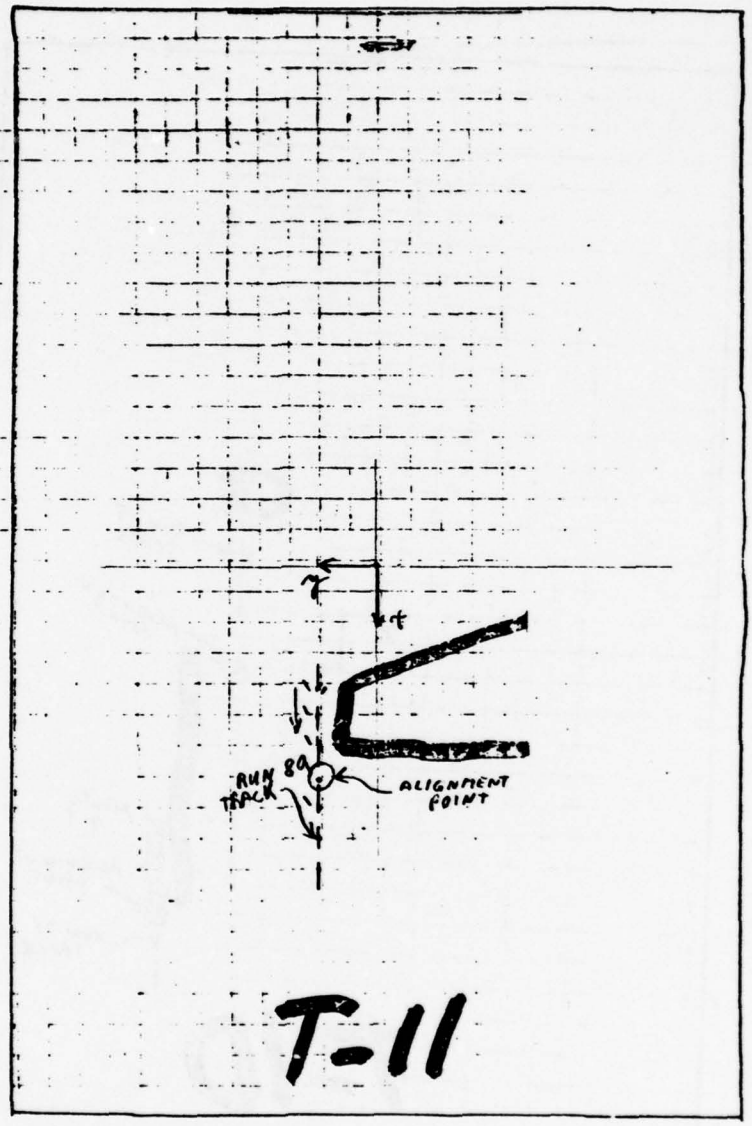

Figure B.25: Sample - T-11
Use - Classifier Design

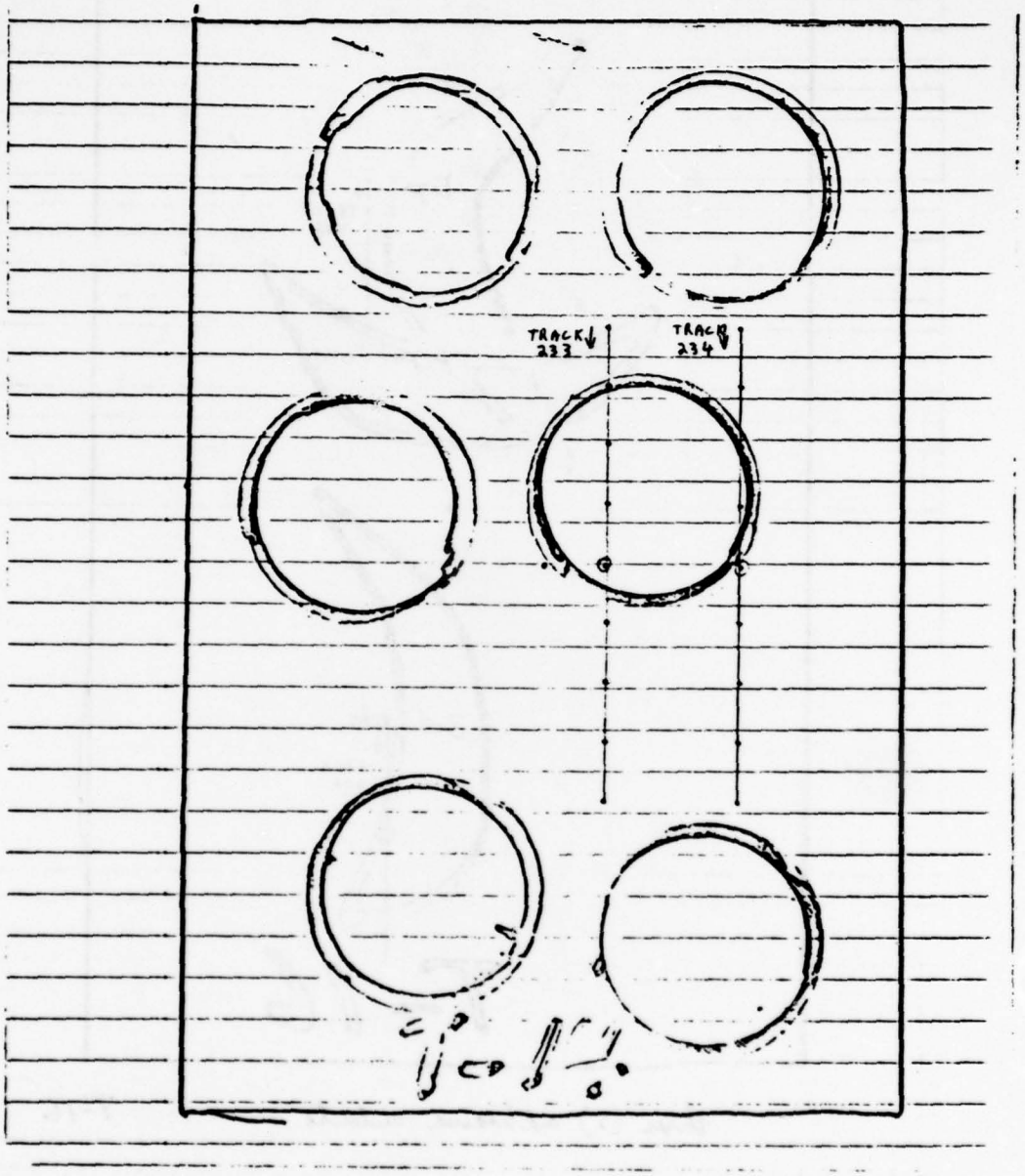

Figure B.26: Sample - T-14
Use - Classifier Evaluation

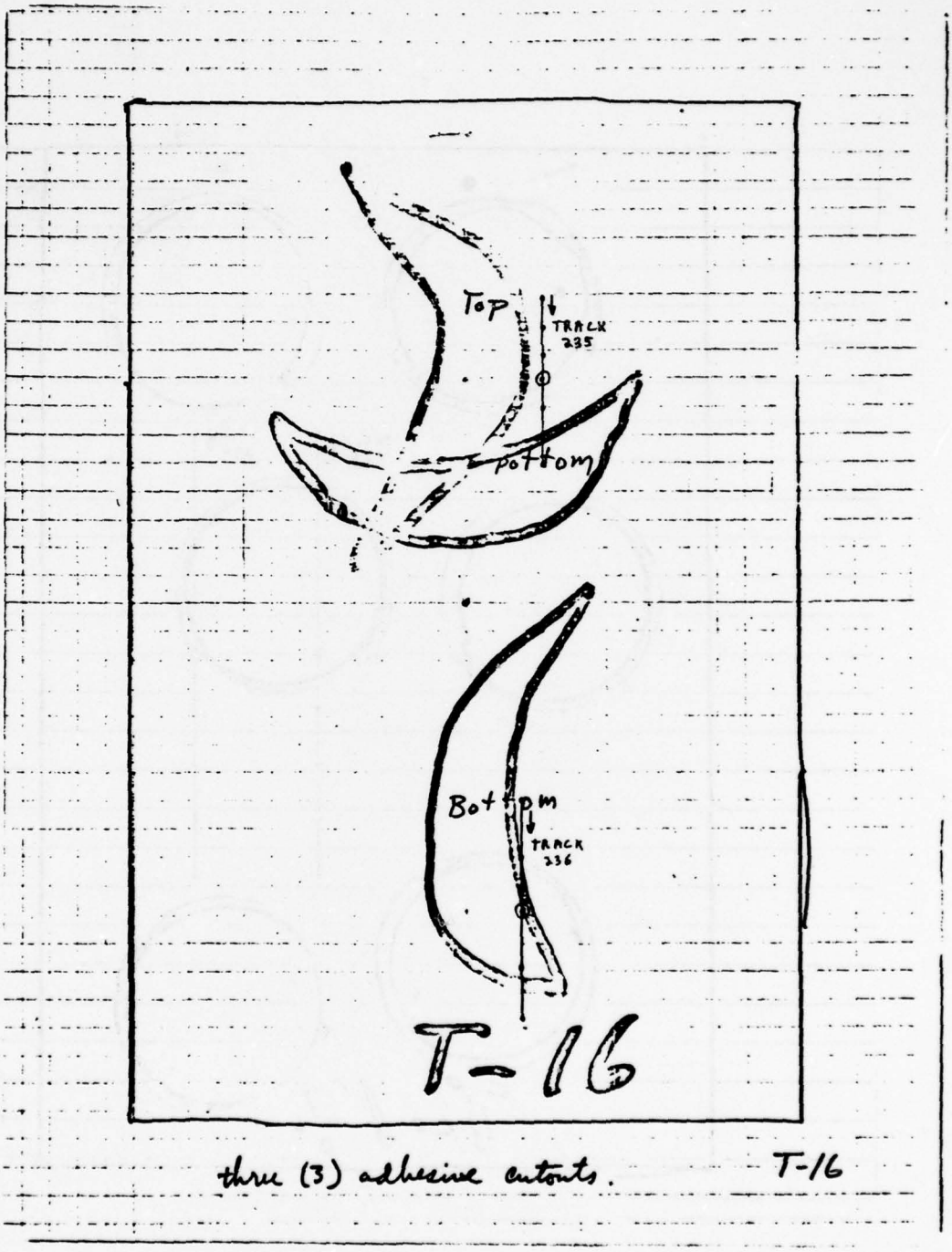

Figure B.27: Sample - T-16
Use - Classifier Evaluation

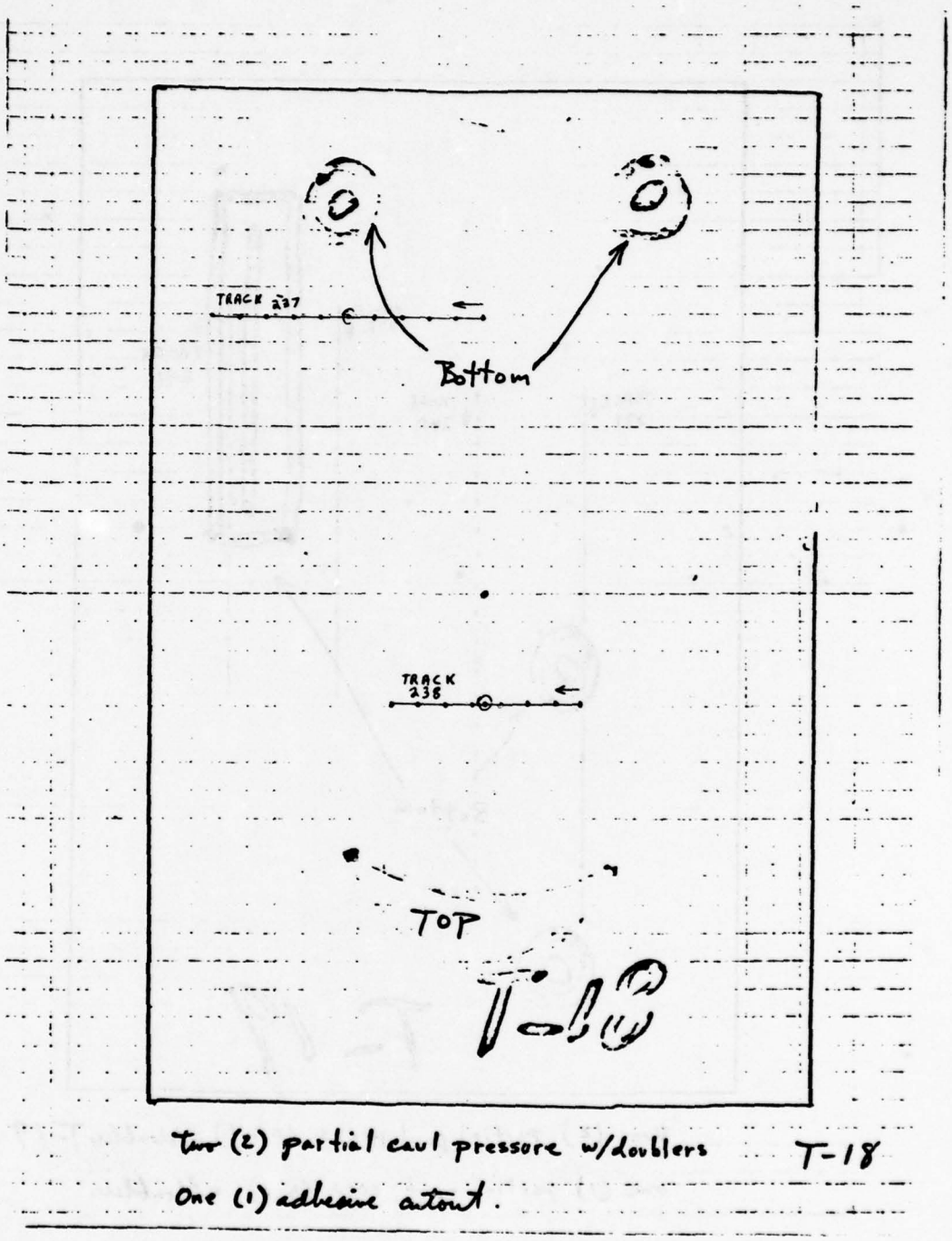

Figure B.28: Sample - T-18
Use - Classifier Evaluation

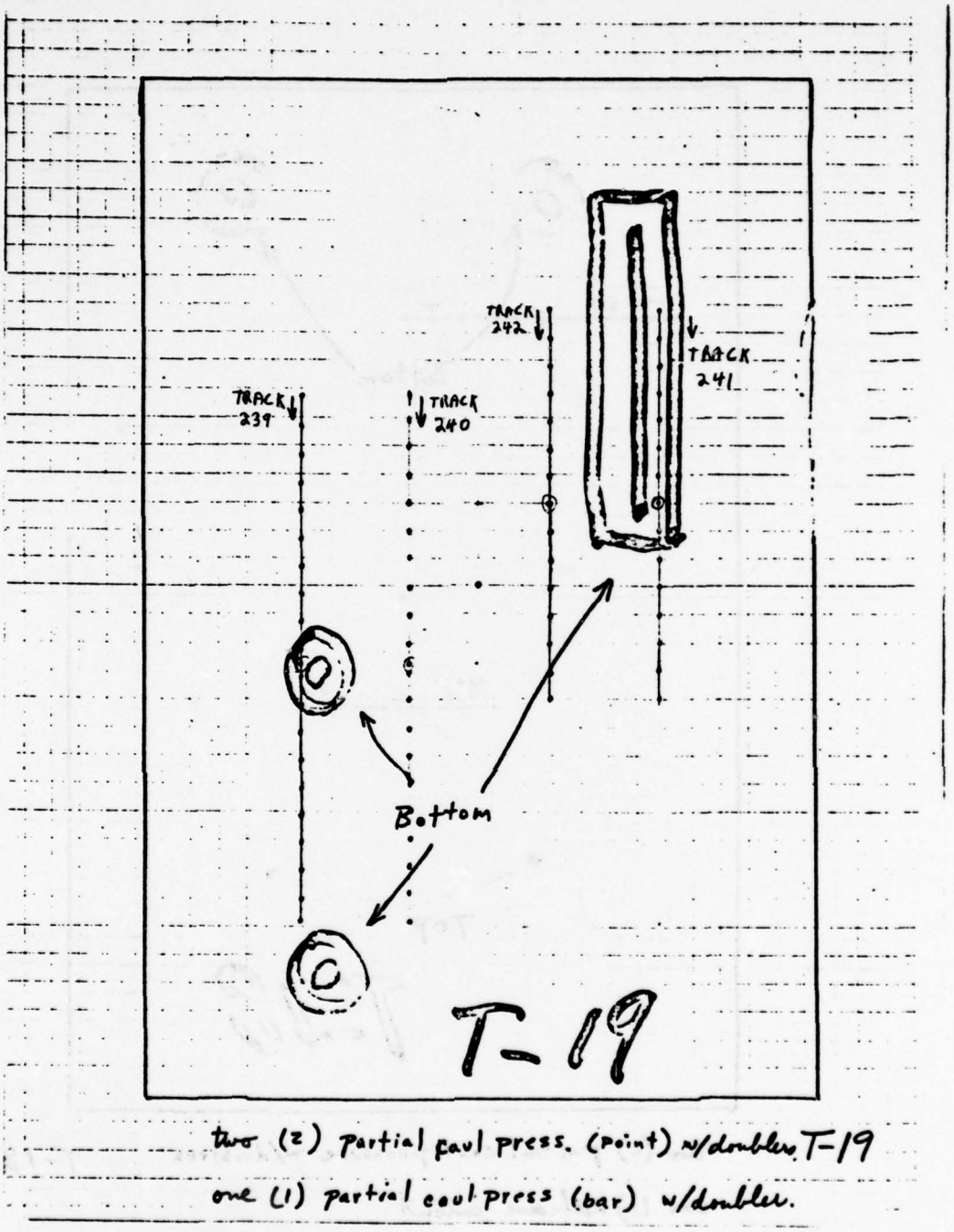

Figure B.29: Sample - T-19
Use - Classifier Evaluation

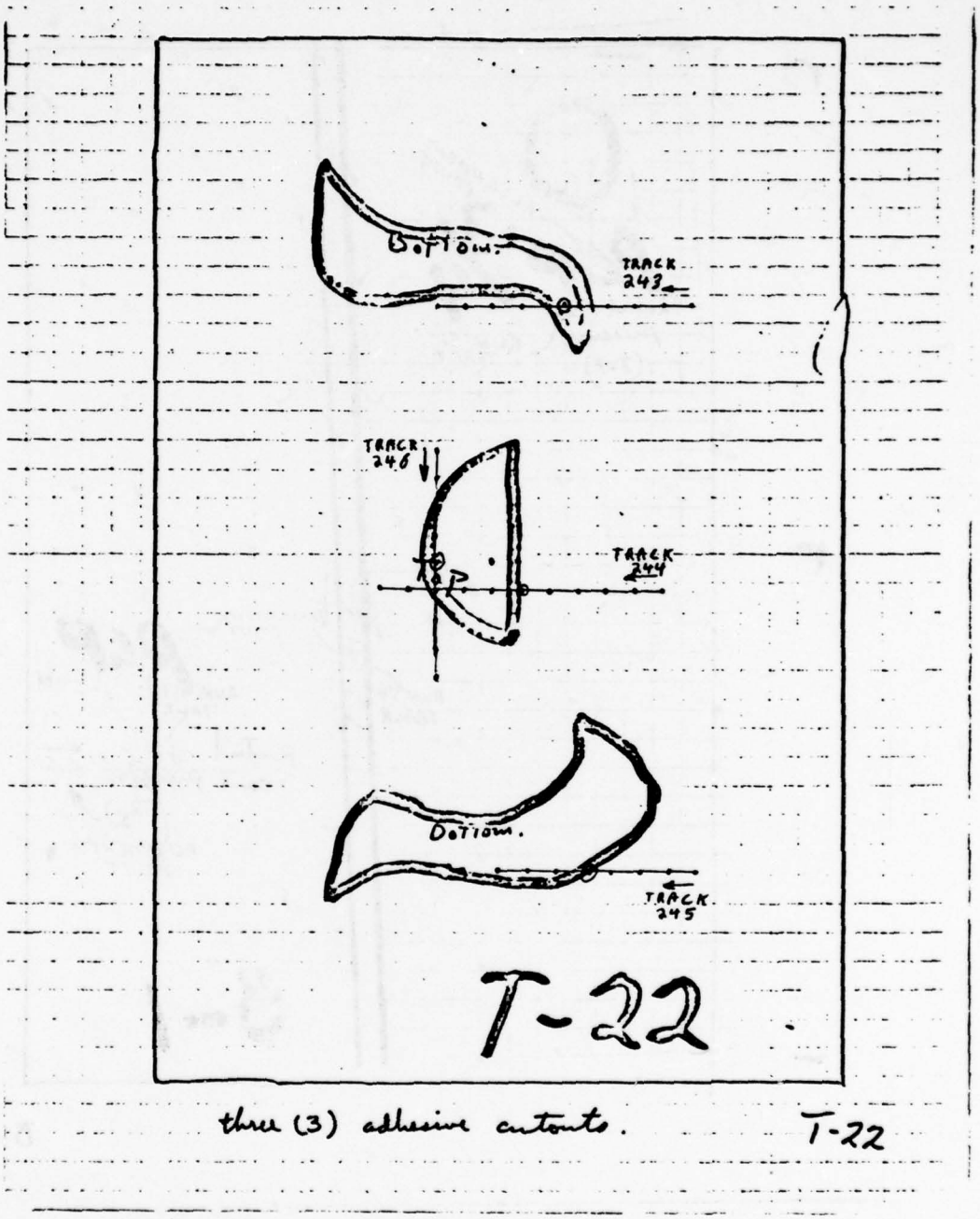

Figure B.30: Sample - T-22
Use - Classifier Evaluation

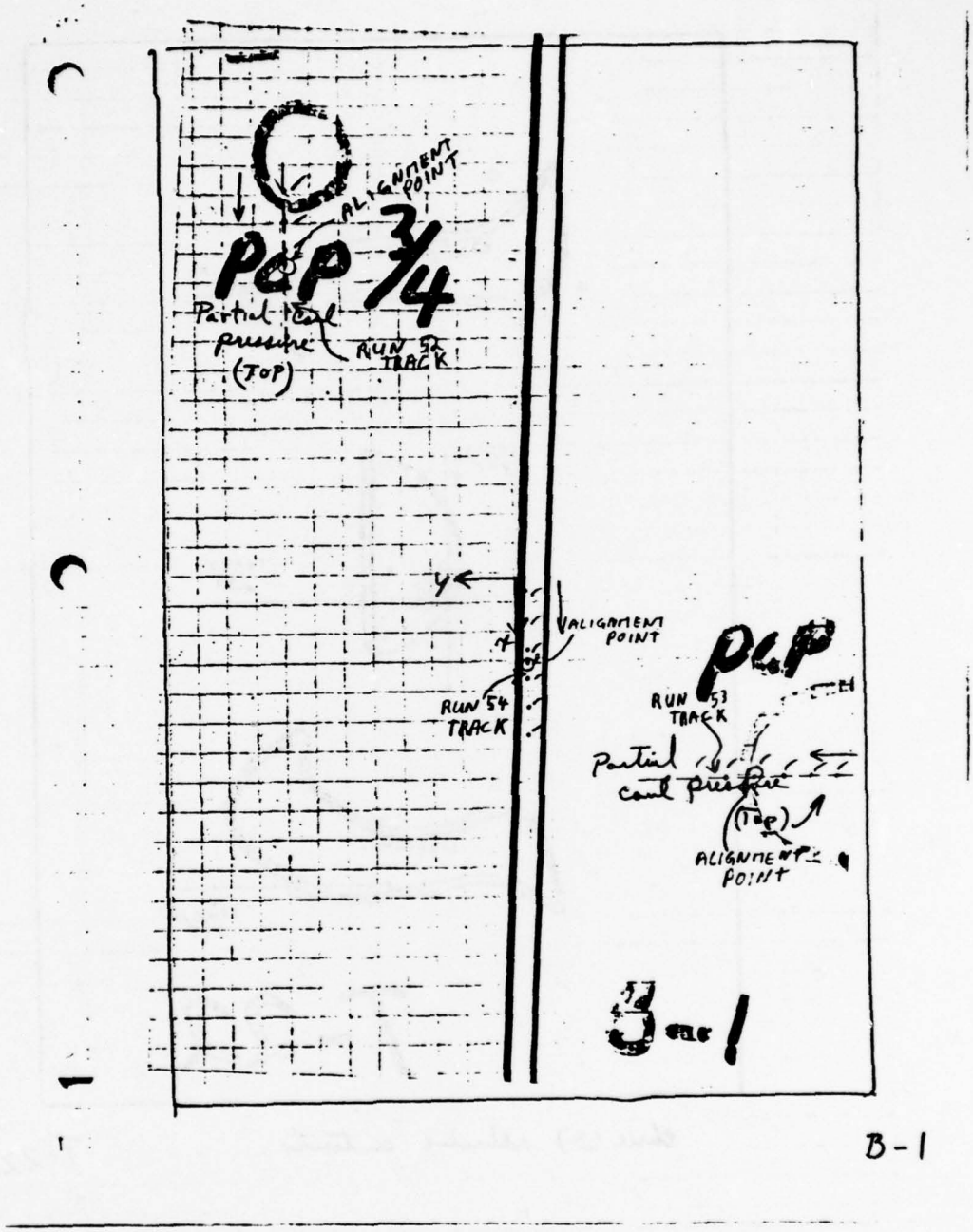

Figure B.31: Sample - B-1
Use - Classifier Design

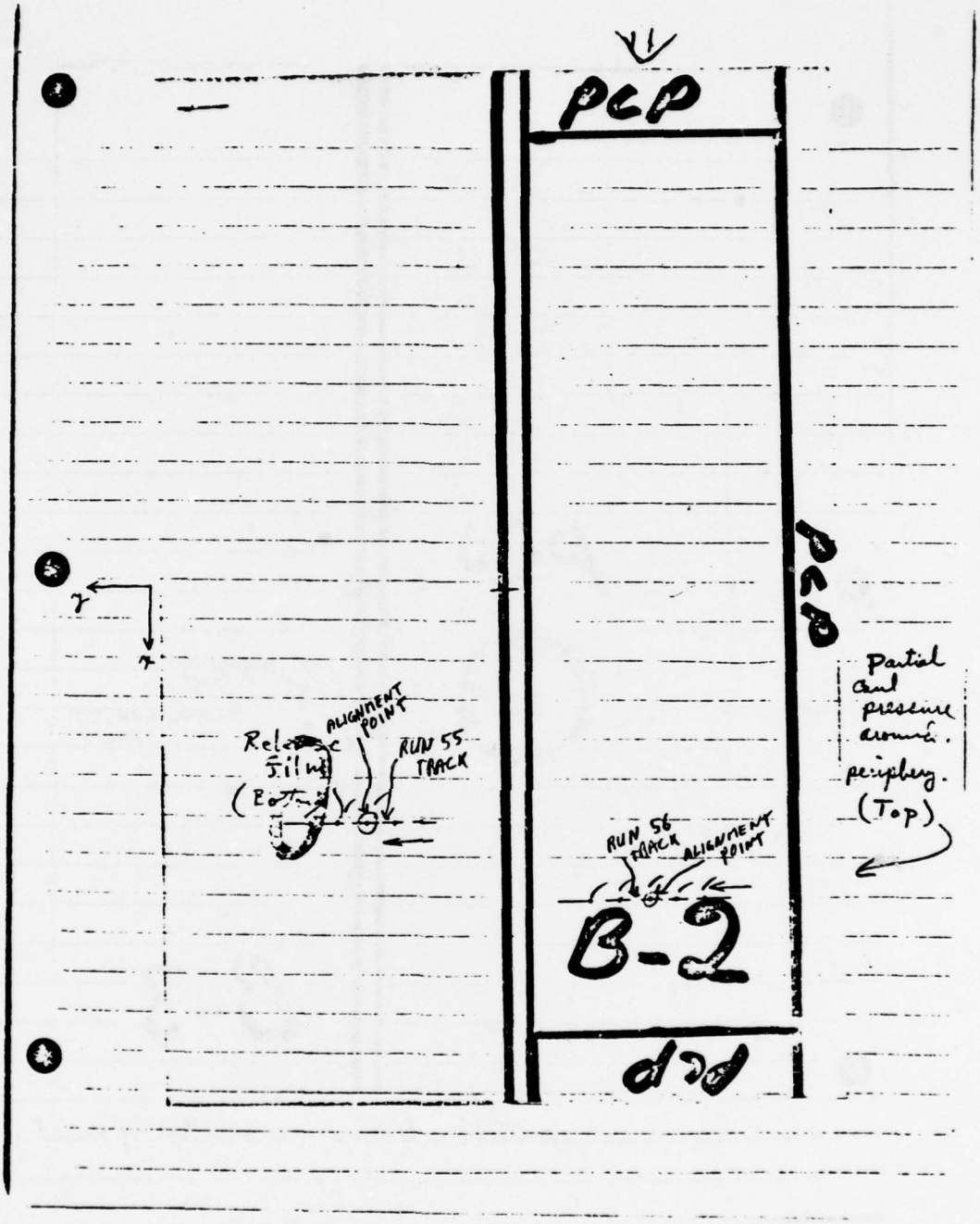

Figure B.32: Sample - B-2
Use - Classifier Design

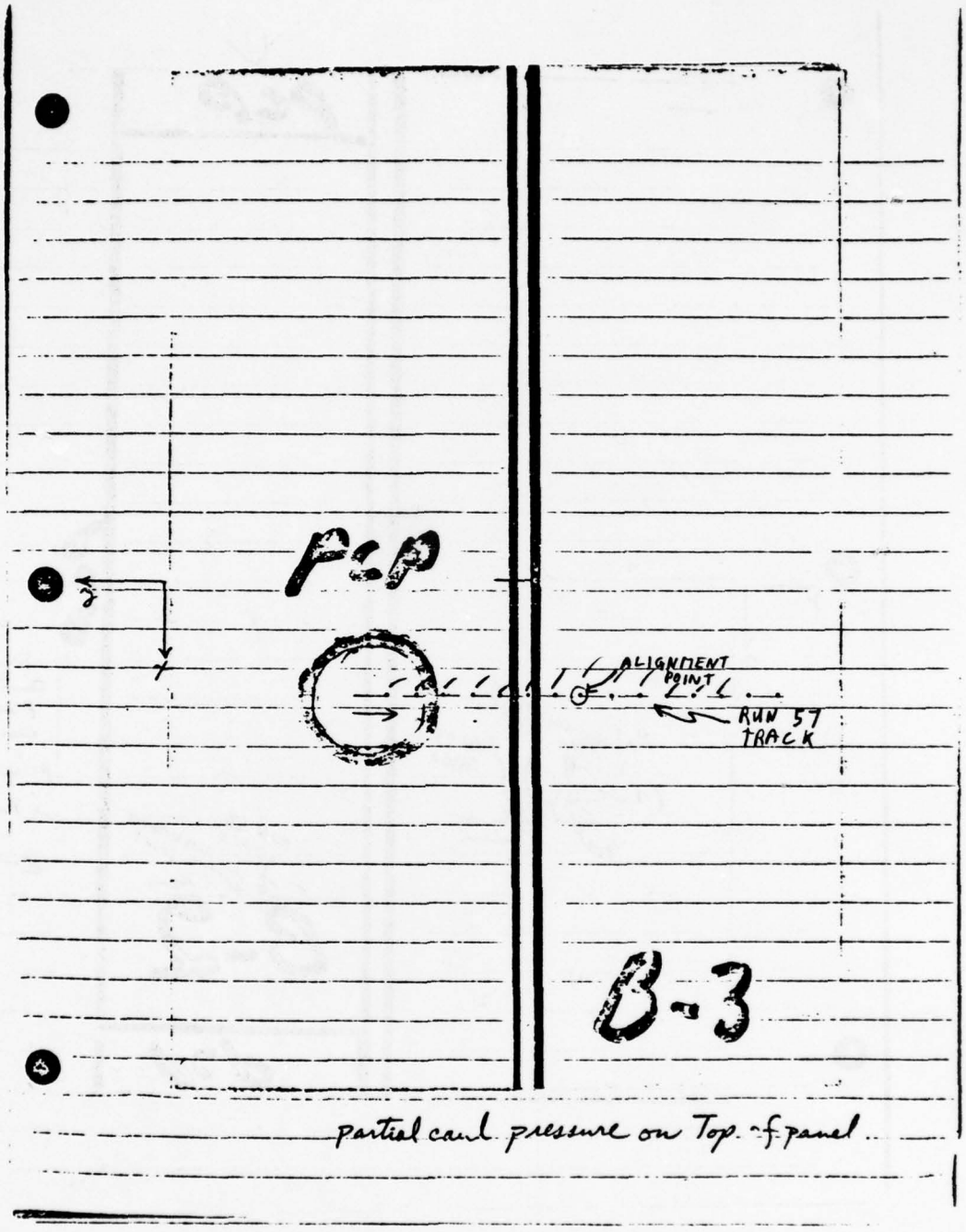

Figure B.33: Sample - B-3
Use - Classifier Design

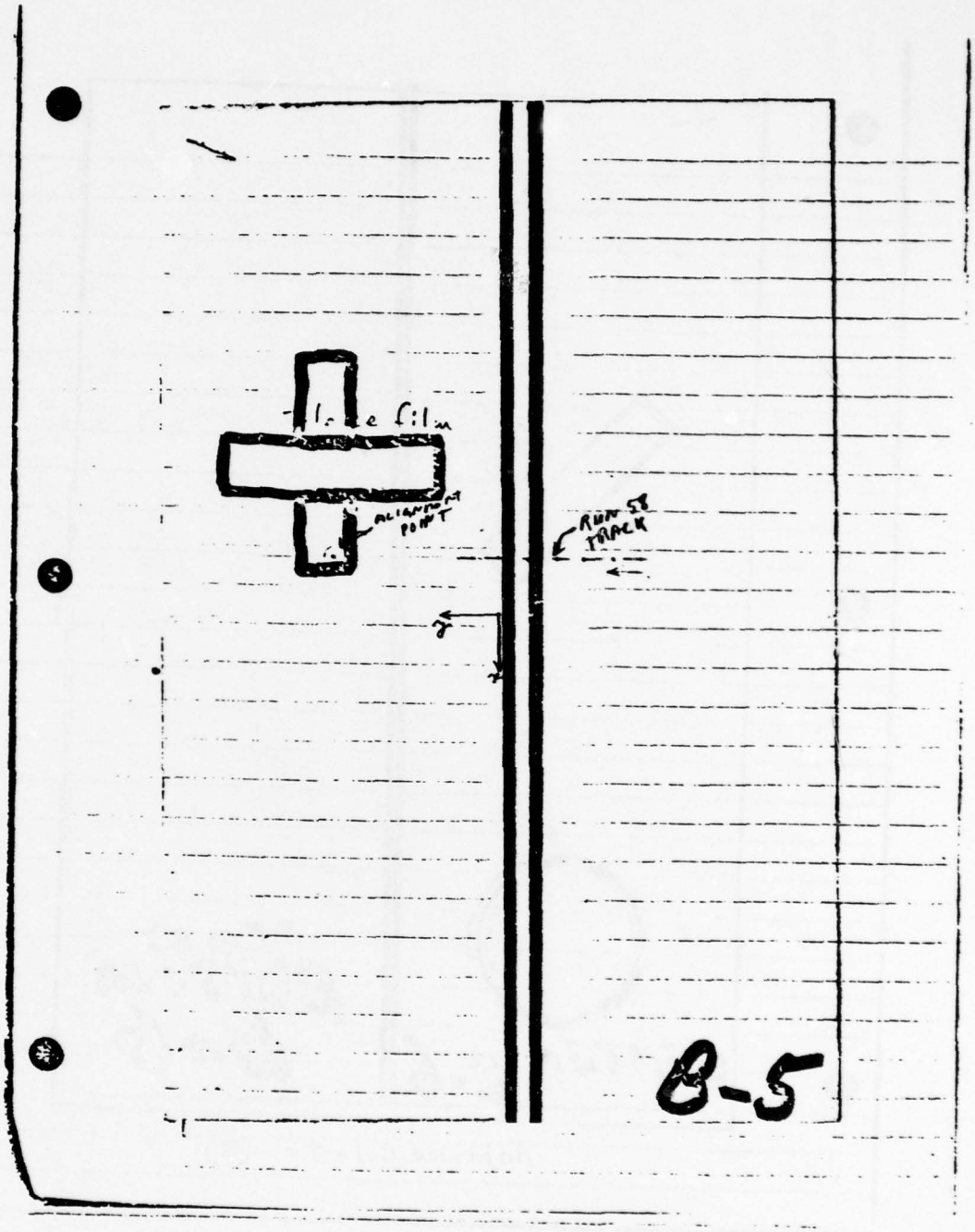

Figure B.34: Sample - B-5
Use - Classifier Design

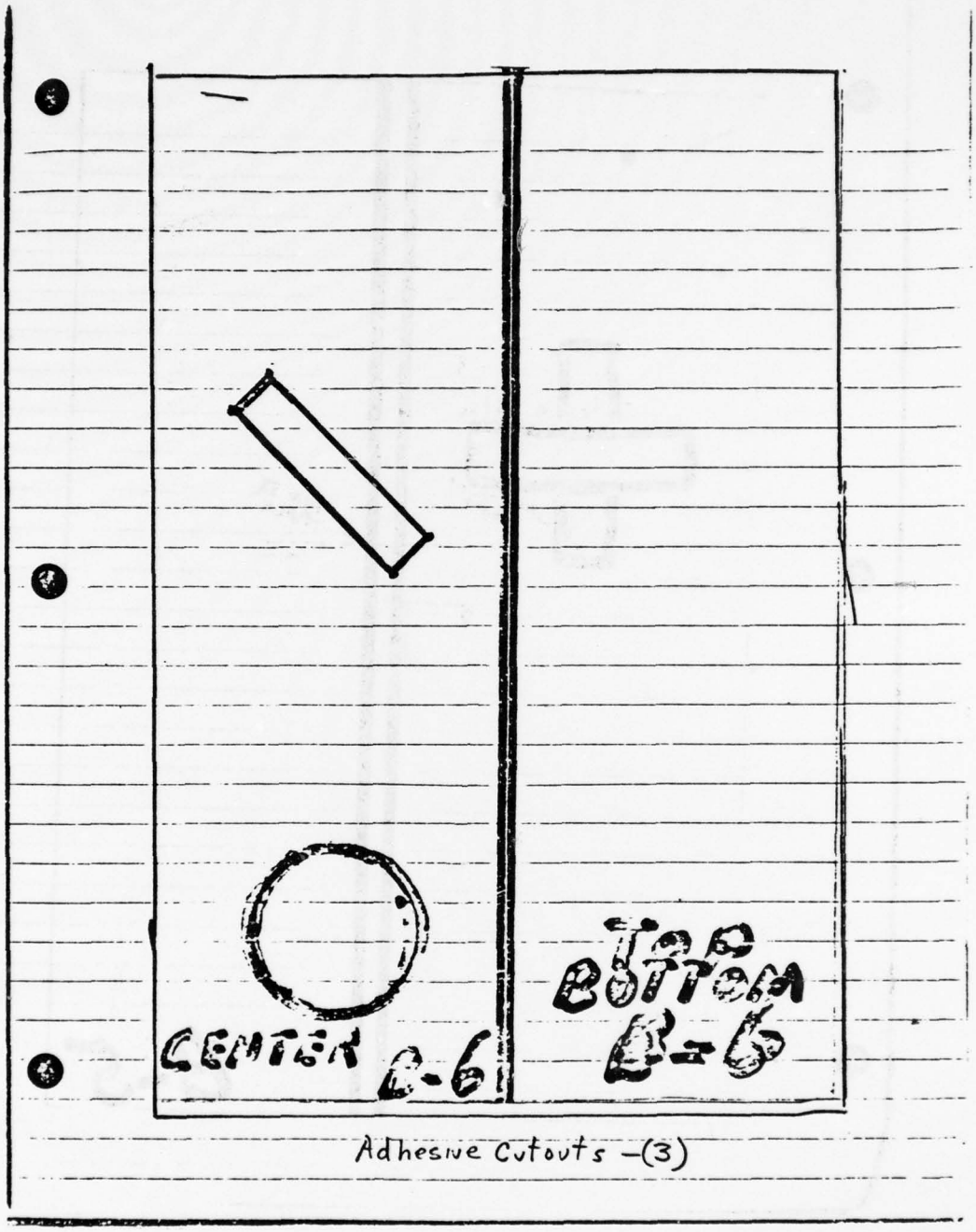

Figure B.35: Sample - B-6
Use - Classifier Design

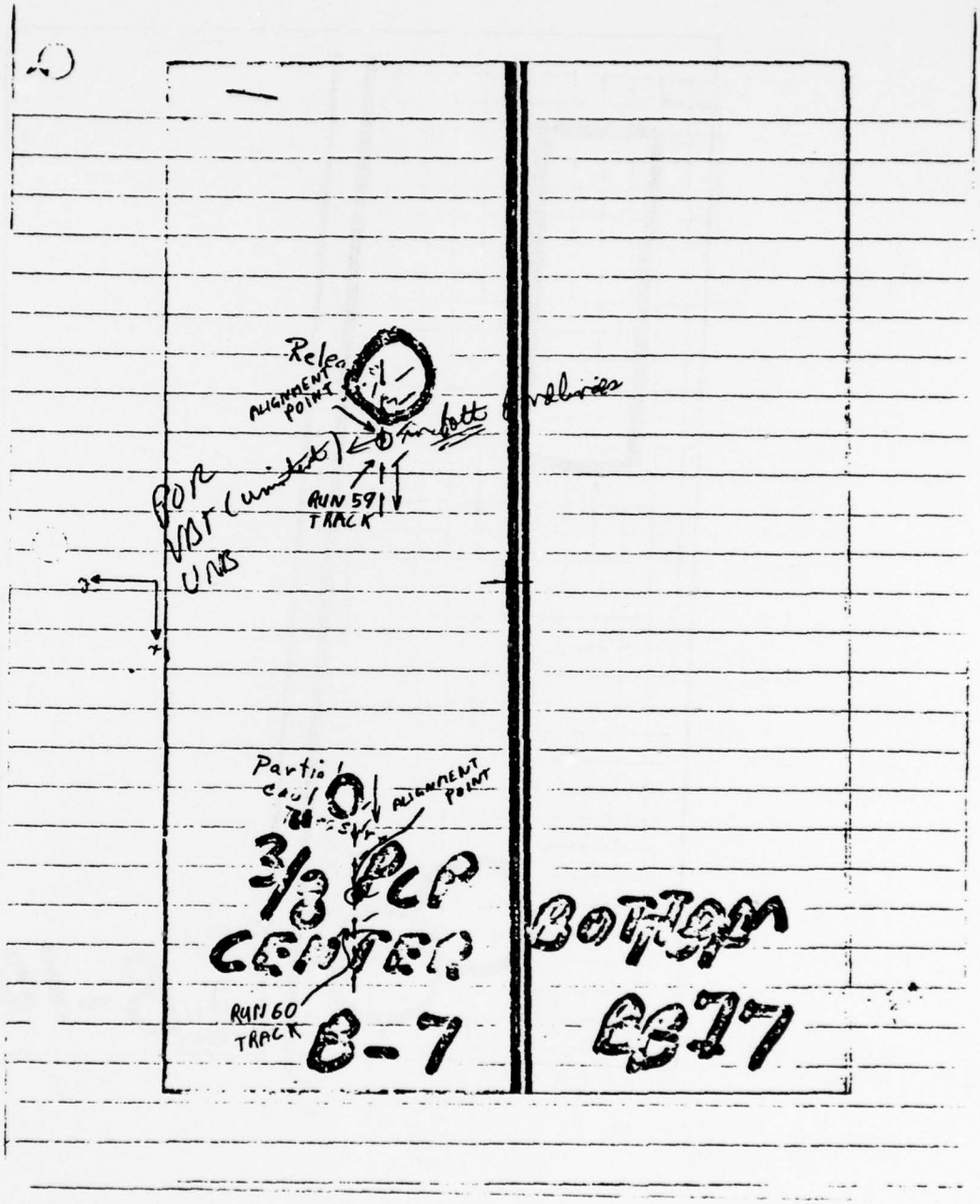

Figure B.36: Sample - B-7
Use - Classifier Design

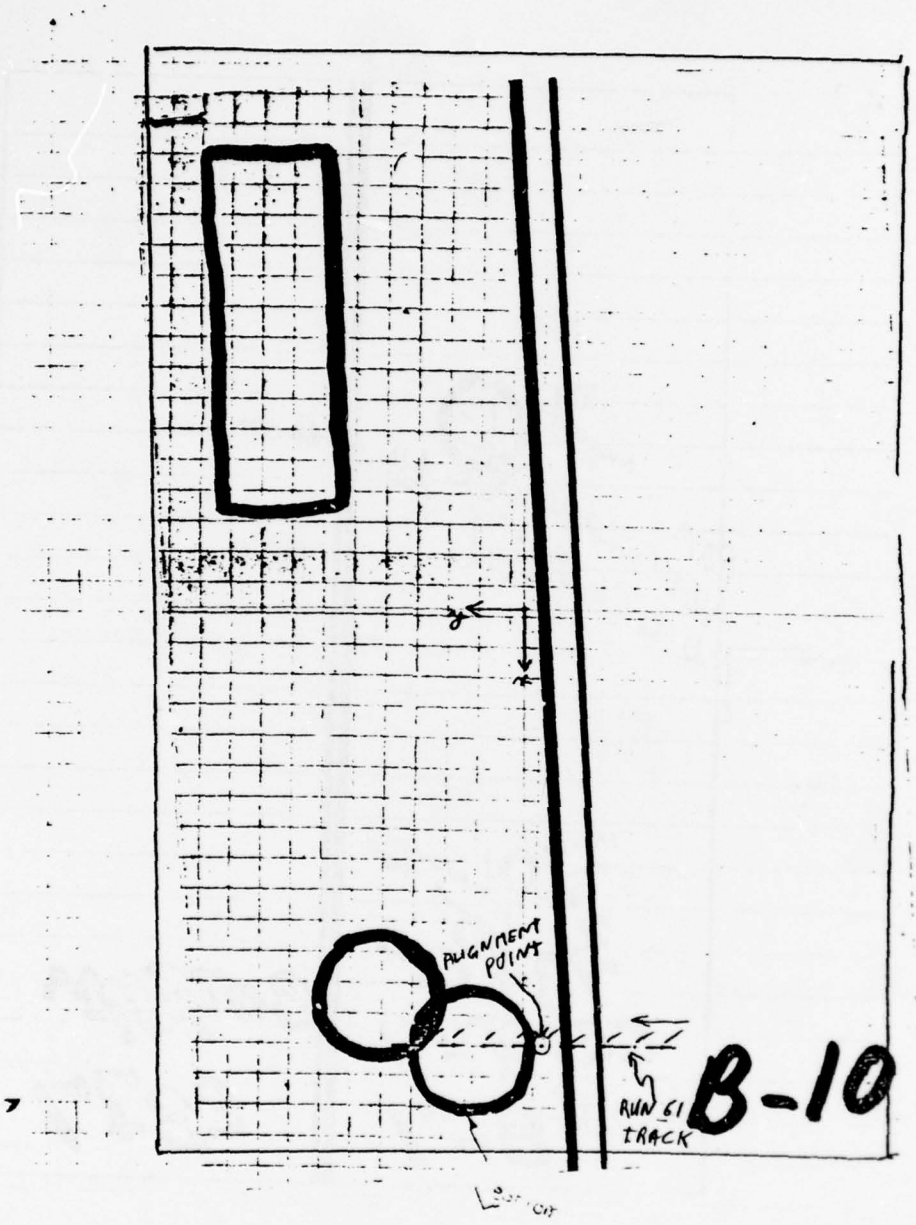

Figure B.37: Sample - B-10
Use - Classifier Design

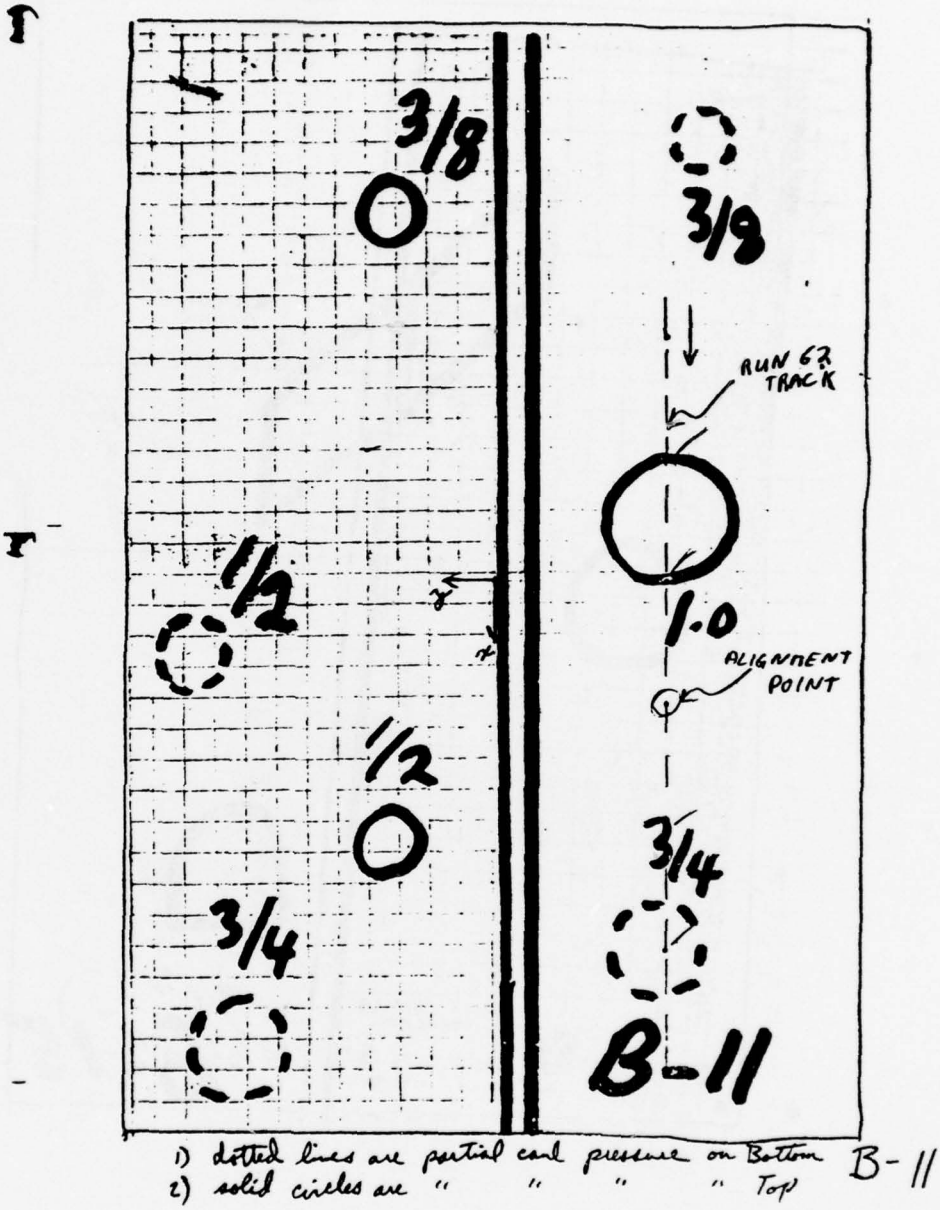

Figure B.38: Sample - B-11
Use - Classifier Design

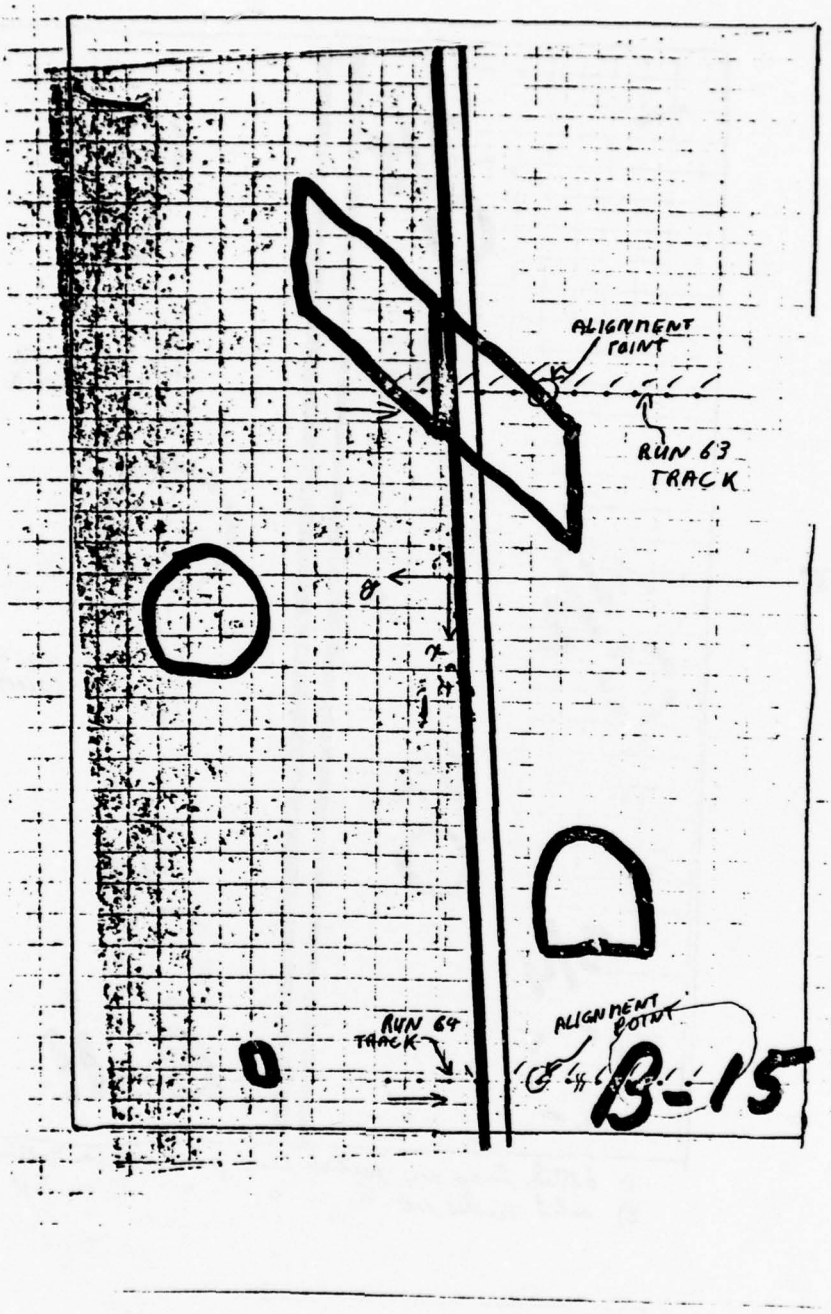

Figure B.39: Sample - B-15
Use - Classifier Design

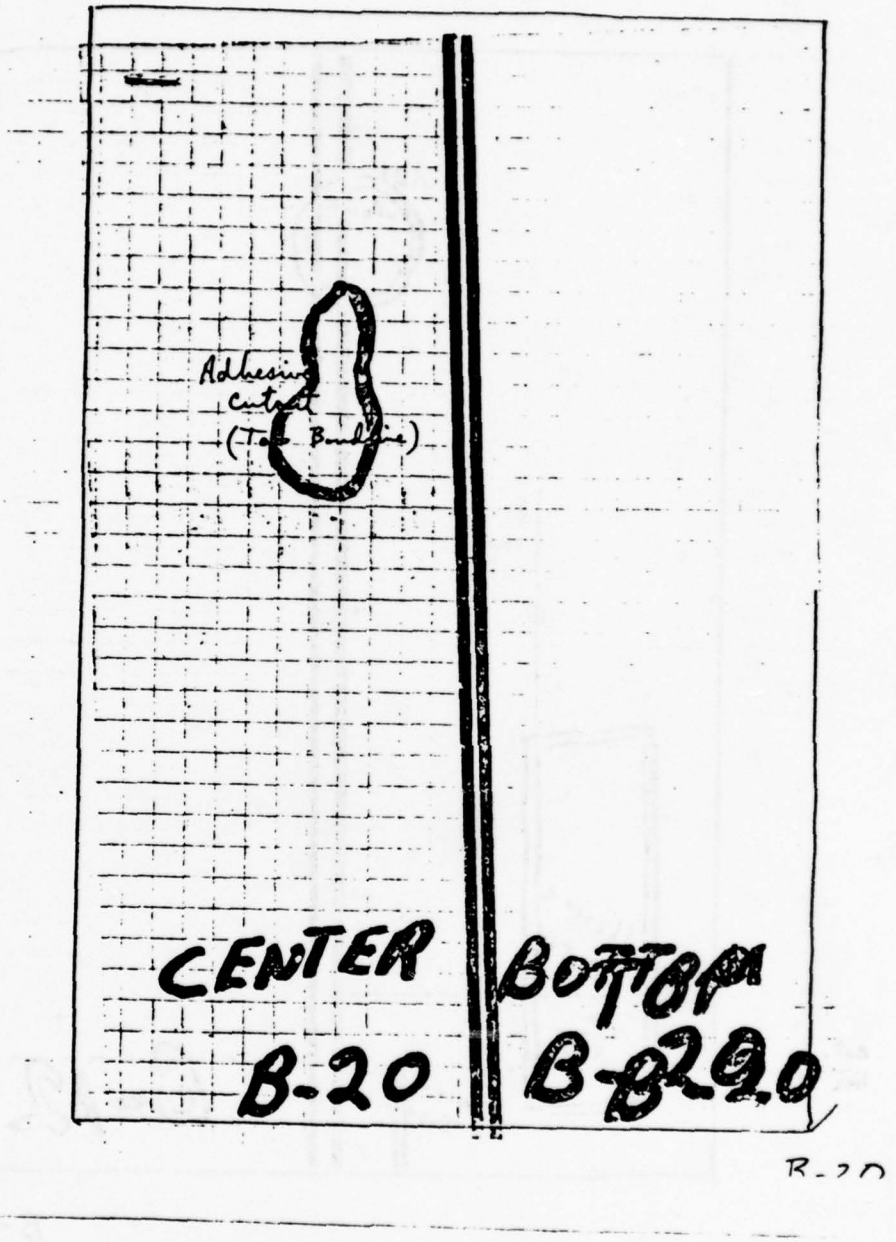

Figure B.40: Sample - B-20
Use - Classifier Design

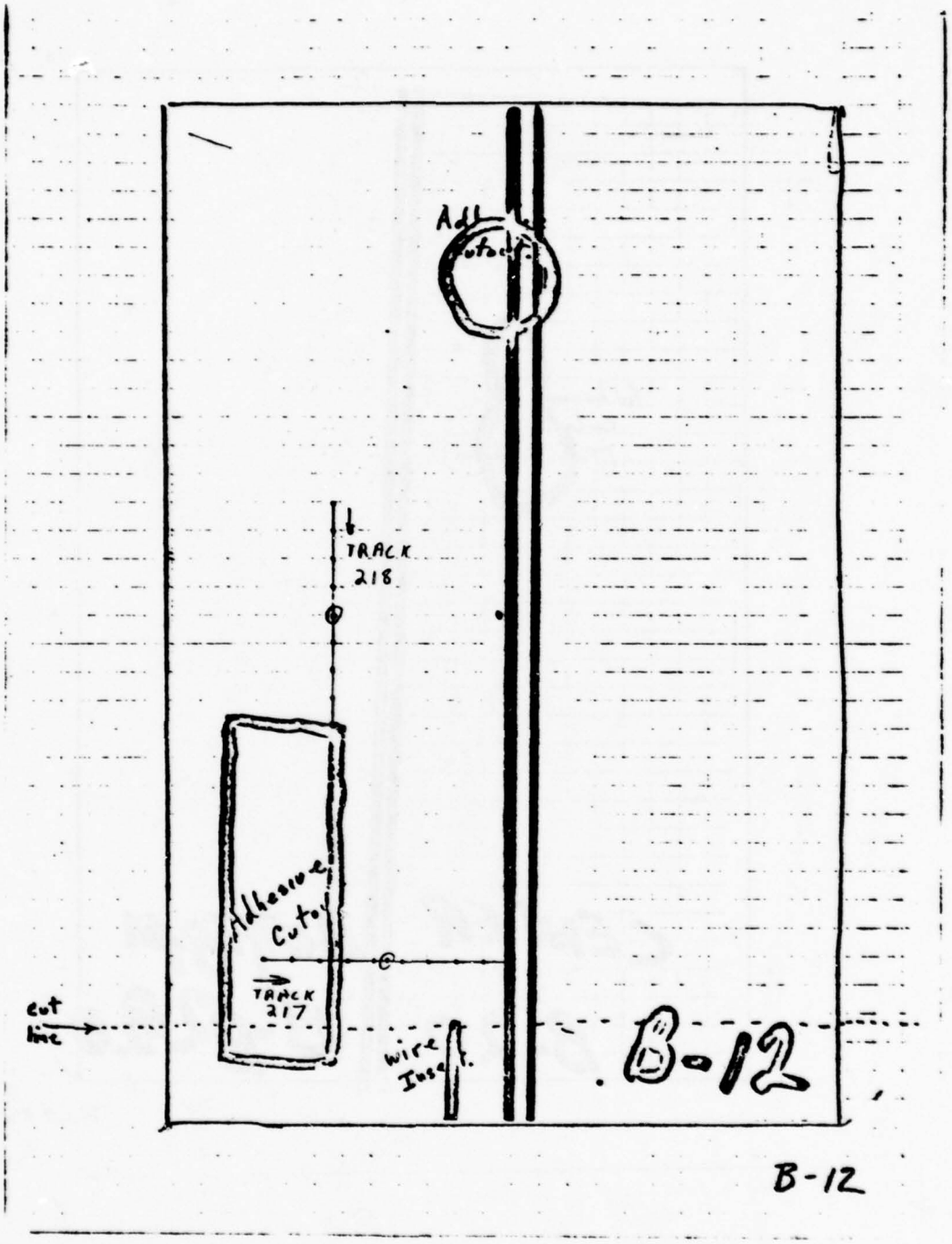

Figure B.41: Sample - B-12
Use - Classifier Evaluation

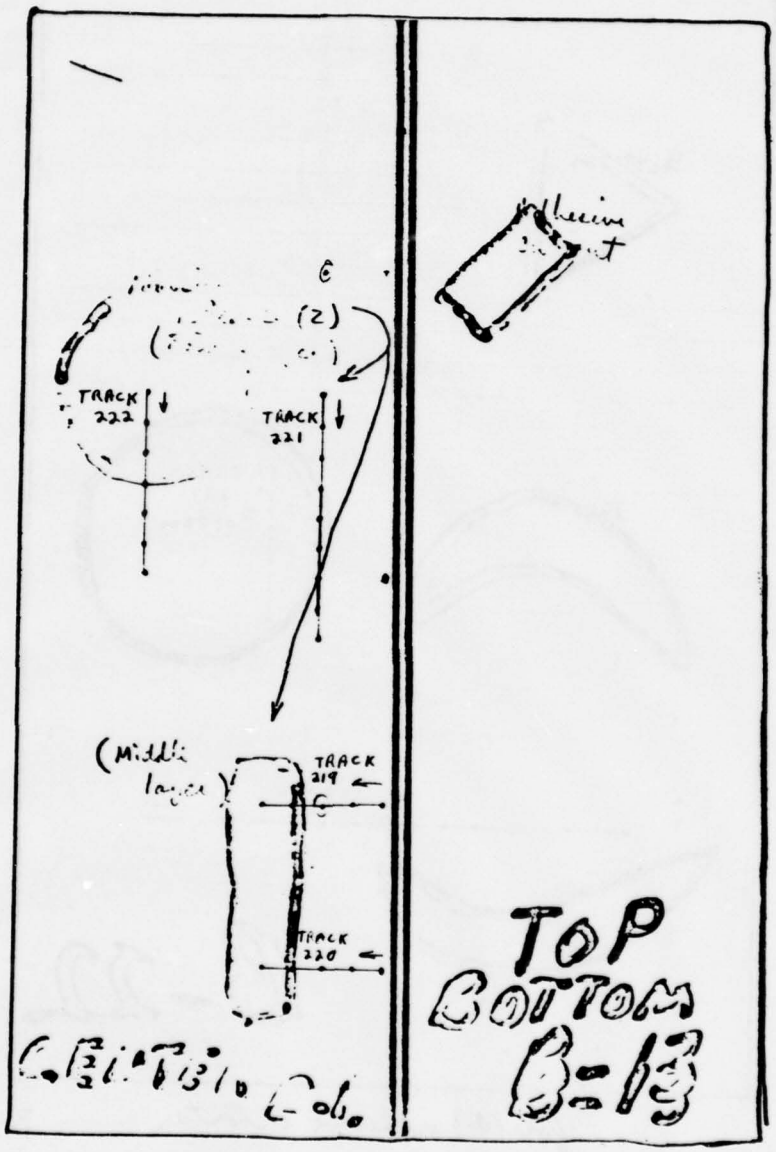

Figure B.42: Sample - B-13
Use - Classifier Evaluation

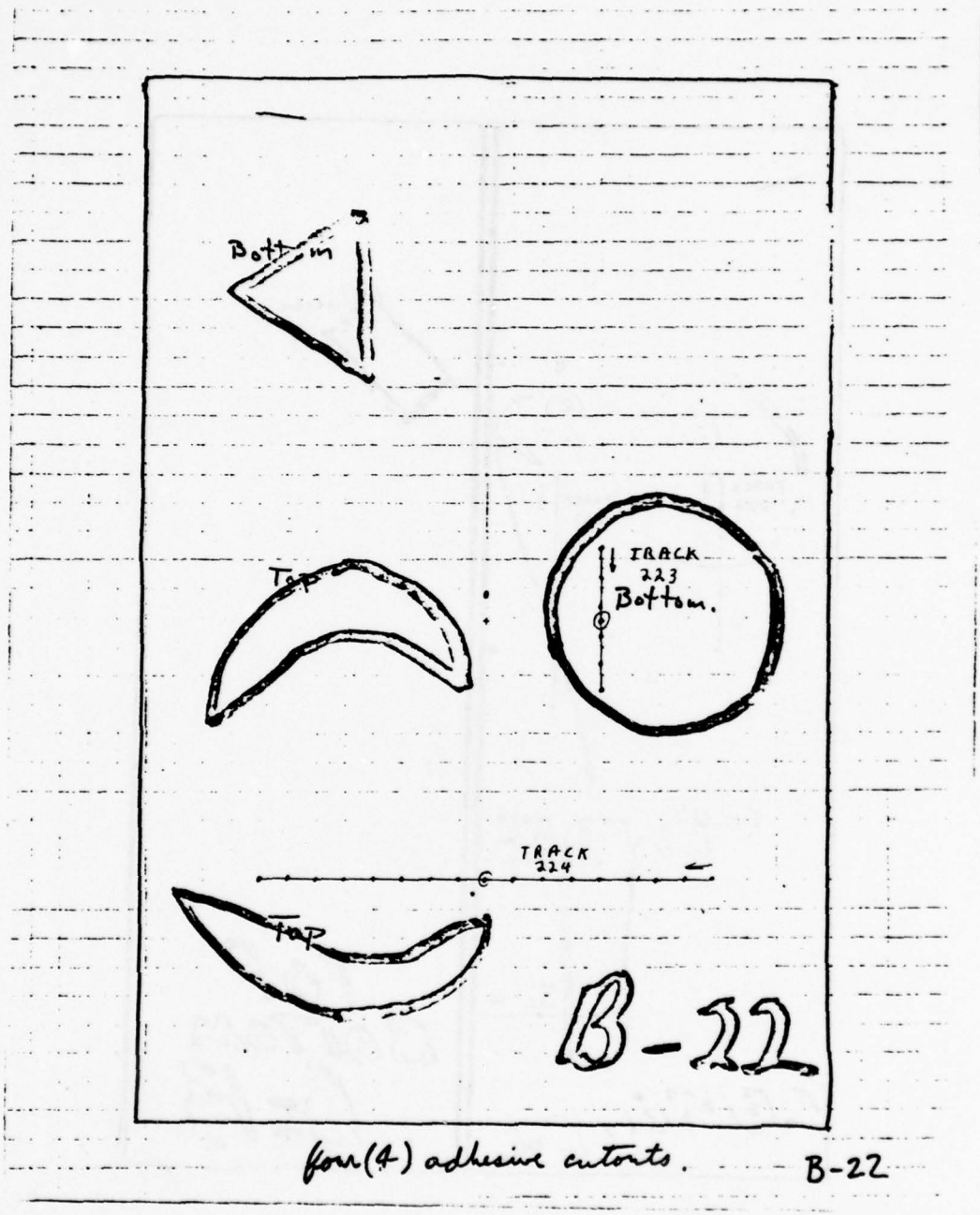

Figure B.43: Sample - B-22
Use - Classifier Evaluation

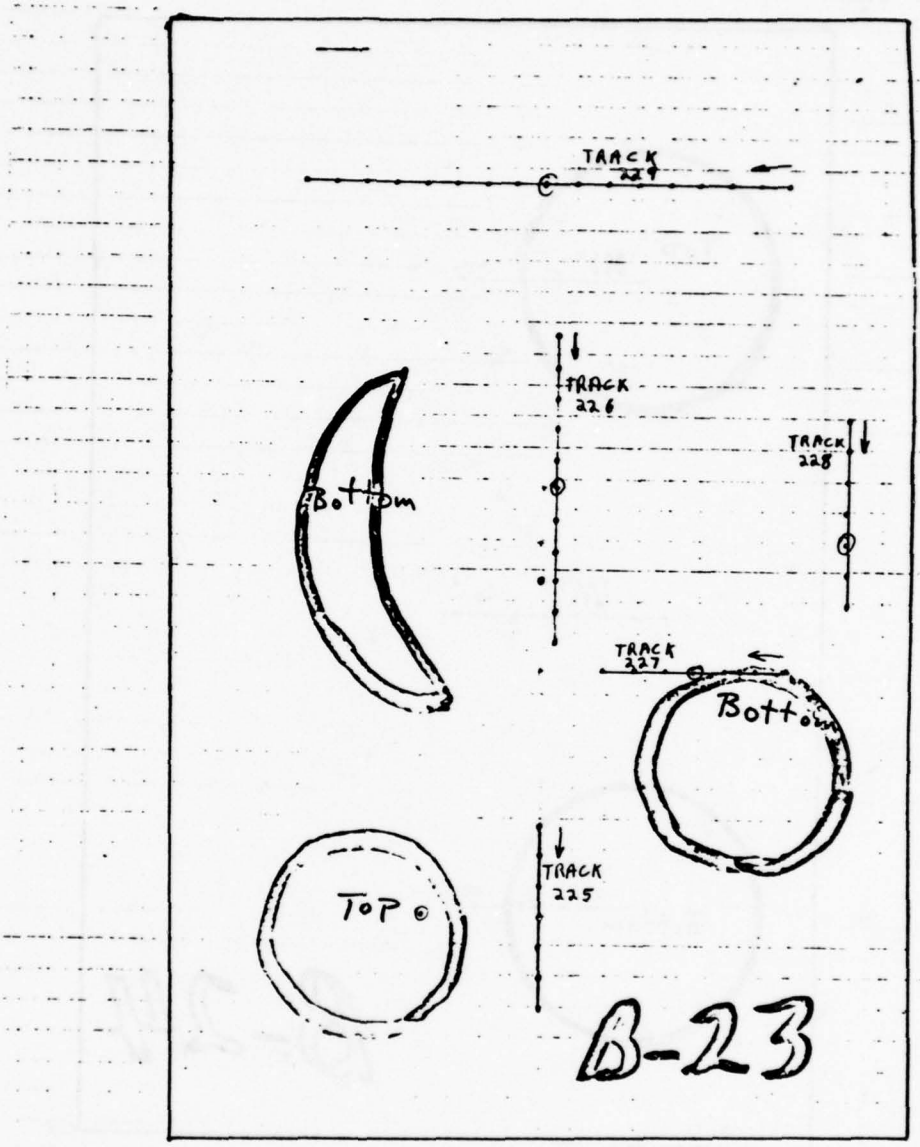

Figure B.44: Sample - B-23
Use - Classifier Evaluation

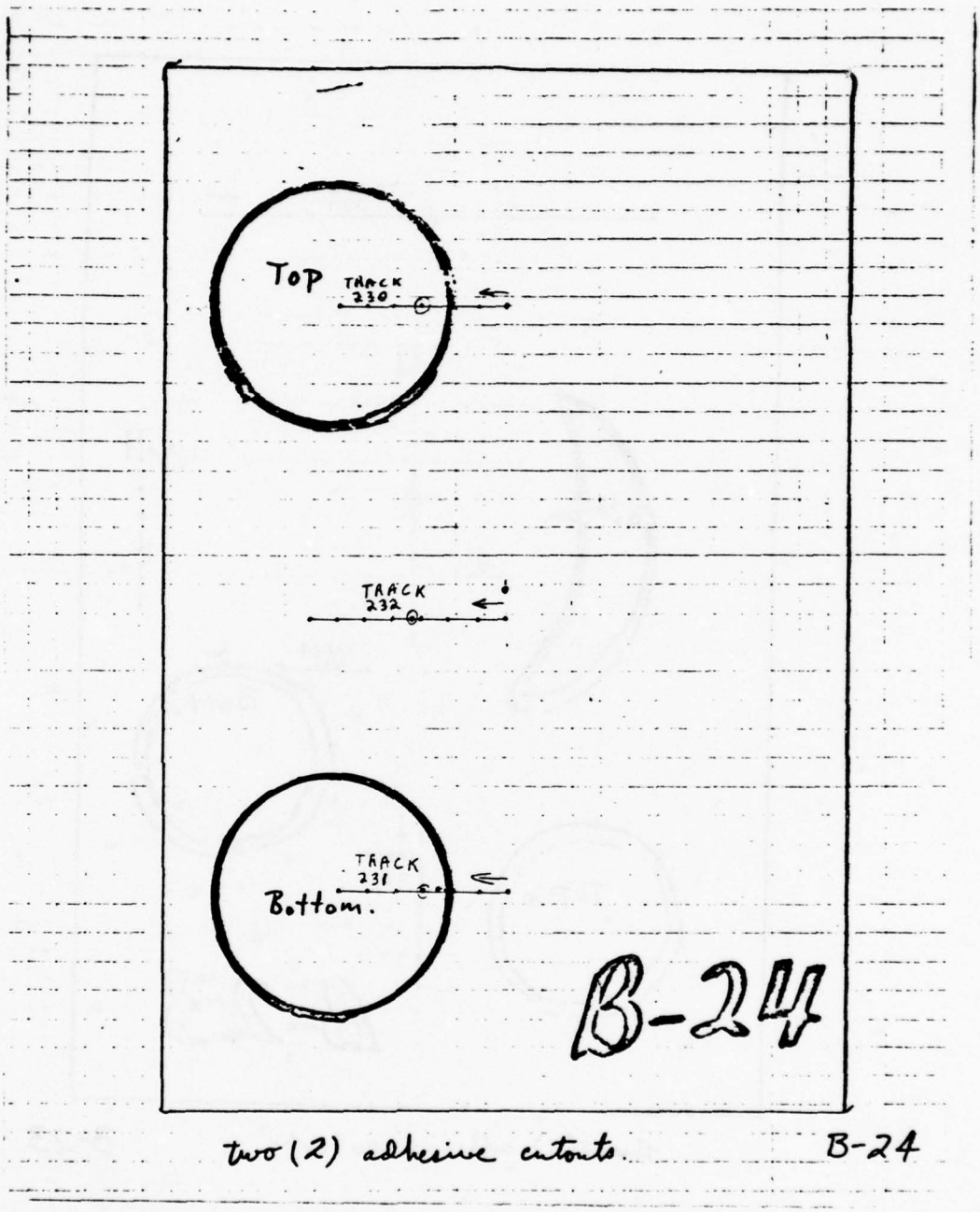

Figure B.45: Sample - B-24
Use - Classifier Evaluation

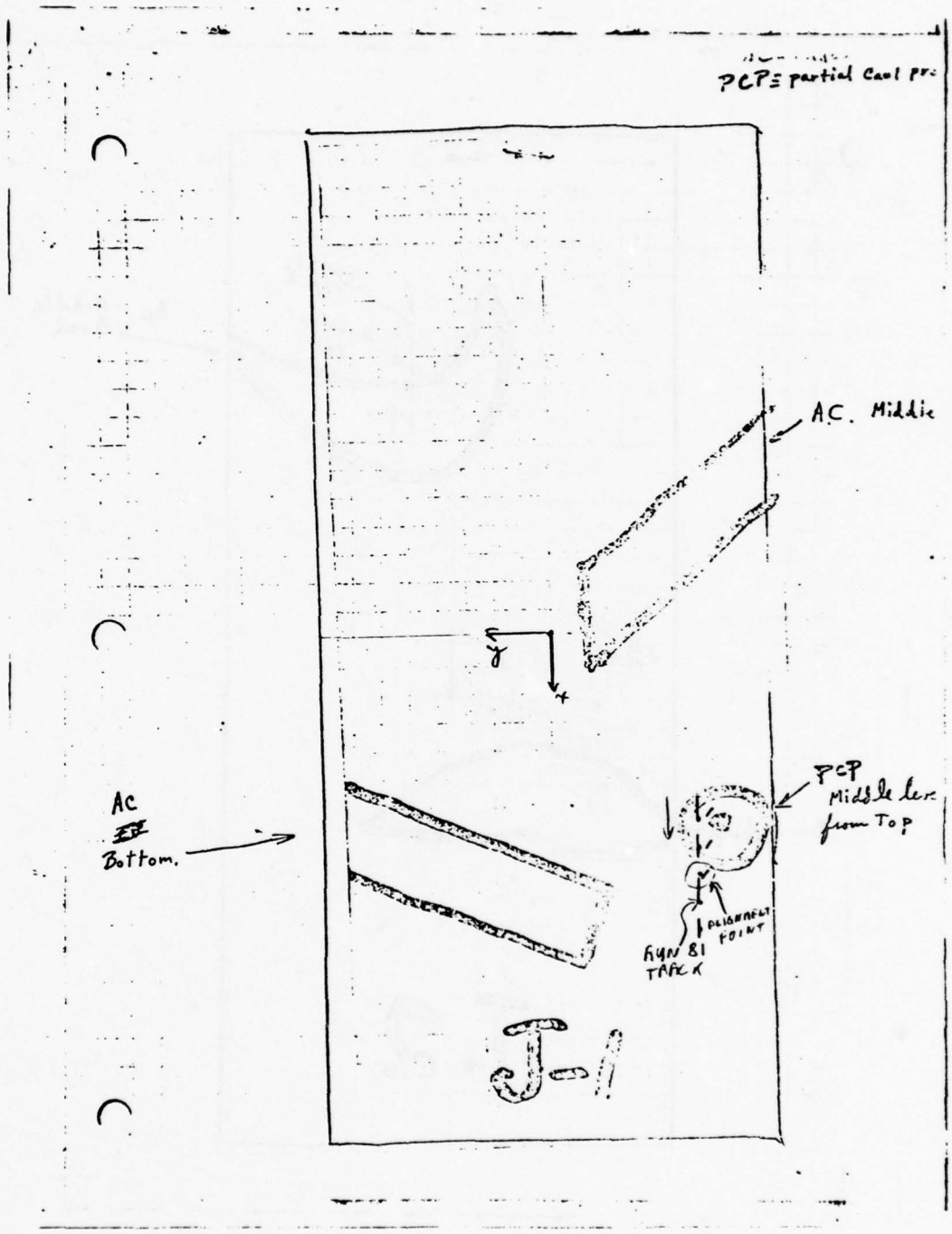

Figure B.46: Sample - J-1
Use - Classifier Design

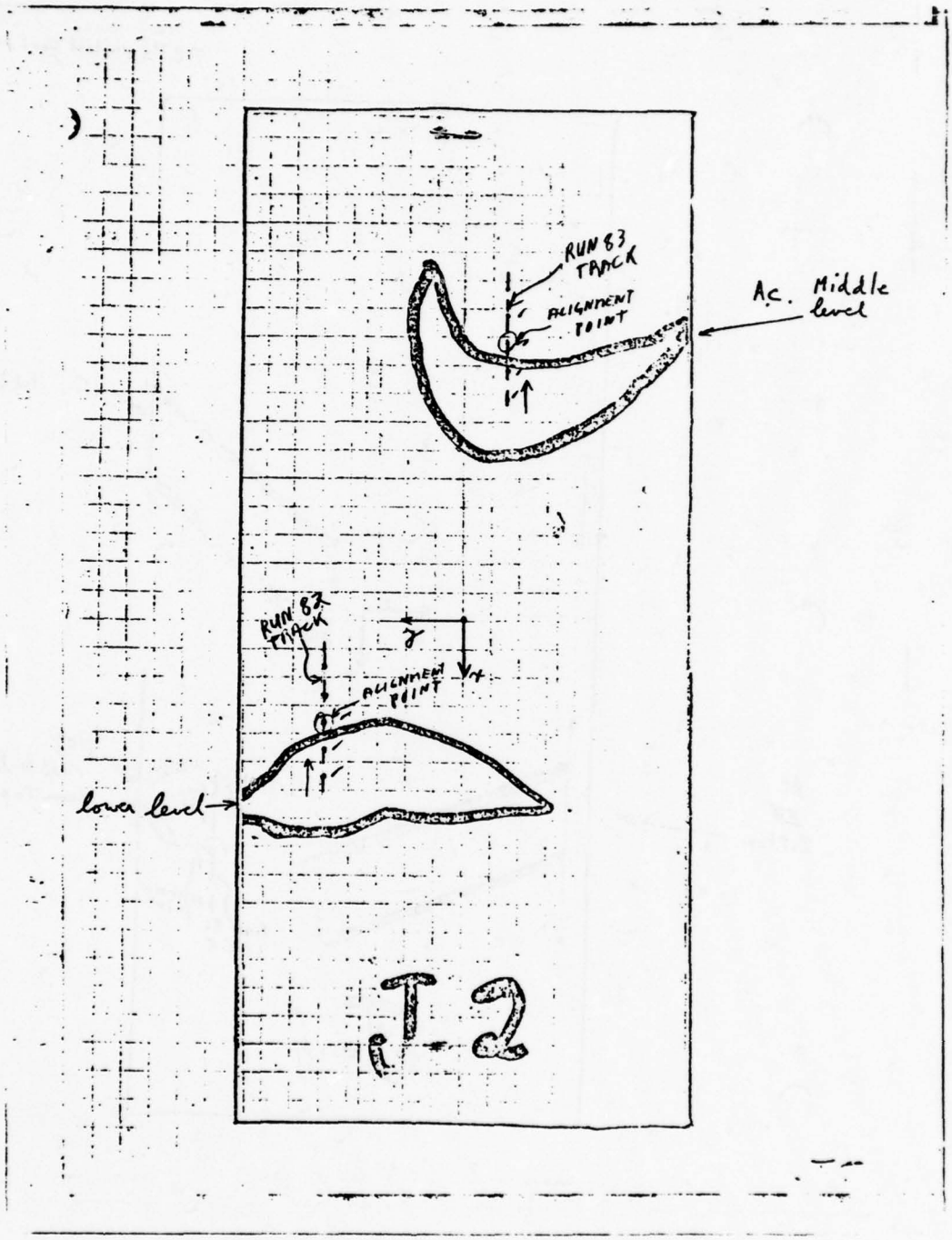

Figure B.47: Sample - J-2
Use - Classifier Design

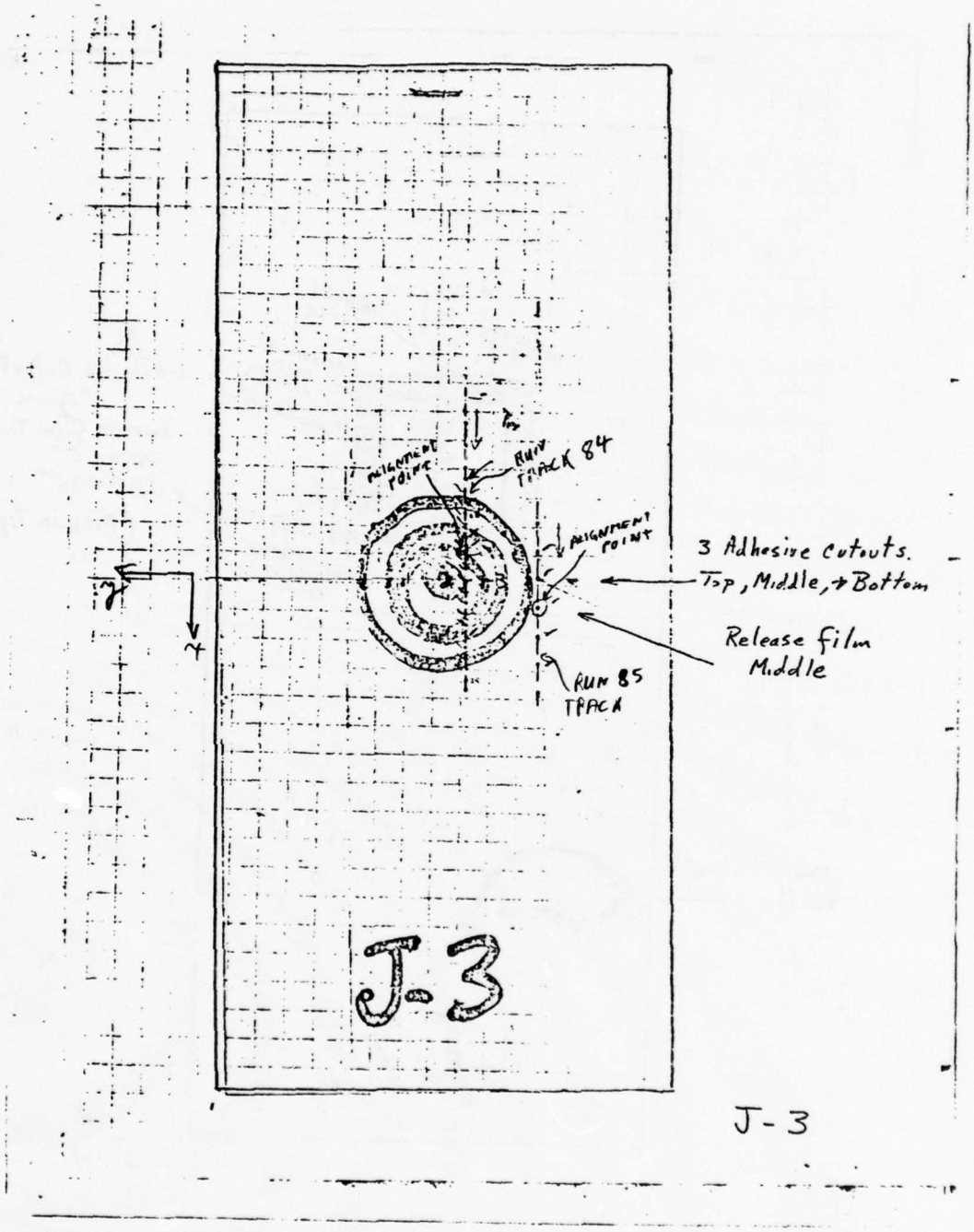

Figure B.48: Sample - J-3
Use - Classifier Design

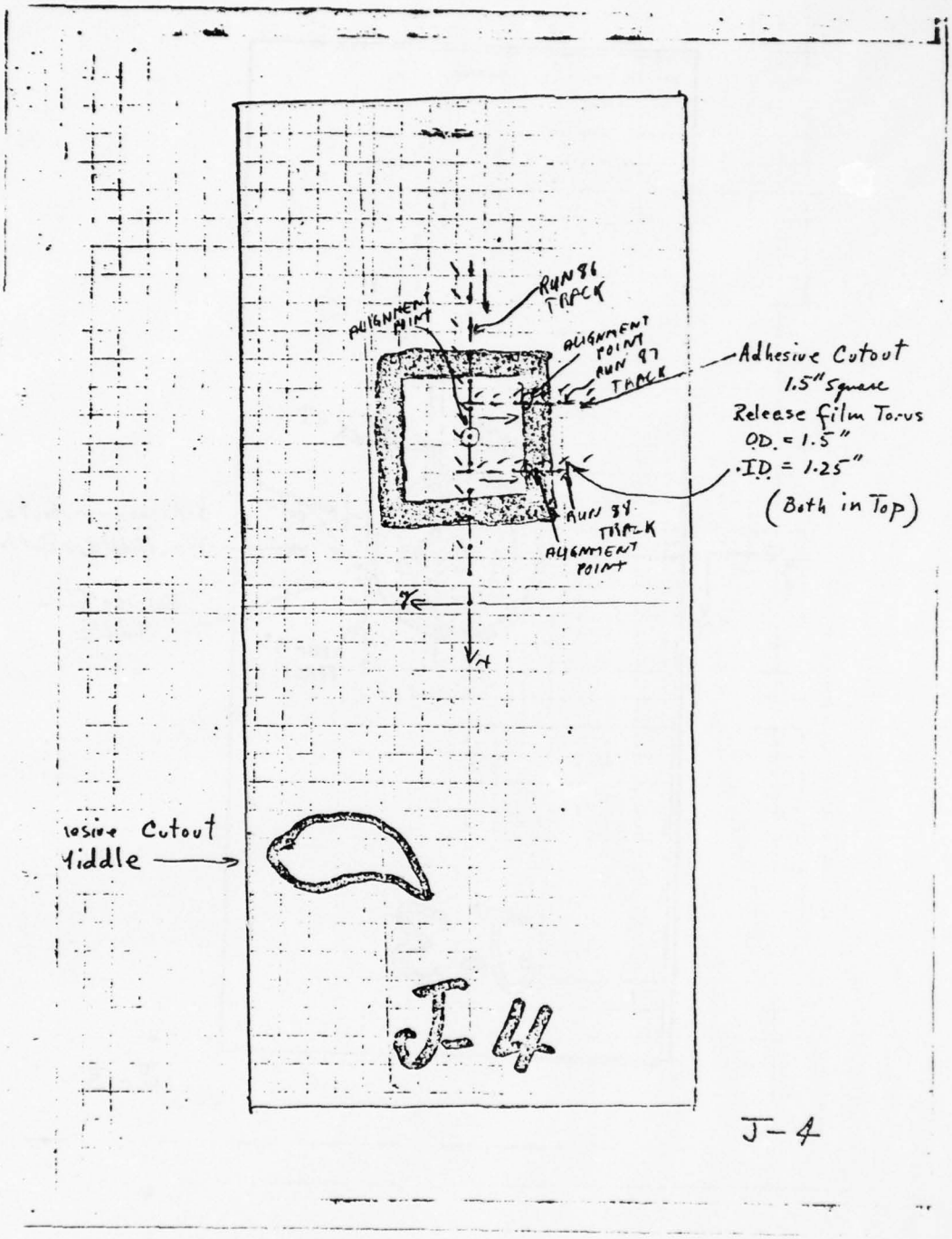

Figure B.49: Sample - J-4
Use - Classifier Design

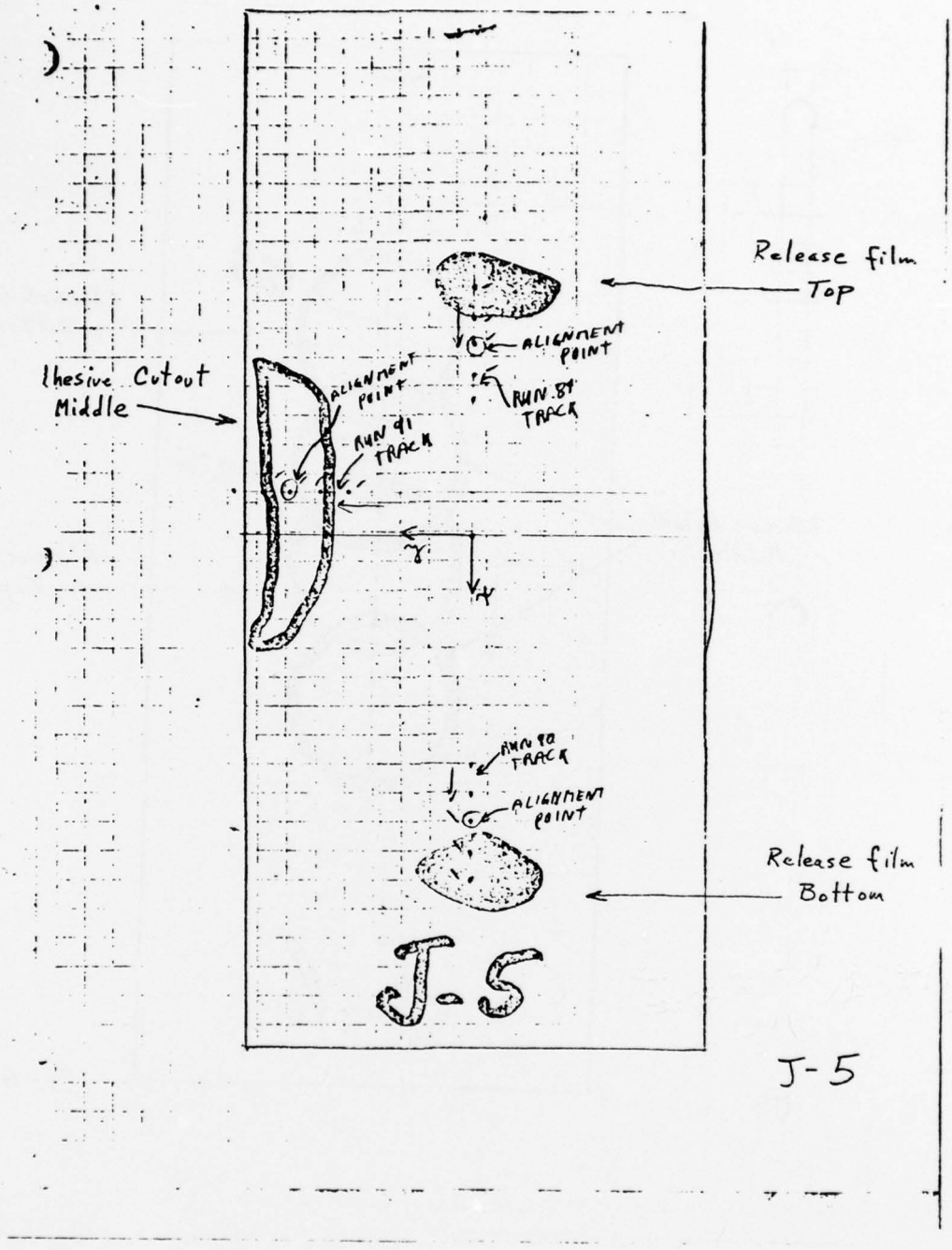

Figure B.50: Sample - J-5
Use - Classifier Design

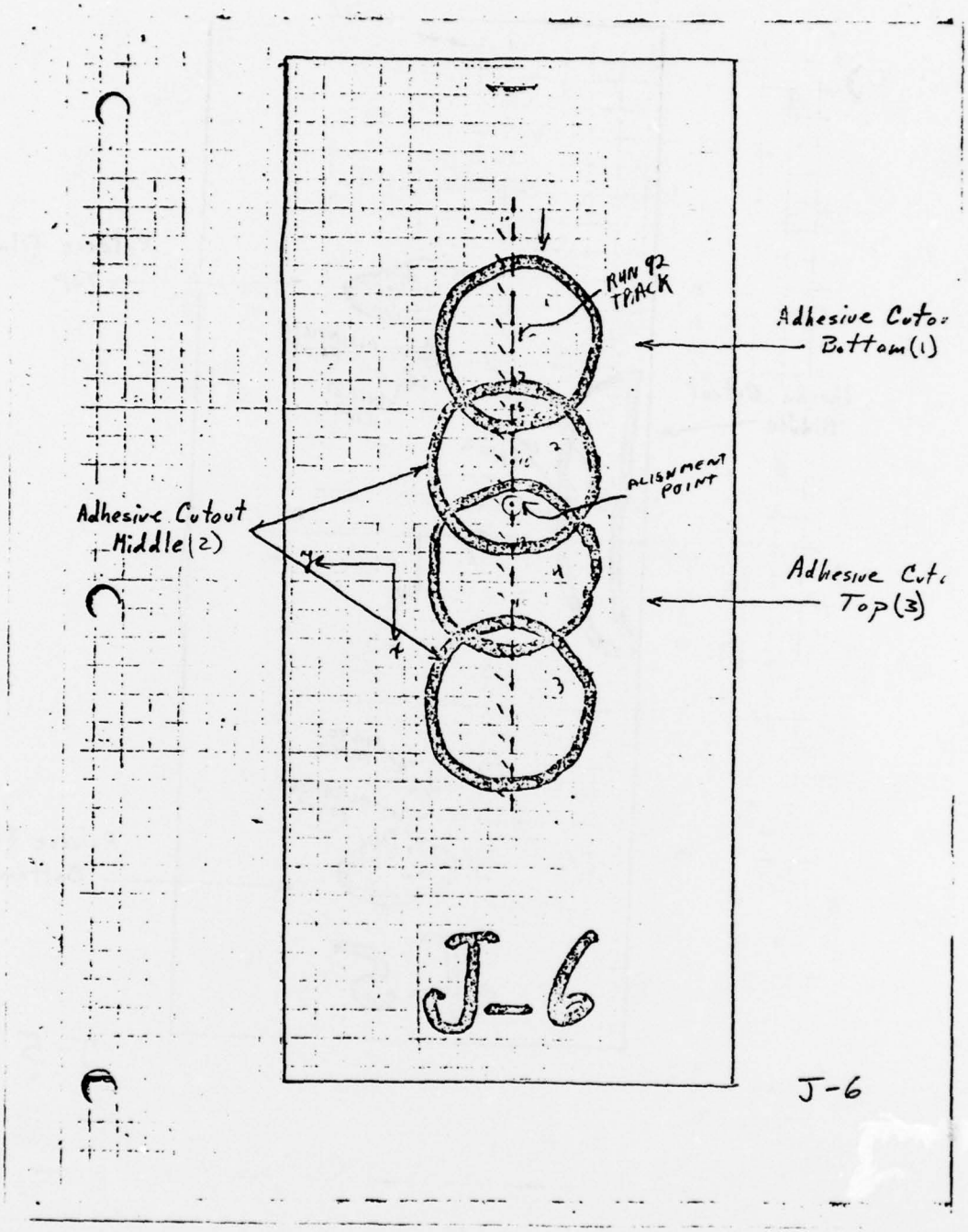

Figure B.51: Sample - J-6
Use - Classifier Design

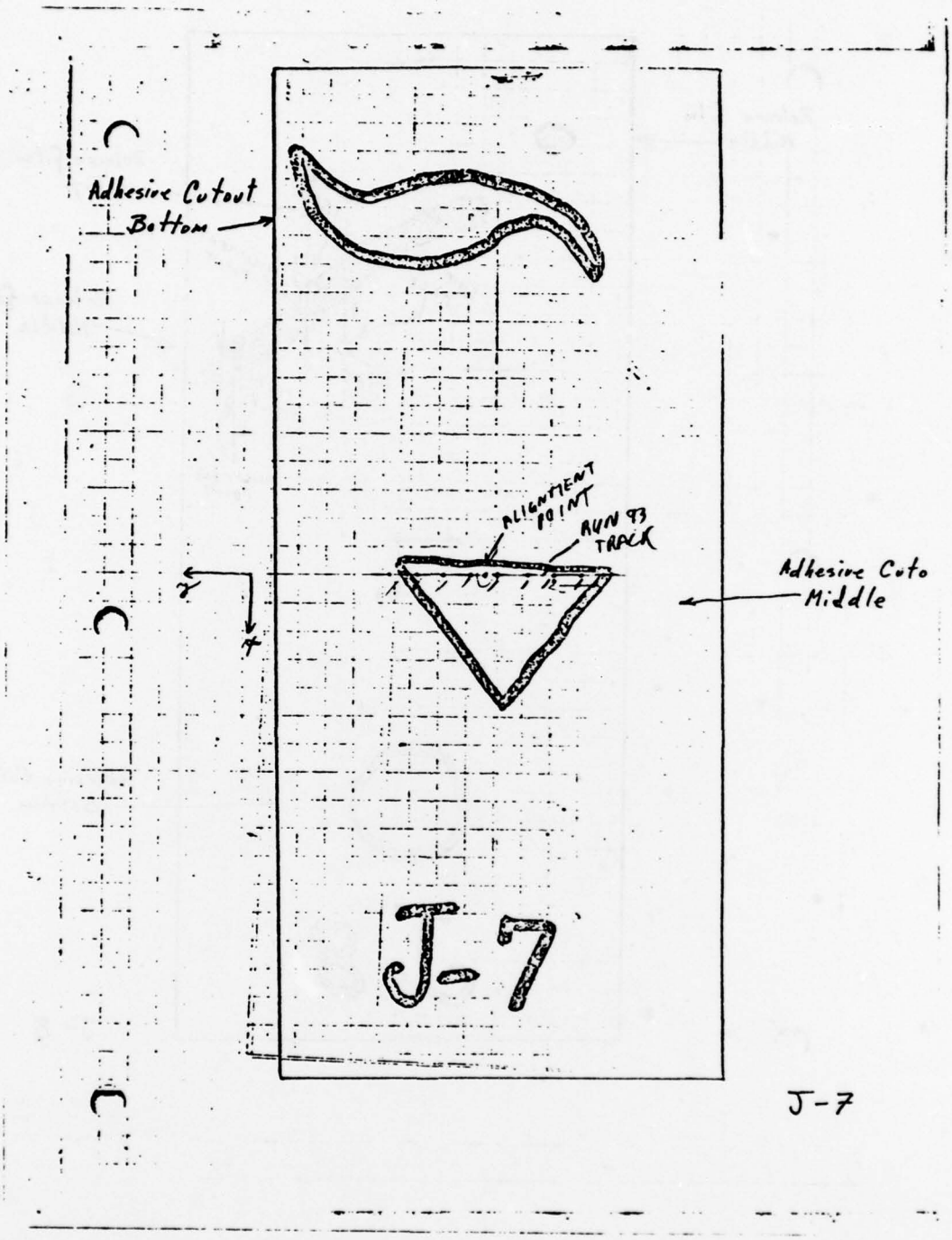

Figure B.52: Sample - J-7
Use - Classifier Design

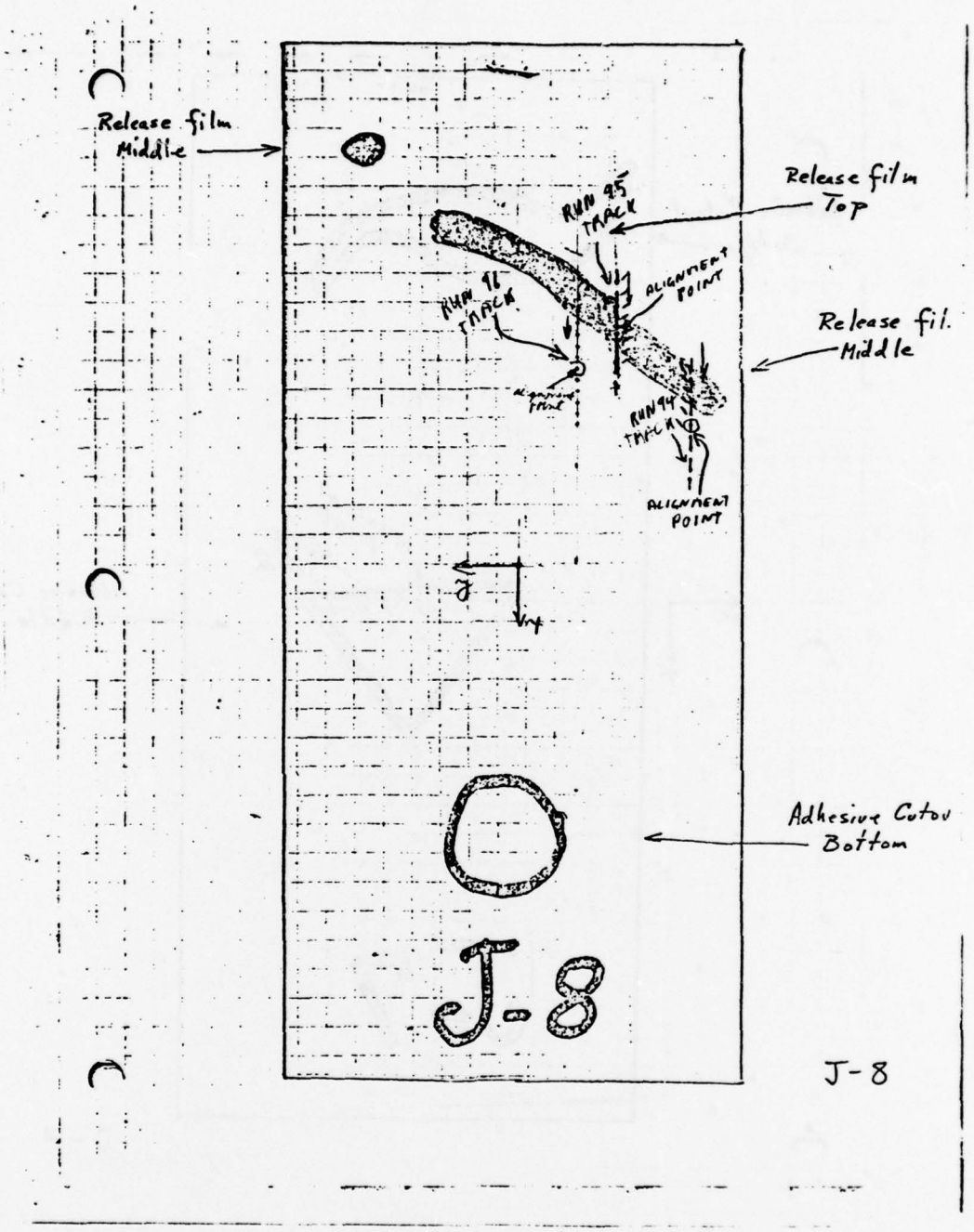

Figure B.53: Sample - J-8
Use - Classifier Design

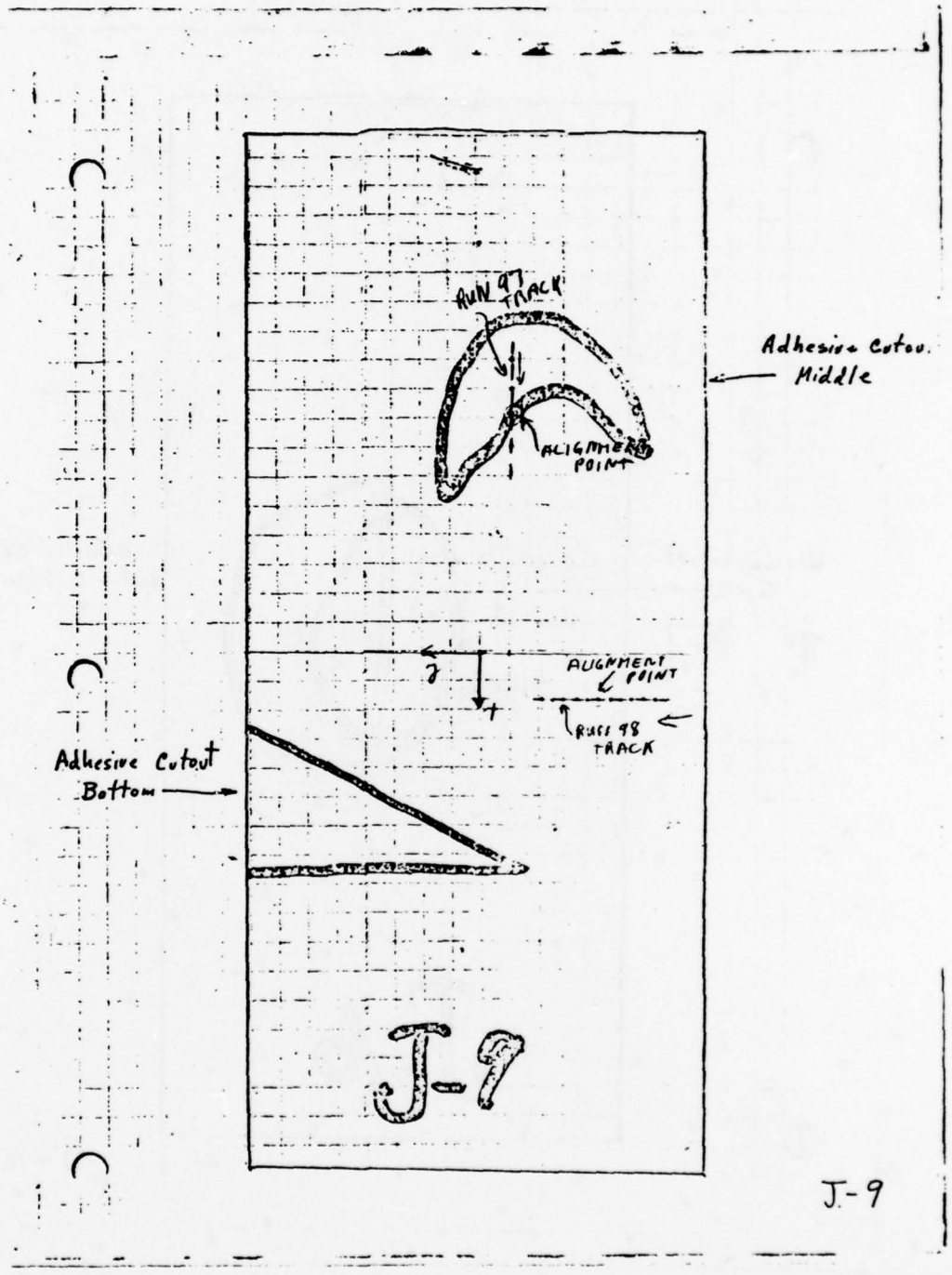

Figure B.54: Sample - J-9
Use - Classifier Design

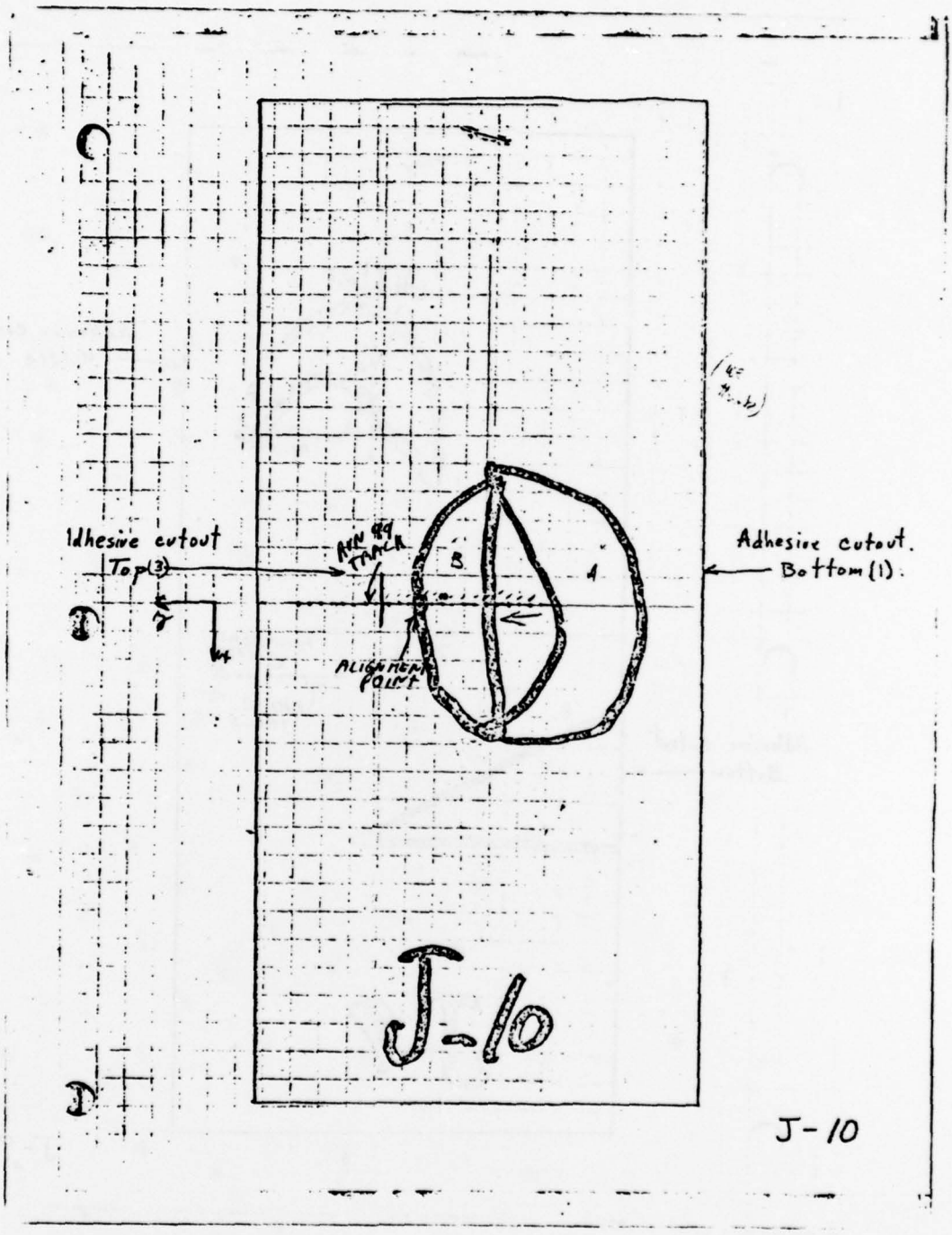

Figure B.55: Sample - J-10
Use - Classifier Design

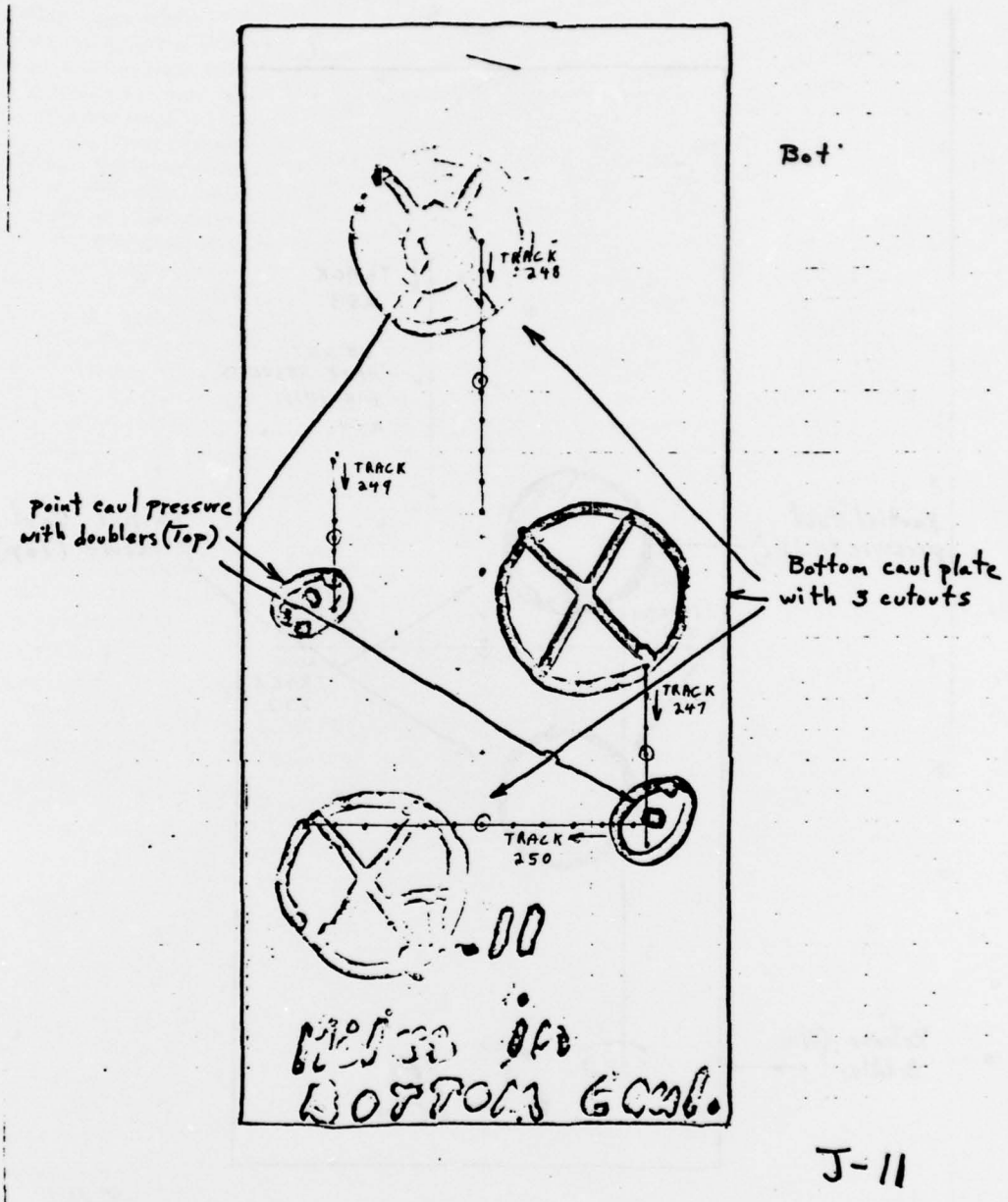

Figure B.56: Sample - J-11
Use - Classifier Evaluation

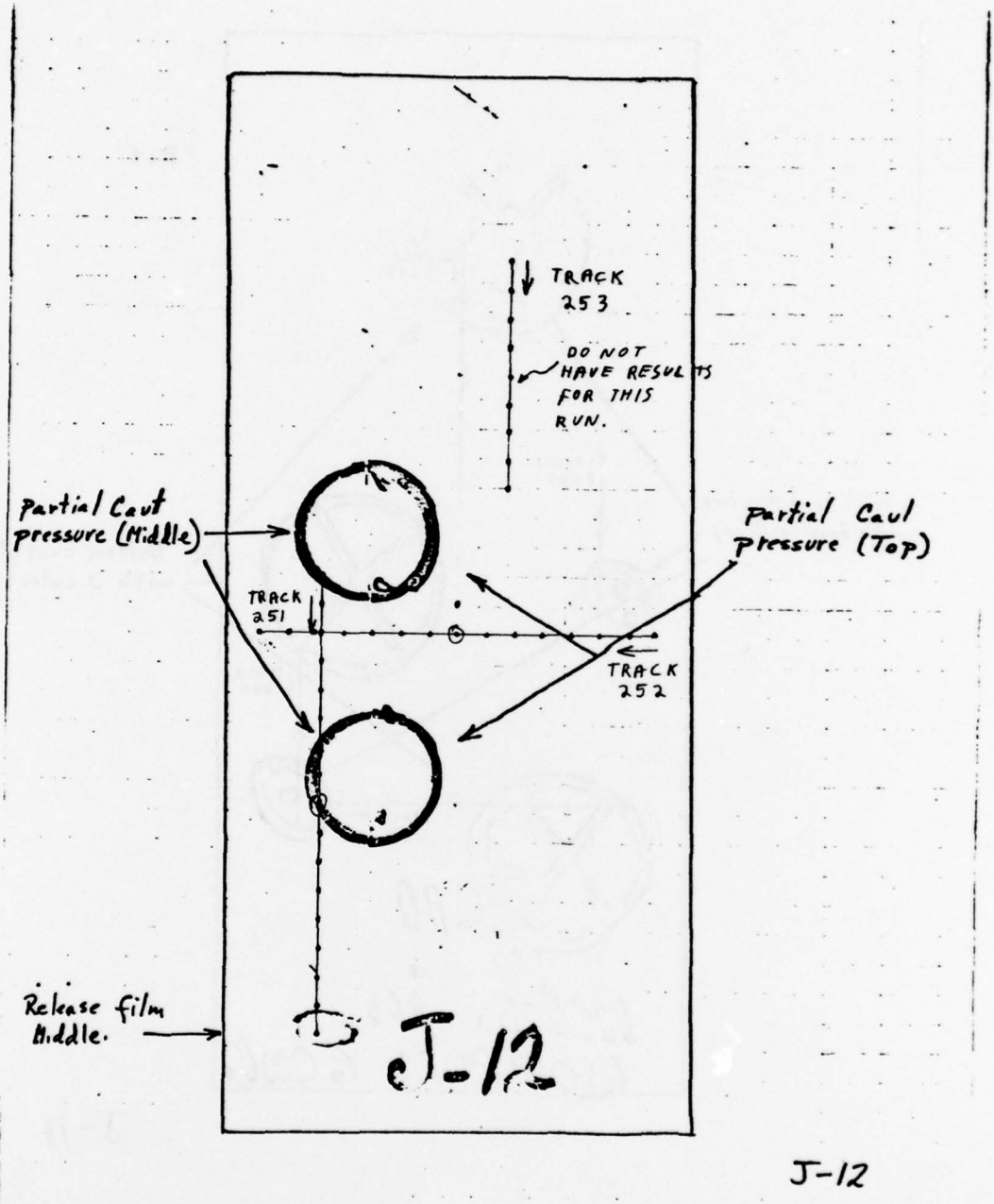

Figure B.57: Sample - J-12
Use - Classifier Evaluation

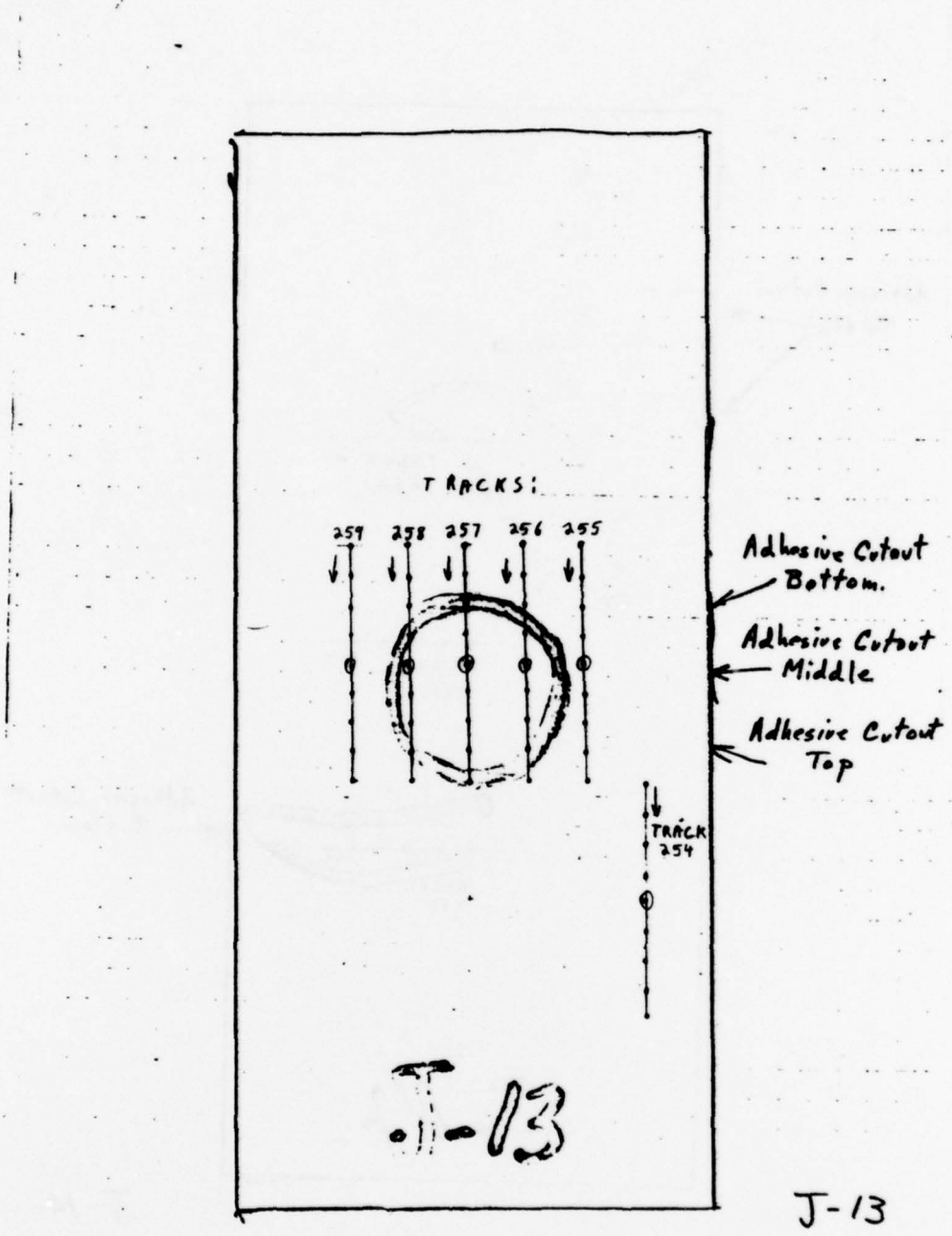

Figure B.58: Sample - J-13
Use - Classifier Evaluation

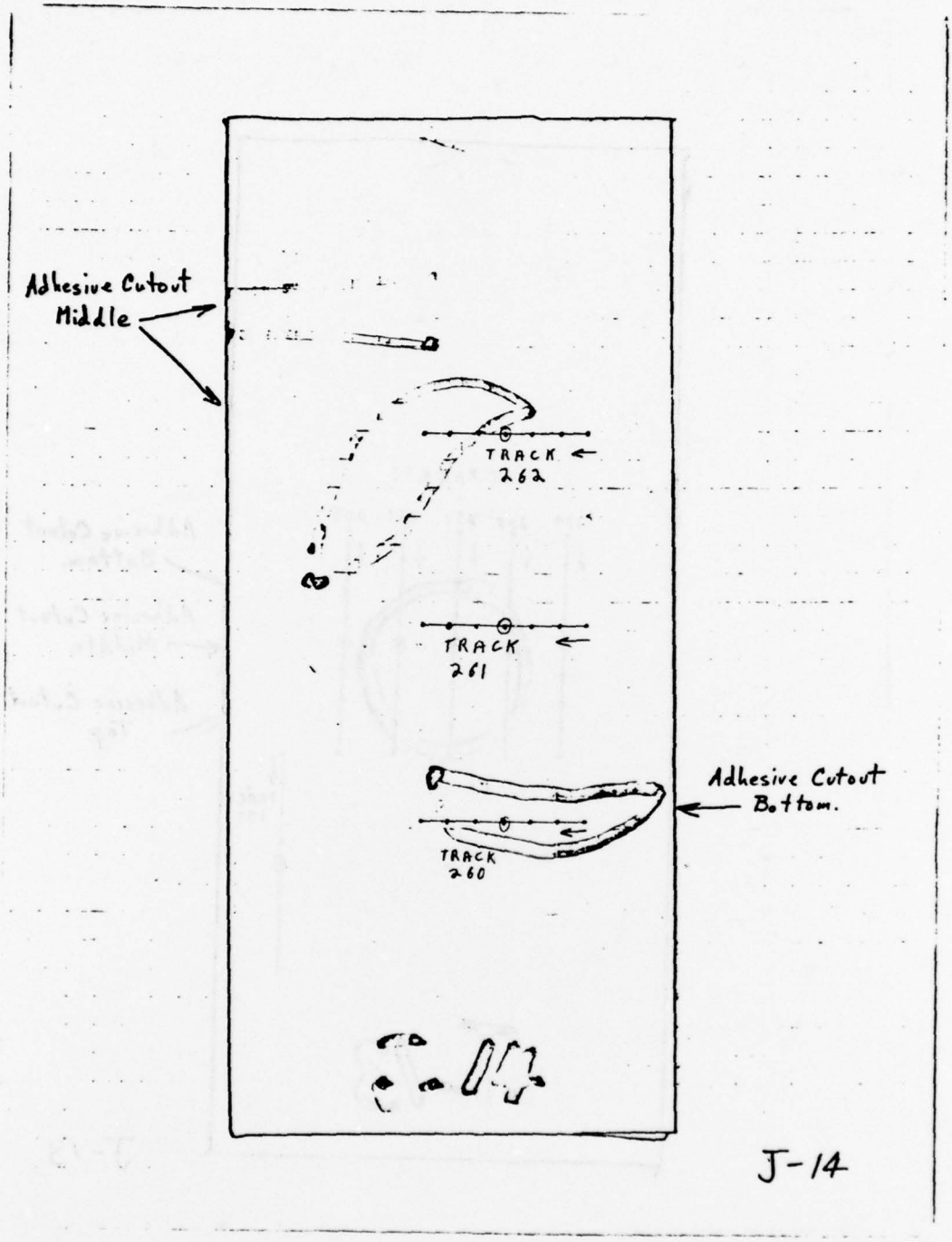

Figure B.59: Sample - J-14
Use - Classifier Evaluation

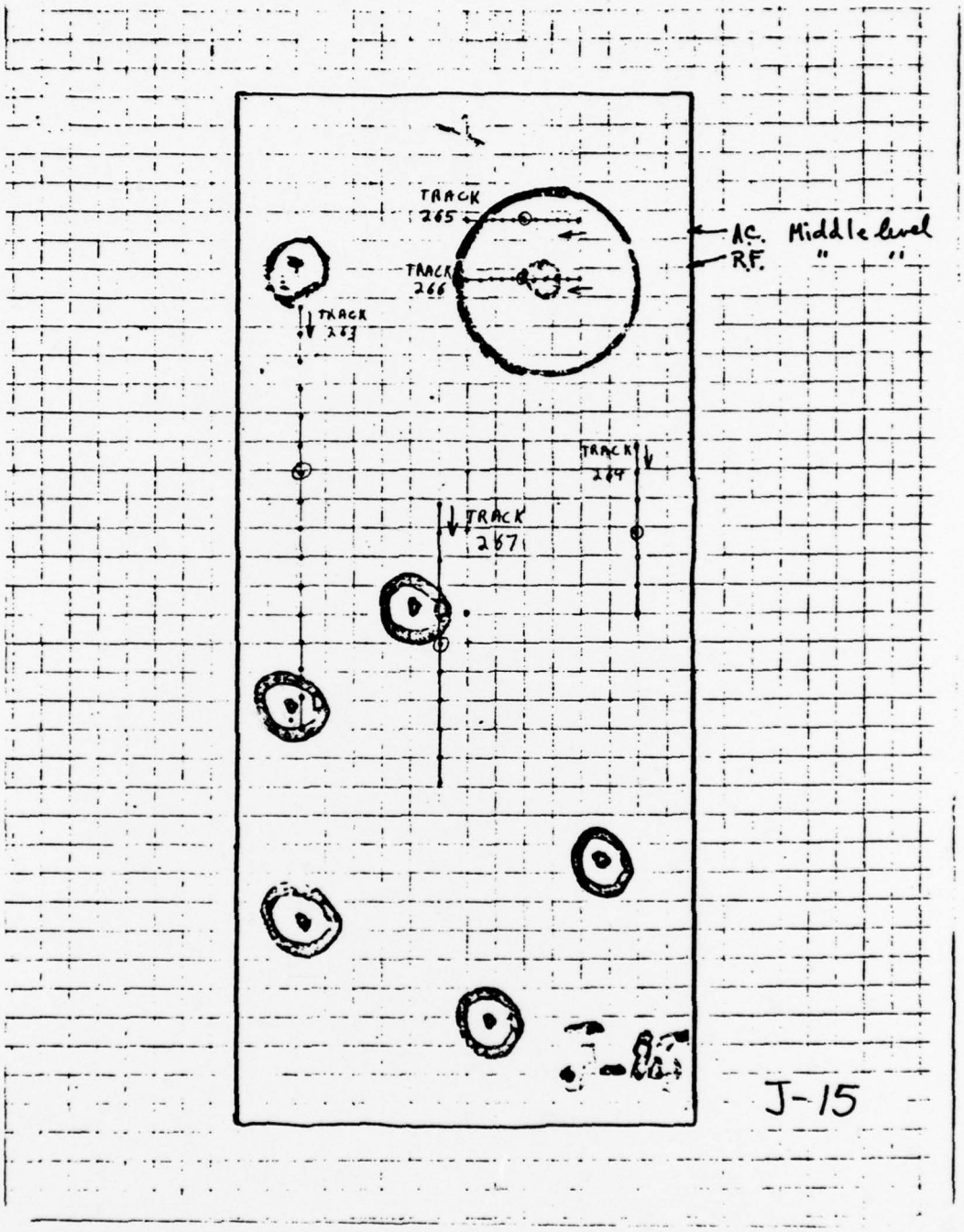

Figure B.60: Sample - J-15
Use - Classifier Evaluation

APPENDIX C

ALTERNATE INSPECTION TECHNIQUES

Angle Beam Thickness Measurements - Angle Beam Thickness Measurement (ABTM) experiments were performed on (1) a 0.40" thick aluminum plate and (2) adhesive bond sample F1, using 15 MHz 1/2" diameter, 1.5" focal length broadband transducers. The aluminum plate experiment demonstrated that pulses reflected in a layer do emerge from the layer displaced along the surface, in accordance with the laws of geometrical acoustics. The ABTM estimate of the thickness of the 0.040" plate was correct to within six percent.

The primary limitation on the accuracy of the measurement was in the ability to locate the position of emergence. The uncertainty in position is a function of the sound beam spot size and was found to be about 0.003 inches.

It is more difficult to perform ABTM on adhesive bond specimens for three reasons. First, because the adhesive bond is thin (0.005"), a given error in position measurement will cause a larger fractional error in the measurement. Second, thinness of the adhesive causes difficulty in separating the echoes from the front and back surfaces of the adhesive. Third, because of the attenuation of (high resolution) high frequencies by the adhesive, the back surface pulse is distorted.

An ABTM measurement at one position on Sample F1 which had an 8 mil adhesive thickness yielded an estimate of 13.4 mils, assuming that it was the first occurrence of the adhesive echo that was being measured, and 6.7 mils if the second adhesive echo was being measured.

The accuracy expected from ABTM on the basis of the aluminum plate experiments is barely adequate for adhesive bond thickness measurements. The accuracy achieved with adhesive bonds themselves is not yet sufficient to be useful.

In-Plane Modes - The use of ultrasonic waves which propagate parallel to the adhesive bond was studied for inspecting metal-to-metal adhesive joints. It was concluded that these wave modes are too difficult (if not impossible) to excite in the finished samples supplied by the Air Force; no further work was done with this technique.

SECTION IX

REFERENCES

1. R. L. Barron, "Learning Networks Improve Computer-Aided Prediction and Control," Computer Design, pp 65-70, August 1975.

2. A. V. Oppenheim, R. W. Schafer, and T. G. Stockham, Jr., "Nonlinear Filtering of Multiplied and Convolved Signals," Proc. IEEE, Vol. 56, pp 1264-1291, August 1968.

3. V. R. Arya and H. D. Holden, "Deconvolution of Seismic Data -- An Overview," IEEE Trans. Geo. Elect., Vol. GE-16, No. 2, pp 95-98, April 1978.

*U.S.Government Printing Office: 1979 — 657-002/13